

Wilfrid Laurier University

Scholars Commons @ Laurier

Theses and Dissertations (Comprehensive)

2023

Spatial and temporal characteristics of historical surface climate over the Northwest Territories, Canada

Bhaleka D. Persaud

Wilfrid Laurier University, pers3479@mylaurier.ca

Follow this and additional works at: <https://scholars.wlu.ca/etd>



Part of the [Atmospheric Sciences Commons](#), [Climate Commons](#), [Hydrology Commons](#), [Meteorology Commons](#), and the [Other Oceanography and Atmospheric Sciences and Meteorology Commons](#)

Recommended Citation

Persaud, Bhaleka D., "Spatial and temporal characteristics of historical surface climate over the Northwest Territories, Canada" (2023). *Theses and Dissertations (Comprehensive)*. 2532.
<https://scholars.wlu.ca/etd/2532>

This Dissertation is brought to you for free and open access by Scholars Commons @ Laurier. It has been accepted for inclusion in Theses and Dissertations (Comprehensive) by an authorized administrator of Scholars Commons @ Laurier. For more information, please contact scholarscommons@wlu.ca.

Spatial and temporal characteristics of historical surface climate over the Northwest Territories, Canada

By:

Bhaleka Devi Persaud

BSc in Physics, University of Guyana, 2002

MSc in Weather, Climate and Modelling, University of Reading, 2005

DISSERTATION

Submitted to the Department of Geography and Environmental
Studies, Faculty of Science

in partial fulfillment of the requirements for

Doctor of Philosophy in Geography

Wilfrid Laurier University

© Bhaleka Devi Persaud 2022

Abstract

Climate change is putting many of the Northwest Territories (NWT) ecosystems, its people and animal populations at risk due to accelerated warming, permafrost thaw, and changing precipitation regimes. As the NWT continues to warm, at disproportionately higher rates when compared to the rest of Canada, threats to the stability of NWT's ecosystems are expected to increase. Consequently, understanding how climate warming has changed historically and its implications on natural ecosystems requires point-to-region-specific, long-term climatic data to elucidate important drivers of observed changes relevant to decision makers at community, Indigenous, Territorial and Federal government levels. However, *in situ* climate data are limited temporally and spatially across the NWT. Hence, the overarching goal of this research is to enhance and improve the understanding of historical surface climate variables trends and patterns (air temperature, precipitation, and shortwave radiation) and its implications at local and regional scales in the continental NWT by using interpolated, reanalysis and remote sensing climate data.

Gridded climate datasets such as interpolated and reanalysis data, can provide reliable estimates for *in situ* observations to compensate for data scarcity, but it is critical that researchers understand how biases in these datasets can impact runoff simulation in the NWT. Thus, the objective of this dissertation was to assess the similarity between daily *in situ* station observations and three gridded datasets (ANUSPLIN, ERA-Interim and MERRA-2) from 1980 to 2013 to support hydrological modelling in the NWT subarctic. The ANUSPLIN maximum and minimum temperature at eight locations aligned closely to the corresponding *in situ* observations and had mean daily biases of less than 0.58°C and 1.33°C, respectively. Precipitation estimates showed that the alternative datasets captured year-to-year variability, but large seasonal biases mainly during spring and summer were evident when precipitation magnitudes were estimated. In addition, this study used gridded data as a

substitute for *in situ* observations in the Cold Regions Hydrological Model (CRHM) to simulate runoff. Simulated runoff generated when using ANUSPLIN and ERA-Interim data as inputs in CRHM captures the timing and magnitude of freshet and baseflow generally well at Scotty Creek. This study suggests that gridded datasets can provide reasonable estimates of *in situ* climate data in data sparse regions and reinforced that the accuracy in representing *in situ* observations over the NWT improves as the spatial resolution of interpolated dataset increases. This research also highlighted that when comparing datasets, it is important use multiple metrics and graphical methods to discern systematic biases.

The presence of oceanic-atmospheric teleconnections patterns can influence weather patterns in northern regions which may lead to an increase in climate related wildland fires. The impact of the Arctic Dipole (AD) anomaly, a northern atmospheric teleconnection, on NWT's surface climate has not been explored. Hence, the second objective of this dissertation used the ANUSPLIN dataset to assess the effects of the AD anomaly on local climate (air temperature, precipitation, and snowmelt) during a 66-year period (1950-2015). For all seasons, from 1950 to 2015, the occurrence of 64 strong positive and 56 strong negative AD modes were identified. The AD pattern revealed significant year-to-year fluctuation, with more frequent strong negative modes observed in the 2000s. In summer, when AD is in its strong negative mode, there is increased variance in the range of local air temperature, which is amplified in the southern, lake and foothill regions of the Taiga Plains. During strong positive AD modes, local air temperature anomalies increased ($>0.8^{\circ}\text{C}$) when compared to long-term mean temperature during summer months. Positive AD modes also lead to earlier commencement of snowmelt by an average of 3 to 5 days. The air temperature/snowmelt onset north-south amplification to the AD is linked to the position and intensity of the geopotential heights ridge axis over the continental NWT. A weak correlation was found between the AD and seasonal

precipitation despite high correlation association between the AD and local air temperature in summer.

Finally, the spatiotemporal patterns of incoming surface shortwave radiation (SSR) were analysed and quantified for the continental NWT to enhance understanding of northern ecosystems energy balance that are undergoing environmental changes. The third objective of this dissertation addressed this knowledge gap by assessing annual and seasonal trends in SSR receipt and to explore relationship between SSR and lake surface water temperature (LSWT) during the warm season. Consequently, the quantity of SSR that reaches Earth's surface may vary. In this study, it is observed that SSR trends display a significant temporal and spatial dependency on NWT's ecozones between 1980 and 2020. The annual mean SSR since 1980 decreased by $\sim 0.8 \text{ Wm}^{-2}\text{decade}^{-1}$ in the Taiga Plains and Northern Arctic ecozones, with mixture of increasing and decreasing trends in both Taiga Shield and Southern Arctic ecozones. Seasonally, SSR decreased significantly in the summer since 1980 over the majority of the Taiga Plains ecozone, with a reduction rate that ranged between 0.6 and $14.6 \text{ Wm}^{-2}\text{decade}^{-1}$. The LSWT in small lakes was positively associated with SSR, while the LSWT in medium and large lakes showed a mix of positive and negative correlation coefficients. The linkage between total cloud cover and SSR in the NWT was largely negative for spring, summer and autumn seasons, with the Taiga Plains ecozone displaying the largest negative correlation. Long-term changes in SSR in the NWT will have an impact on the seasonal and annual energy balance of the region's lakes. The impact of SSR changes on lake energy balances will have a wide range of consequences, particularly for NWT communities that rely on lakes for their transportation networks. These networks are already being adversely impacted by climate change-driven alterations in warming lake ice phenology.

The collective findings of this study demonstrate the feasibility of using gridded and remote sensing datasets to characterize historical changes in local and regional weather and climate, building an

understanding of northern climatology and providing best estimates of long-term trends with implications for ecosystem change in the future, such as increased rates of shrubification and frequency of wildland fires. In the absence of consistent *in situ* climate data, these gridded and remote sensing datasets aid our understanding of the physical links between climate change and northern ecosystems, which must be accounted for in forecast models used to predict future hydroclimate scenarios and to provide enhance climate services in northern regions. Improved understanding of how local and regional climate has changed in the NWT will inform policymakers in their efforts to develop and improve climate adaptation and mitigation policies in local communities across the territory.

Dedication

To Marie Boodram and family --who in challenging times readily shared their home and hearts that made the foundations of my post secondary education possible. I am forever grateful!

Acknowledgements

It is often said that “*it takes a village to raise a child*”. I also believe these words are applicable for me completing this PhD dissertation. This research would not have been possible without the divine blessings from Bhagavān Ganesha (God) and the support and cheering from a village consisting of many great people whom I was very fortunate to interact with along this PhD marathon.

I benefited from the guidance of my doctoral advisory committee who provided invaluable guidance throughout this marathon. I am thankful to Dr. William Quinton who sparked my interest in northern climatology and for introducing me to this PhD research. Thank you to my supervisors Dr. Brent Wolfe and Dr. Michael English whose thoughtful conversations, attention to details and valuable discussions and feedback helped propel me to this marathon’s finish line even after several detours and pauses. I would also like to thank Dr. Laura Chasmer, Dr. Homa Kheyrollah Pour and Dr. Paul Whitfield, for their mentorship at various stages of this PhD research. I appreciate all your interest, engagement, and insightful conversations throughout this marathon!

A special thank you to Dr. Mary-Louise Byrne, Dr. Margaret Walton-Roberts and Mr. Dilip Jaigopaul for offering kind words, and counsel when I was heading on a different route. I appreciate all of your wisdom and directions that led to this marathon completion! I am grateful for the support provided by Dr. Philippe Van Cappellen, Dr. Jimmy Lin and Dr. Fereidoun Reza Nezhad; they provided a flexible work environment and engaged me in interdisciplinary studies that provided transferable research skills that also aided this journey. I would also like to thank the staff of Wilfrid Laurier Writing Centre, especially Dr. Elliot Worsfold, for his guidance on editing strategies in academic writing. I enjoyed the camaraderie of numerous colleagues and peers from research groups across several universities; in particular, those who I met along this marathon path that willingly shared

many academic and non academic skills and experiences – especially Emily Haughton, Dr. Ryan Connon, Caren Ackley, Lindsay Stone, Dr. Geoff Kershaw, Nick Wilson, Ela Mastej, Stephanie Slowinski, Dr. Zahra Akbarzadeh, Dr. Christina Smeaton, Dr. Chris Parsons, Julie Grant, Ariel Lisogorsky, Gifty Attiah, Krysha Dukacz, Nancy Goucher and Dr. Juliane Mai.

Throughout this marathon, my family and friends have been an incredible source of encouragement. Huge thanks to my sister Rameka, my rakhi bhai Rajiv, my cousins Jaya, Ryan, Randy, and my pals, Geeta, and Petal for your love and many cheering up phone calls, messages, and impromptu visits to Canada, especially when I needed it the most during this marathon. Thank you to Annie, Garvin and Lyndon for providing entertaining chats that served as timely reminders of this marathon motivation. I am also grateful for the support from my friends in the Vista Hills community (Hajra, Jennifer, Lorelei, Milena, Sharon, Raneem, Thurka and Terrie) for putting extra effort to ensure that I can keep up with my children’s school and extracurricular activities, while simultaneously trying to get to this dissertation across the finish line. A special thank you to all my extended family (paternal, maternal, and in-laws) for always offering encouraging words and sending delicious treats, especially my aunt and uncle (Marla & Balwant), both of whom have been source of tremendous support in this journey.

I owe immense gratitude to my parents (Nandlall & Pramela Seulall) for choosing to spend most of their retirement in an atypical climate to provide endless grand(parenting) care and for their unwavering love and steadfast belief in my abilities always. My heartfelt appreciation to my beloved husband Heemant and my wonderful children (Neelam & Ajay) for their infinite love, sacrifices, and tolerance throughout this marathon. My amazing husband spared no effort to provide the best possible home environment for me to pursue this research and has been a steady source of optimism and calming voice of reasoning during this journey!

Declaration of Co-authorship/Previous Publications

I hereby declare that I am the main author of this dissertation and all research within this dissertation the product of my own work. I developed the conceptual ideas under the guidance of my doctoral advisory committee, carried out the analyses, and prepared the manuscripts. This dissertation is also the result of collaborative work with the coauthors listed on each publication. Chapters 2, 3, and 4 represent the main body of this dissertation and contain content that has been published (Chapters 2 & Chapter 3) or will be submitted to a journal to be considered for publication (Chapter 4).

Chapter 2:

Coauthors, Dr. Paul Whitfield and Dr. William Quinton, contributed to the refinement of the conceptual ideas, reviewed and edited the chapter, while a coauthor, Lindsay Stone, applied the Cold Regions Hydrological Model over Scotty Creek and provided the output hydrological data so that a comparative analysis could be conducted to test the sensitivity of the model to various input data.

Chapter 3:

All coauthors (Drs. Michael English, Brent Wolfe, Laura Chasmer and William Quinton) assisted with refinement of conceptual ideas, reviewed, and edited this chapter.

Chapter 4:

Gifty Attiah provided the lake surface water temperature data and downloaded ERA5 cloud data while Drs. Michael English, Brent Wolfe, Laura Chasmer and Homa Kheyrollah Pour assisted with refinement of conceptual ideas, reviewed, and edited this chapter.

Statement of Originality

I hereby declare that the work presented in this dissertation is the result of my own analysis. This work has not been submitted in whole, or in part, for recognition at Wilfrid Laurier University or any other University. All ideas presented in this paper are either original or have been properly cited and attributed.

Table of Contents

Abstract	ii
Dedication	vi
Acknowledgements	vii
Declaration of Co-authorship/Previous Publications	ix
Statement of Originality	x
Table of Contents	xi
List of Tables.....	xiv
List of Figures	xv
1 General Introduction	1
1.1 Climatology of the Northwest Territories	1
1.2 Vulnerability of the Northwest Territories to climate change.....	3
1.3 Northern hydroclimate research data challenges and opportunities.....	6
1.4 Research objective.....	10
1.5 Dissertation structure.....	11
1.6 References	13
2 Evaluating the suitability of three gridded datasets and their impacts on hydrological simulation at Scotty Creek in the southern Northwest Territories, Canada.....	22
2.1 Abstract.....	23
2.2 Introduction	24
2.3 Study Area	27
2.4 Data and Methods.....	28
2.4.1 Data and datasets.....	28
2.4.2 Statistical evaluation	31
2.4.3 Sensitivity analysis using Cold Regions Hydrological Model.....	33
2.5 Results	34
2.5.1 Population statistics comparison.....	34
2.5.2 Temporal structure	41
2.5.3 Hydrological sensitivity to differences in gridded datasets	46
2.6 Discussion.....	49
2.7 Conclusions	56

2.8	Acknowledgements	58
2.9	Data Availability Statement.....	58
2.10	References	59
3	Sensitivity of seasonal air temperature and precipitation, and onset of snowmelt, to Arctic dipole modes across the Taiga Plains, Northwest Territories, Canada	71
3.1	Abstract.....	72
3.2	Introduction	73
3.3	Data and Methods.....	77
3.3.1	Study Area.....	77
3.3.2	Arctic Dipole index	80
3.3.3	Climate data.....	81
3.3.4	Statistical Analysis	83
3.4	Results	84
3.4.1	Temporal distribution of the seasonal Arctic Dipole index	84
3.4.2	Geopotential height patterns during periods of strong negative and positive AD mode	86
3.4.3	Positive and negative modes of the AD index and air temperature	87
3.4.4	Positive and negative modes of the AD index and precipitation amount	90
3.4.5	Positive and negative modes of the AD index and onset of snowmelt	93
3.5	Discussion.....	94
3.5.1	Mechanistic interactions between the AD and climate in the Taiga Plains	95
3.5.2	Implications of AD and surface climate variability on terrestrial ecosystem in the Taiga Plains.....	97
3.5.3	Recommendations for future study	100
3.6	Conclusion.....	101
3.7	Acknowledgements	103
3.8	Data availability statement	103
3.9	References	104
4	Trend analysis of surface shortwave radiation across continental Northwest Territories, Canada (1980-2020).....	118
4.1	Abstract.....	119
4.2	Introduction	121

4.3	Study Area	125
4.4	Data and Methods.....	126
4.4.1	Databases.....	126
4.4.2	Statistical Analysis	130
4.5	Results	131
4.5.1	Characterizing trends in annual and seasonal mean SSR in the NWT.....	131
4.5.2	Correlation between total cloud cover and SSR.....	135
4.5.3	Correlation between SSR and lake surface water temperature in North Slave Region	138
4.6	Discussion.....	142
4.6.1	Causes of observed changes in SSR trends.....	142
4.6.2	Response of LSWT to SSR changes	144
4.6.3	Implications of warming lakes for northern communities and ecosystems	145
4.6.4	Use of gridded and remote sensing data, potential limitations, and opportunities.....	147
	Conclusion.....	149
4.7	Acknowledgements	152
4.8	Data availability statement	152
4.9	References	153
5	General conclusion and recommendations	168
5.1	Summary of major findings.....	169
5.1.1	Chapter 2	169
5.1.2	Chapter 3	170
5.1.3	Chapter 4	171
5.2	Future research recommendations.....	172
5.2.1	Applications of interpolated, reanalysis and remote sensing data	172
5.2.2	Atmospheric-oceanic teleconnections and predictions	173
5.2.3	Radiation budget and LSWT.....	174
5.3	References	176
	Appendices	181
	Supplemental information for Chapter 2.....	181
	Supplemental information for Chapter 4.....	185

List of Tables

Table 2.1 Summary of the characteristics of the three gridded datasets over study domain.	30
Table 2.2 Kolmogorov-Smirnov test to assess the distributional similarity between the observations and gridded datasets. For values ≤ 0.05 , underlined, the null hypothesis is rejected, i.e., observations and gridded datasets do not represent the same continuous distribution.	36
Table 2.3 Berusch-Pagan test to assess for homoscedasticity of residuals of the regression of gridded against observations at Fort Simpson. For values ≤ 0.05 , underlined, the null hypothesis is rejected, i.e., observations and gridded residuals are not homoscedastic.	44
Table 3.1 p-values the Kruskal–Wallis test for AD events exceeding the ± 0.5 AD index thresholds were examined to quantify whether the mean climate variables anomalies (air temperature, precipitation, and onset date of sustained snowmelt) were significantly different during these positive and negative AD modes For p values ≤ 0.05 (bold and underlined) the null hypothesis is rejected (i.e., there is no change in the mean of climate variables anomaly (air temperature, precipitation and onset date of sustained snowmelt) during the positive and negative AD modes.....	89

List of Figures

Figure 1.1 Examples of air temperature and precipitation long-term average variation for selected towns for the period 1981 to 2010 for a) Inuvik, b) Normal Wells, c) Yellowknife and d) Fort Simpson. Total mean precipitation is represented as bars, while lines on graphs represent air temperature. (Source: ECCCC, 2022)	2
Figure 1.2 a) Location of the 1735 surface weather and climate monitoring stations in Canada and b) temporal evolution of the monitoring stations in Canada and its peak and subsequent decline of the monitoring network in Canada from 1990s. (Source: From Figures 1 and 2 in Mekis et al., 2018) ...	8
Figure 2.1 Topography of the southern NWT showing the location of the seven climate stations (black dots) and Scotty Creek Research Watershed (white dot) and of the study area in Canada	28
Figure 2.2 Statistical properties of gridded data against observations. Daily maximum temperature (a, d, g, j), daily minimum temperature (b, e, h, k) and daily precipitation (c, f, i, l); mean (central tendency), standard deviation (spread), skewness (symmetry) and kurtosis (peakedness) of the eight stations for observations, ANUSPLIN, ERA-Interim, and MERRA-2.....	35
Figure 2.3 a) Daily maximum temperature and (b) daily minimum duration curves for observations, ANUSPLIN, ERA-Interim, and MERRA-2 for Fort Simpson, NWT, from 1980 to 2013.	38
Figure 2.4 Example for Fort Simpson demonstrating the relationship of (a-c) observed maximum and (d-f) observed temperatures against the gridded data for ANUSPLIN (a & d), ERA-Interim (b & e), and MERRA-2 (c & f) from 1980 to 2013. In each case, the dashed line is the regression line of the gridded data to the observations, and the black line is the 1:1 line; also presented are the mean error (ME), mean absolute error (MAE), root mean square error (RSME), Nash-Sutcliffe model efficiency (NSE), and Wang-Bovick statistic (WB). The total number of observations N is $12000 < N \leq 12410$ between 1980 and 2013.....	39
Figure 2.5 Daily observed precipitation against the daily gridded data at Fort Simpson, (a) ANUSPLIN, (b) ERA-interim and (c) MERRA-2. Dashed line is the regression line of the gridded data to the observations, and the black line is the 1:1 line; also presented are the mean error (ME), mean absolute error (MAE), root mean square error (RSME), Nash-Sutcliffe model efficiency (NSE),	

and Wang-Bovic statistic (WB). The total number of observations N is $12000 < N \leq 12410$ between 1980 and 2013.40

Figure 2.6 The ratio of the relative frequency ANUSPLIN/OBSERVED, ERA/OBSERVED, and MERRA-2/OBSERVED daily precipitation. The dashed line at 1.0 indicates the count per intensity category that would be expected if the gridded data were equal to the observed data.41

Figure 2.7 a) Example of monthly averaged daily mean absolute error between gridded and observed temperatures for ANUSPLIN, ERA-Interim and MERRA-2 at Fort Simpson, NWT. Maximum temperature (solid lines) and minimum (dashed lines), b) Example of monthly averaged mean absolute error between gridded and observed precipitation.43

Figure 2.8 a) Deviation onset date of melt from long term average for Fort Simpson computed as the first day on which mean daily air temperature was above 0°C, following the last five-day period between March and April, when the daily mean air temperature was below 0°C; and b) deviation of onset date of freezing from long term average observed onset date. The onset date of freezing was defined as the first day on which mean daily air temperature was below 0°C following the last five-day period between October and November when daily mean air temperature was above 0°C.46

Figure 2.9 Comparing daily simulated runoff forced by observations against forces by gridded data. Dashed line is the regression line of the gridded data to the observations, and the black line is the 1:1 line; also presented are the mean error (ME), mean absolute error (MAE), root mean square error (RSME), Nash-Sutcliffe model efficiency (NSE), and Wang-Bovic statistic (WB). The total number of observations is 1825.47

Figure 2.10 Daily simulated runoff using Cold Region Hydrological Model (CRHM) for a 0.45 km² drainage area at Scotty Creek for 2011 when driven by temperature and precipitation input from observations, and ANUSPLIN, ERA-Interim and MERRA-2 datasets. Inset: Flow duration curves for runoff (on a log scale) simulated using CRHM driven by four different input forcing datasets (temperature and precipitation): observations and three different gridded datasets.49

Figure 3.1 Locations of the study domain (inset map) and study sites (black stars) within the four regions.78

Figure 3.2 Example multi-year composite sea level pressure (SLP) anomaly patterns, that is SLP deviation from long term averages, in Summer (June-July-Aug) during a) the strong negative AD mode from 2007 to 2012 and b) the strong positive AD mode from 1988 to 1991. Data are from the NCEP–NCAR Reanalysis through the NOAA/Earth Systems Research Laboratory (NOAA, 2020).81

Figure 3.3 Standardized AD for a) winter, b) spring, c) summer and d) autumn. Grey bars are negative AD anomalies and black bars are positive AD anomalies. Indices exceeding ± 0.5 threshold (dashed lines) are defined as strong \pm AD modes. The blue boxes highlight areas mentioned in the text.85

Figure 3.4 Summer multi-year composite during a period strong negative AD modes 2007 to 2012 for the a) 700 hPa geopotential height mean and b) 700 hPa geopotential height anomaly and during a strong positive AD mode (1988 to 1991) c) mean 700 hPa geopotential height and d) 700 hPa geopotential height anomaly. Data and plotting tool used for data are from the NCEP–NCAR Reanalysis through the NOAA/Earth Systems Research Laboratory (NOAA, 2020). Solid red lines on figures represent the ridge axis.....87

Figure 3.5 Boxplots showing the distribution of winter, spring, summer and autumn AD modes exceeding the ± 0.5 threshold and its corresponding mean temperature anomaly. Anomalies are departures from 1950 to 2015 seasonal mean air temperatures. Black boxes represent positive AD mode while grey boxes represent negative AD mode, while black dots represent outliers.....90

Figure 3.6 Boxplots displaying precipitation anomalies during positive (black boxes) and negative (grey boxes) modes of the AD index in winter, spring, summer, and fall. Anomalies are departures from 1950 to 2015 seasonal total precipitation. A positive anomaly indicates the observed precipitation was greater than the long-term total average while a negative anomaly indicates the observed precipitation was less than the long-term average. Black dots represent outliers.92

Figure 3.7 Deviation in the timing of snowmelt (in days) from the mean date of snowmelt during spring AD modes exceeding an index threshold of ± 0.5 . Black boxes represent positive AD mode and grey boxes represent negative AD mode. Black dots represent outliers. Positive anomaly on y axis = later snowmelt; negative anomaly on y axis= earlier snowmelt.93

Figure 4.1 Map shows the study area with the SSR, and cloud cover data grid points (black dots) extracted from Daymet and ERA5 databases, respectively. Different colours in the map indicate ecozones of the Northwest Territories. Three independent weather stations are shown in red & black circles and the location of selected lakes within the North Slave region are shown with the blue shapefiles. 126

Figure 4.2 Spatial distribution of mean annual SSR trends magnitudes across the NWT for the following periods: a) 1980 to 2020, b) 1980-2000, and c) 2001-2020. Cross denotes the long-term trends at grids are significant at $p \leq 0.05$. The values are estimated for each grid and rate of change in colour bar is expressed as $W m^{-2} decade^{-1}$ 132

Figure 4.3 Distribution of mean shortwave radiation trend for a) Spring, b) Summer and c) Autumn from 1980 to 2020 across continental NWT. Cross denotes the long-term trends at grids are significant at $p \leq 0.05$. The values are estimated for each grid and rate of change on colour bar is expressed as $W m^{-2} decade^{-1}$ 134

Figure 4.4 Annual normalized total cloud cover (blue) and Daymet shortwave radiation estimates (red) for Inuvik, Yellowknife and Fort Simpson during summer seasons. The zero line is the 1980-2020 long term average. 136

Figure 4.5 Scatter plot showing relationship between mean total cloud cover and shortwave radiation in summer for three locations in the NWT. 137

Figure 4.6 Correlation Coefficient R between total cloud cover and shortwave radiation over NWT from 1980 to 2020 during a) Spring b) Summer and c) Autumn. Cross denotes the correlation coefficient at grids are significant at $p \leq 0.05$ 138

Figure 4.7 Trend analysis in a) shortwave radiation, b) lake surface water temperature estimates annual summer from 1984 to 2020 for North Slave Region. Solid red or blue triangle indicate trends are significant at $p \leq 0.05$ 139

Figure 4.8 a) Spatial distribution of the correlation coefficient across the North Slave Region during summer (June, July, August) for 1984-2020. Blue circles represent a negative correlation between LSWT compared with SSR, while red circles represent a positive correlation. b) Correlation

coefficient between SSR and LSWT during summer months for lakes in the North Slave Region for the period of 1984-2020. Lakes $<1 \text{ km}^2$ area are considered small (n=64), while lakes between 1 km^2 and 100 km^2 are medium (n=464) and lakes greater than $>100 \text{ km}^2$ are large (n=12). Asterisks indicate that differences in correlations value among lake sizes are significant at $p \leq 0.05$141

1 General Introduction

1.1 Climatology of the Northwest Territories

The continental Northwest Territories (NWT), located between 60° and 70°N, spans several ecozones and covers over 1.0 million km² (GWNT, 2018). The majority of this territory is underlain by permafrost of varying thickness dominated by many lakes, glaciers, rivers, forests, and various types of wetlands such as swamps, bogs, and fens, which are affected by climate (Prowse & Ommanney, 1990; Bailey et al., 1997). The NWT climate varies temporally, locally and regionally, but is typically characterized by long cold winters and short cool summers (Phillips, 1990). Mean daily January air temperatures typically range from -17°C to -29°C, while mean daily July air temperatures range from about 7°C to 17°C (see Figure 1.1) (ECCC, 2022). Large diurnal temperature variability is not uncommon (Serreze & Barry, 2014). Annual shortwave radiation typically ranges between 100 and 250 Wm⁻² (Bailey et al., 1997). Incoming solar shortwave radiation also arrives at relatively low angles, limiting energy reaching the ground surface during winter, although this effect is offset during long summer days (Phillips, 1990; Bailey et al., 1997). Snow and ice have high albedos, reflecting large amounts of incoming shortwave radiation (Serreze & Barry, 2011). Annual precipitation is low (200–400 mm), with the highest amounts received in the Boreal Cordillera, Taiga Cordillera, southern Taiga Plain, and Taiga Shield ecozones. There is also a general decrease in precipitation with increasing latitude (Phillips, 1990; Bailey et al., 1997) and precipitation mainly falls as snow from November through March and rain from April to October (Phillips, 1990) peaking during the summer months (see Figure 1.1).

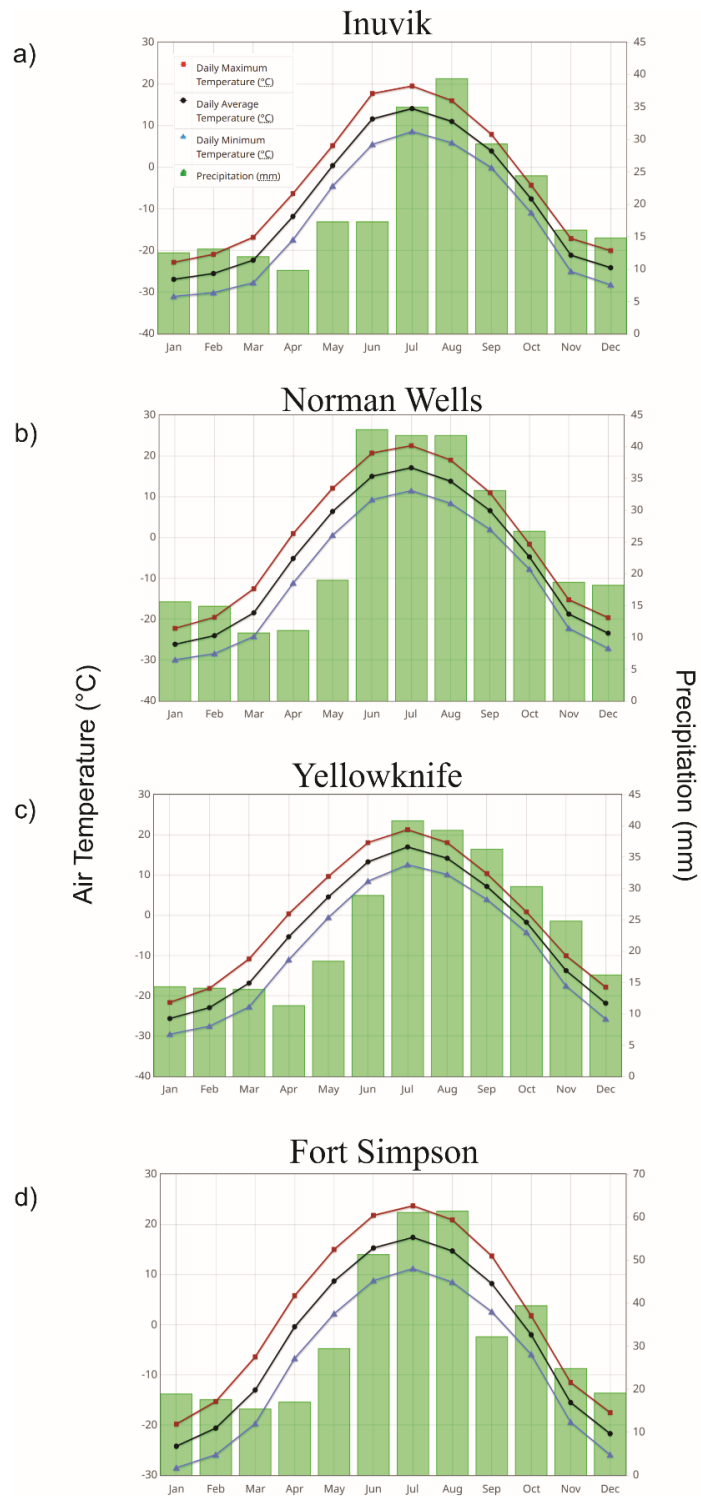


Figure 1.1 Examples of air temperature and precipitation long-term average variation for selected towns for the period 1981 to 2010 for a) Inuvik, b) Norman Wells, c) Yellowknife and d) Fort Simpson. Total mean precipitation is represented as bars, while lines on graphs represent air temperature. (Source: ECCC, 2022)

The climate of the NWT is dependent upon several conditions. These include: i) latitude, and its influence on solar radiation received; ii) air mass influences; iii) location of high and low atmospheric pressure systems; iv) proximity to oceans, lakes and rivers; v) location of mountain barriers; vi) prevailing global wind patterns; and vii) elevation (Phillips, 1990; Bailey et al., 1997). The Mackenzie River basin is an important source region for anticyclones and thus plays a significant role in mixing cold dry Arctic air masses with warm moist air masses from the south (Phillips, 1990; Lackmann & Gyakum, 1996; Szeto 2008; Szeto et al., 2008). These interactions generate a complex climate and add uncertainty to weather and climate predictions over the NWT (Woo & Thorne, 2008).

1.2 Vulnerability of the Northwest Territories to climate change

The high latitude regions of Canada are responding to climate warming at unprecedented, disproportionate rates (Zhang et al., 2000; Vincent et al., 2015; Bush & Lemmen, 2019; Arias et al., 2021). Vincent et al. (2015) reported that surface air temperature from 1948 to 2012 in NWT increased by 4.0°C to 6.0°C in winter and by 1.5°C to 2.0°C in summer. The southern and northern NWT surface air temperatures have also increased by at least two and four times, respectively, when compared with the rate of increase for the rest of Canada (GNWT, 2018). According to the Coupled Model Intercomparison Project version 5 (CMIP5) multi-model ensemble, under the business as usual emission scenario (RCP8.5), average surface air temperature for all seasons is expected to rise from 4.5 °C to 12.5°C by end of 2100 in the NWT (Bush & Lemmen, 2019; Li & Li, 2021). Some of the largest rate of change will continue to occur in winter (Bush & Lemmen, 2019; Li & Li, 2021).

Trend analysis from 1945 to 2012 indicates significant increases in total annual precipitation by 10% to 50% for the majority of NWT locations (Vincent et al., 2015). Although distinctive regional precipitation trends are less easily discerned than regional temperature, statistically significant increasing trends in precipitation appear to be more predominant in the Taiga Plains and Southern Arctic ecozones compared with the rest of the continental NWT (Whitfield et al., 2004; Vincent et al., 2015; Bush & Lemmen, 2019). Under the CMIP 5 RCP 8.5 ensemble scenario, the NWT annual mean precipitation is anticipated to increase by approximately 20 to 50% by the end of 2080s (Bush & Lemmen, 2019). These projected changes are also consistent with climate model projections for future changes in global high latitude air temperature and precipitation (Arias et al., 2021).

The scale and rapidity of observed warming-induced changes in the NWT and other high latitude areas have been attributed to number of processes including increasing global greenhouse emissions, aerosol changes, sea ice feedback, and snow-albedo feedback (Bush & Lemmen, 2019; IPCC, 2021). Others have also highlighted that changes in surface air temperature and precipitation are also driven by atmospheric-oceanic circulation patterns (Déry et al., 2009; Vincent et al., 2015). These include northern atmospheric–oceanic circulations such as the Arctic Oscillation (AO) and Arctic Dipole (AD) anomaly (Thompson & Wallace, 1998; Wang et al., 2009). For example, the negative AO has led to southward expansion of the Arctic blocking high pressure system that has led to enhanced temperature variability and warming in Alaska and the Northwest Territories (Thompson & Wallace, 1998; NOAA, 2009). In contrast to the AO, the AD impacts on surface air temperature and precipitation are yet to be explored over the NWT. Thus, it would be appropriate to analyse the relationships between large-scale modes of atmospheric-oceanic circulation and

hydroclimatic variables at shorter time scales as they are poorly understood in climatology and can behave differently from year to year. Hence, improved knowledge of the interaction between various northern atmospheric-oceanic circulation patterns and surface climate variables will help strengthen our understanding of the existing pattern of climate change and the frequency and intensity of climate events. Quantifying the long-term trends of essential surface climate variables and the mechanisms that maybe responsible for these trends will aid in refining weather and climate-related predictions across the globe including the NWT (Doblas-Reyes et al., 2013; Bojinski et al., 2014).

The implications of the current and projected climate warming extend beyond the scope of meteorological variability (Bates et al., 2008). This implication is especially true for the NWT where the consequences of climate change have lead to many rapid ecosystem and landscape changes since mid-1990s to early 2000s (Rouse, et al., 1997; Kokelj et al., 2007; Chasmer & Hopkinson, 2017; GNWT, 2018). For example, permafrost degradation has led to the conversion of forests to wetlands (Quinton et al., 2011) and tundra forest to shrub vegetation, all of which have been exacerbated since 2000s (Chapin et al, 2005; Wilcox et al., 2019). Moreover, permafrost degradation has a direct impact on the NWT infrastructure such as roads, industrial and residential buildings, bridges, and pipelines, which is estimated to cost Canadians at least an additional \$51 million annually to repair (Hjort et al., 2022). Climate warming has also affected the hydrology in NWT through a variety of mechanisms, including changing the distribution and routing of water over the NWT particularly over the Taiga Plains wetland areas (Connon et al., 2015; GNWT, 2018). Altered flow pathways and changing water quality regimes have affected the function of streams, rivers, and lakes, including main waterways used for potable water supply, hydropower

and transportation (GNWT, 2018). Warming may also lead to greater lake productivity because of longer growing seasons and more favourable conditions for growth (van de Poll, 2021). These climate related changes also directly threaten the health, wellbeing, safety and livelihoods of NWT communities (GNWT, 2018).

Despite the heightened interest in climate warming and its impacts in the NWT, there are many northern communities where weather and climate patterns are still not sufficiently monitored as they do not have weather stations (CARI, 2008; GNWT, 2018). Understanding the linkages between past and present seasonal patterns of northern climate and hydrological processes at local and regional scales assists greatly with projecting possible changes to these systems (Debeer et al., 2021; GNWT, 2018). While the focus on long-term trends has been placed primarily on surface air temperature and precipitation (Bush & Lemmen, 2019), there remains limited information on the characteristics of other important climate variables, such as surface shortwave radiation, and linkages of air temperature and precipitation with northern atmospheric-oceanic teleconnection patterns across the NWT. Thus, as the climate warms there is a gap between understanding changes in large scale atmospheric teleconnection phases and impacts on temperature and precipitation at local and regional scales that need to be addressed over the NWT.

1.3 Northern hydroclimate research data challenges and opportunities

In general, the knowledge gaps in long-term surface hydroclimatology research for northern regions partially originate from limited *in situ* climate observations and restricted access to existing data held by other scholars and institutions (CARI, 2008; Viglione et al., 2010; Beniston et al., 2012). It may also take many months or years before some *in situ* data are made publicly available (GNWT, 2018). There are various institutions and research groups that are operating climate

stations in NWT including Environment and Climate Change Canada (ECCC). However, it is noted that there is non-uniform and inadequate distribution of the existing climate stations in northern Canada, having only selected observed climate elements and sparse data records both spatially and temporally (Figure 1.2a) (Prowse & Ommanney 1990; Mekis et al., 2018; GNWT, 2018). Additionally, Mekis et al. (2018) reported several types of hydroclimate variables collected by ECCC, but the summary inventory presented as of September 2016, emphasizes air temperature, precipitation, and other essential climate elements (see Table 1 in Mekis et al., 2018 for additional details). However, it is not clear if incoming surface shortwave radiation (SSR) data for locations shown in Figure 1.2a are still collected and curated for long-term preservation by ECCC. Consequently, SSR data are more challenging to obtain than surface air temperatures and precipitation. Nonetheless, historical trends and implications in SSR regimes for Canada have been studied for earlier temporal periods but these existing studies are restricted to certain geographic regions that did not include the continental NWT (Weston et al., 2007; Cutforth & Judiesch, 2007). Climate stations are also often located near populated areas, and therefore may not adequately capture synoptic climate characteristics of more-remote locations (e.g., small lakes or high altitude and latitude areas; Beniston et al., 2012). Moreover, changing government policies and limited access to government funding or long-term dedicated funding may result in further reduction of monitoring stations (Figure 1.2b; Shiklomanov, Lammers & Vörösmarty, 2002; Mlynowski et al., 2011; Orihel, Swanson & Venkiteswaran, 2014; Lavoie, 2017).

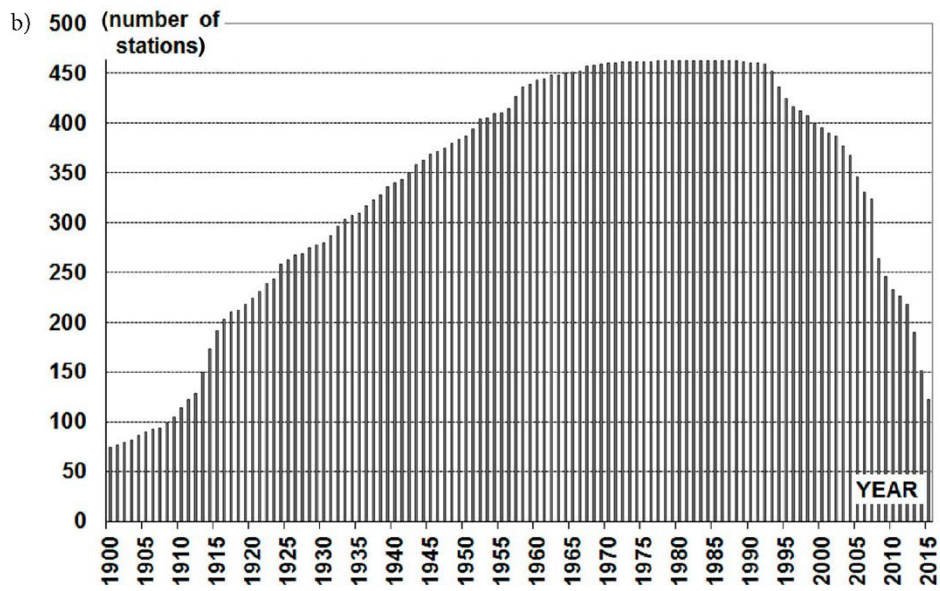
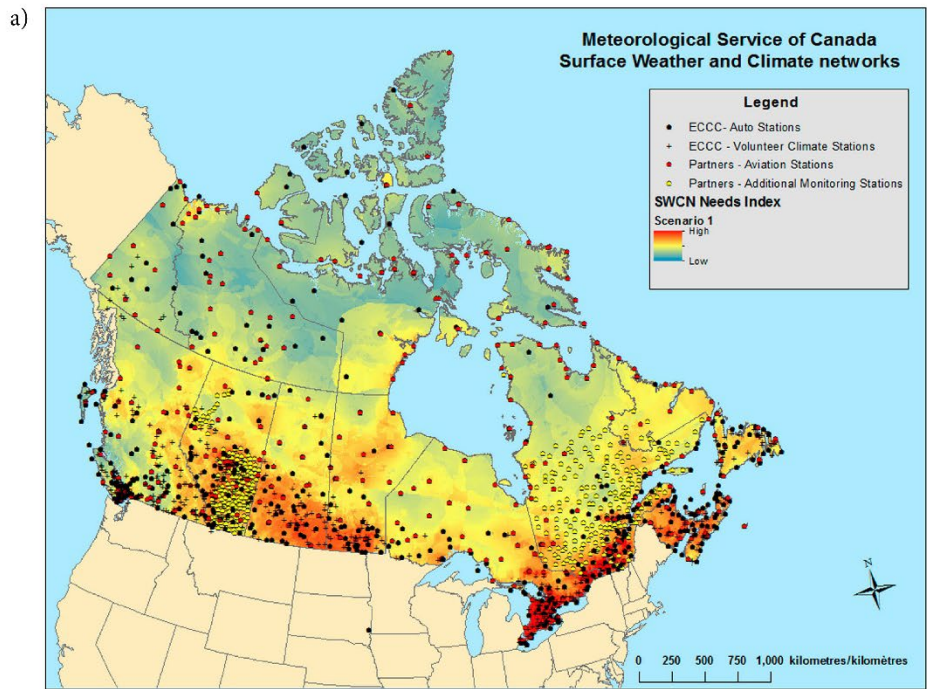


Figure 1.2 a) Location of the 1735 surface weather and climate monitoring stations in Canada and b) temporal evolution of the monitoring stations in Canada and its peak and subsequent decline of the monitoring network in Canada from 1990s. (Source: From Figures 1 and 2 in Mekis et al., 2018)

In situ climate measurement in the NWT can also be challenging as monitoring stations are costly to purchase, install and operate, and may be poorly situated or relatively inaccessible in remote areas (Prowse & Ommanney, 1990; GNWT, 2018). In addition, problems may arise due to harsh climate conditions, mechanical failures, and interference by wildlife, creating large data gaps when monitoring stations go months without servicing (Prowse & Ommanney 1990). The uncertainty regarding observed climate in the northern regions is further increased by measurement biases, such as in solid precipitation, which can be underestimated by at least 50% due to wind at the time of observation (Goodison et al., 1998; Smith et al., 2019). Thus, the lack of reliable data is a major constraint for studying long-term climate change in high latitudes, and new approaches are needed to identify and diagnose these changes.

Proxy, remote sensing, and gridded meteorological modelled data products offer an alternative for assessing northern hydroclimatological change with large spatial and continuous temporal coverage (Dee et al., 2011; Li et al., 2020). While some alternative data are interpolated from *in situ* measurements over grids, others use various assimilation techniques that amalgamate data from many observation sources (*in situ* meteorological stations, upper air stations, ships, weather radars, and satellite products) with numerical weather simulations to provide the best estimates that are representative of *in situ* data (Hutchinson et al., 2009; Rienecker et al., 2011; Dee et al., 2011). Much of this gridded data are also available to the academic community at no cost. These datasets have led to improved process-based understanding and have allowed for plausible assessments of current and future climatic change at local, regional and global scales (e.g., Zhang et al., 2000; Derksen, et al., 2008; Murfitt & Brown 2017; Lilhare et al., 2019; Li & Li, 2021; Arias et al., 2021). These gridded data are available to fill gaps in weather and climate research across

the NWT and are increasingly being improved in their resolution and physical representation of local and regional weather and climate conditions. However, due to the limited number of weather stations in the NWT, gridded air temperature, precipitation, and incoming shortwave radiation along with spatial inputs from satellite data and general circulation models are important for understanding how the climate is changing in northern environments. This requires validation of gridded datasets at local scales using available weather station and alternative data sources and proxy-indicators. Also, once gridded data have been validated, both long-term trends in these climate variables and weather changes associated with shorter-term atmospheric teleconnection patterns such as the Arctic Dipole atmospheric circulation need to be examined as they have received considerably less attention in the NWT when compared to other regions in Canada and across the globe.

1.4 Research objective

The primary objective of this dissertation is to improve the understanding of historical climate variables trends and patterns across the continental NWT and its implications at local and regional scales. This is accomplished by using gridded climate data and focusing on air temperature, precipitation, and shortwave radiation to answer the following questions:

1. Can gridded datasets (interpolated and reanalyzed) be used as reliable alternative sources for *in situ* observations in climate and hydrological applications in the NWT subarctic?
2. Are continental NWT seasonal surface climate variables (air temperature, precipitation & snowmelt onset) sensitive to concurrent strong Arctic Dipole atmospheric circulation modes?

3. Are there systematic trends of SSR during the past 40 years (1980-2020) across the continental NWT, and are they consistent over spatial and temporal scales? and ii) Do SSR changes drive changes in lake surface water temperature during the warm season?

The continental NWT is the primary focus for this dissertation because this territory is among the most rapidly warming regions in Canada, resulting in a series of environmental consequences (GNWT, 2018). It is envisioned that an assessment of the NWT climate primarily using gridded datasets can provide a baseline and serve as a prototype for similar studies in data-sparse regions.

1.5 Dissertation structure

This dissertation is in manuscript form. Following the general introduction in Chapter 1 are three core data chapters, each of which is presented as an individual manuscript that has been published or will be submitted for publication. To answer research question 1, Chapter 2 evaluates whether gridded datasets are reliable alternatives that can be used in NWT climate research. Chapter 3 and Chapter 4 apply two high spatial resolution gridded datasets to answer research questions 2 and 3 outlined in the preceding section.

The first manuscript (Chapter 2), titled “*Evaluating the suitability of three gridded datasets and their impacts on hydrological simulation at Scotty Creek in the southern Northwest Territories, Canada*” has been published in Hydrological Processes. This chapter compares the atmospheric interpolated/reanalysis data and *in situ* climate data from 1980 to 2013 and elucidates that in the absence of long term *in-situ* data in data sparse regions such as the NWT, gridded data can provide reasonable estimates that can be used as surrogate observations. Results highlight that the higher the spatial resolution of a dataset, the closer it will accurately represent *in situ* climate observations for the NWT. Chapter 3, the second manuscript, entitled “*Sensitivity of seasonal air temperature*

and precipitation, and onset of snowmelt to Arctic Dipole modes across the Taiga Plains, Northwest Territories, Canada” was published in the International Journal of Climatology. This chapter explores the linkages between NWT surface climate variables and their association with strong AD modes. A topic poorly understood in the literature is how AD anomaly circulation historically influenced the surface climate variability in the NWT. The third manuscript (Chapter 4) titled “*Trend analysis of surface shortwave radiation in continental Northwest Territories, Canada (1980-2020)*” focuses on whether there are systematic changes in trends of SSR across the continental NWT and quantifies the sensitivity of SSR received to cloud cover and its influence on lake surface water temperatures. Finally, Chapter 5 summarises key findings drawn from the various analyses presented in the preceding chapters and suggests research recommendations for the future.

1.6 References

- Arias, P.A., N. Bellouin, E. Coppola, R.G. Jones, G. Krinner, J. Marotzke, . . . , & K. Zickfeld, 2021: Technical Summary. In *Climate Change 2021: The Physical Science Basis. Contribution of Working Group I to the Sixth Assessment Report of the Intergovernmental Panel on Climate Change* [Masson-Delmotte, V., P. Zhai, A. Pirani, S.L. Connors, C. Péan, S. Berger, N. Caud, Y. Chen, L. Goldfarb, M.I. Gomis, M. Huang, K. Leitzell, E. Lonnoy, J.B.R. Matthews, T.K. Maycock, T. Waterfield, O. Yelekçi, R. Yu, and B. Zhou (eds.)]. Cambridge University Press, Cambridge, United Kingdom and New York, NY, USA, pp. 33–144. doi:10.1017/9781009157896.002.
- Bailey, W. G., Oke, T. R., & Rouse, W. R. (1997). *The surface climates of Canada*. Montreal: McGill-Queen's University Press.
- Bates, B., Kundzewicz, Z., Wu, S. & Palutikof, J.P eds. (2008). *Climate Change and Water. Technical Paper of the Intergovernmental Panel on Climate Change, IPCC Secretariat, Geneva, 210 pp.* <https://archive.ipcc.ch/pdf/technical-papers/climate-change-water-en.pdf>.
- Beniston, M., Stoffel, M., Harding, R., Kernan, M., Ludwig, R., Moors, E., . . . Tockner, K. (2012). Obstacles to data access for research related to climate and water: Implications for science and EU policy-making. *Environmental Science & Policy*, 17, 41-48. doi: <https://doi.org/10.1016/j.envsci.2011.12.002>.
- Bojinski, S., Verstraete, M., Peterson, T. C., Richter, C., Simmons, A., & Zemp, M. (2014). The concept of essential climate variables in support of climate research, applications, and

- policy. *Bulletin of the American Meteorological Society*, 95(9), 1431-1443. doi
<https://doi.org/10.1175/BAMS-D-13-00047.1>
- Bush, E. & Lemmen, D.S., eds. (2019). *Canada's Changing Climate Report* Government of
Canada, Ottawa, ON. 444 p. <https://changingclimate.ca/CCCR2019/>.
- Chapin, F. S., Sturm, M., Berginger, J., Chapman, W. L., Epstein, H. E., Euskirchen, E. S., . . .
Schimel, J. P. (2005). Role of land-surface changes in arctic summer warming
Science, 310(5748), 657-660. doi:10.1126/science.1117368.
- Chasmer, L., & Hopkinson, C. (2017). Threshold loss of discontinuous permafrost and landscape
evolution. *Global Change Biology*. 23(7), 2672-2686. doi:10.1111/gcb.13537.
- Connon, R. F., Quinton, W. L., Craig, J. R., Hanisch, J., & Sonnentag, O. (2015). The hydrology
of interconnected bog complexes in discontinuous permafrost terrains. *Hydrological
Processes*, 29 (18), 3831-3847. doi: <https://doi.org/10.1002/hyp.10604>.
- Cutforth, H. W., & Judiesch, D. (2007). Long-term changes to incoming solar energy on the
Canadian Prairie. *Agricultural and Forest Meteorology*, 145(3), 167-175. doi:
<https://doi.org/10.1016/j.agrformet.2007.04.011>.
- Dee, D. P., Uppala, S. M., Simmons, A. J., Berrisford, P., Poli, P., Kobayashi, S., . . . Vitart, F.
(2011). The ERA-interim reanalysis: Configuration and performance of the data
assimilation system. *Quarterly Journal of the Royal Meteorological Society*, 137(656), 553-
597. doi: <https://doi.org/10.1002/qj.828>.

- Derksen, C., Brown, R., & MacKay, M. (2008). Mackenzie Basin Snow Cover: Variability and Trends from Conventional Data, Satellite Remote Sensing, and Canadian Regional Climate Model Simulations. In: Woo, M. (eds) Cold Region Atmospheric and Hydrologic Studies. The Mackenzie GEWEX Experience. Springer, Berlin, Heidelberg. doi: https://doi.org/10.1007/978-3-540-73936-4_13.
- Déry, S. J., Hernández-Henríquez, M. A., Burford, J. E., & Wood, E. F. (2009). Observational evidence of an intensifying hydrological cycle in northern Canada. *Geophysical Research Letters* 36(13), L13402-n/a. doi:10.1029/2009GL038852.
- Doblas-Reyes, F. J., García-Serrano, J., Lienert, F., Biescas, A. P., & Rodrigues, L. R. (2013). Seasonal climate predictability and forecasting: status and prospects. *Wiley Interdisciplinary Reviews: Climate Change*, 4(4), 245-268. doi: <https://doi.org/10.1002/wcc.217>
- ECCC (2022), Canadian Climate Normal. Retrieved June 14, 2022, from https://climate.weather.gc.ca/climate_normals/index_e.html.
- Goodison, B. E., Louie, P. Y., & Yang, D. (1998). WMO solid precipitation measurement intercomparison. WMO/TD-No. 872, 88pp+212pp Annex, *World Meteorological Organisation.*, Geneva https://library.wmo.int/doc_num.php?explnum_id=9694.
- Government of the Northwest Territories [GNWT]. (2018). 2030 NWT Climate Change Strategic Framework. https://www.enr.gov.nt.ca/sites/enr/files/resources/128-climate_change_strategic_framework_web.pdf.

- Hjort, J., Streletskiy, D., Doré, G., Wu, Q., Bjella, K., & Luoto, M. (2022). Impacts of permafrost degradation on infrastructure. *Nature Reviews Earth & Environment*, 3(1), 24-38. doi:10.1038/s43017-021-00247-8.
- Hutchinson, M. F., McKenney, D. W., Lawrence, K., Pedlar, J. H., Hopkinson, R. F., Milewska, E., & Papadopol, P. (2009). Development and testing of Canada-wide interpolated spatial models of daily Minimum–Maximum temperature and precipitation for 1961–2003. *Journal of Applied Meteorology and Climatology*, 48(4), 725-741. doi:10.1175/2008JAMC1979.1.
- International Expert Panel on Science Priorities for the Canadian Arctic Research Initiative [CARI]. (2008). Vision for the Canadian Arctic Research Initiative: assessing the opportunities. <https://www.cca-reports.ca/wp-content/uploads/2018/10/2008-11-05-cari-report.pdf>.
- Kokelj, S. V., Tunnicliffe, J., Lacelle, D., Lantz, T. C., Chin, K. S., & Fraser, R. (2015). Increased precipitation drives mega slump development and destabilization of ice-rich permafrost terrain, northwestern Canada. *Global and Planetary Change*, 129, 56-68. doi:10.1016/j.gloplacha.2015.02.008.
- Lackmann, G. M., & Gyakum, J. R. (1996). The synoptic- and planetary-scale signatures of precipitating systems over the Mackenzie River basin. *Atmosphere-Ocean*, 34(4), 647-674. doi:10.1080/07055900.1996.9649581.
- Lavoie, J. (2017). Key Arctic Research Station Set to Close Because of Liberal Government's Funding Cuts. Access on August 15th, 2022, from <https://thenarwhal.ca/key-arctic-research-station-set-close-because-liberal-government-s-funding-cuts/>.

- Li, L., Li, Y., & Li, Z. (2020). Object-based tracking of precipitation systems in western Canada: The importance of temporal resolution of source data. *Climate Dynamics*, 55(9), 2421-2437. doi:10.1007/s00382-020-05388-y.
- Li, Y., & Li, Z. (2021). High-resolution weather research forecasting (WRF) modeling and projection over western Canada, including Mackenzie watershed. In D. Yang, & D. L. Kane (Eds.), *Arctic hydrology, permafrost and ecosystems* (pp. 815-847). Cham: Springer International Publishing. doi:10.1007/978-3-030-50930-9_28 Retrieved from https://doi.org/10.1007/978-3-030-50930-9_28.
- Lilhare, R., Déry, S. J., Pokorny, S., Stadnyk, T. A., & Koenig, K. A. (2019). Intercomparison of multiple hydroclimatic datasets across the lower Nelson River basin, Manitoba, Canada. *Atmosphere-Ocean*, 57(4), 262-278. doi:10.1080/07055900.2019.1638226
- Mekis, E., Donaldson, N., Reid, J., Zucconi, A., Hoover, J., Li, Q., . . . Melo, S. (2018). An overview of surface-based precipitation observations at environment and climate change Canada. *Atmosphere-Ocean*, 56(2), 71-95. doi:10.1080/07055900.2018.1433627.
- Mlynowski, T. J., Hernández-Henríquez, M. A., & Déry, S. J. (2011). An evaluation of hydrometric monitoring across the Canadian Pan-Arctic region, 1950–2008. *Hydrology Research*, 42(6), 479-490. doi:10.2166/nh.2011.105.
- Murfitt, J., & Brown, L. C. (2017). Lake ice and temperature trends for Ontario and Manitoba: 2001 to 2014. *Hydrological Processes*, 31(21), 3596-3609. doi: <https://doi.org/10.1002/hyp.11295>.

- NOAA (2009), Climate Variability: Arctic Oscillation. Retrieved June 13, 2022, from <https://www.climate.gov/news-features/understanding-climate/climate-variability-arctic-oscillation>.
- Orihel, D., Swanson, H., & Venkiteswaran, J. (2013). Scientists on saving science. *Limnology and Oceanography Bulletin*, 22(3), 76-78. doi: <https://doi.org/10.1002/lob.201322376>.
- Phillips, D. W. (1990). *The climates of Canada*. Ottawa, Ontario: Supply and Services Canada.
- Prowse, T. D., & Ommanney, C. S. (1990). *Northern hydrology: Canadian perspectives*. Saskatoon, Sask., Canada: National Hydrology Research Institute.
- Quinton, W. L., Hayashi, M., & Chasmer, L. E. (2011). Permafrost-thaw-induced land-cover change in the Canadian subarctic: Implications for water resources. *Hydrological Processes*, 25(1), 152-158. doi: <https://doi.org/10.1002/hyp.7894>.
- Rienecker, M. M., Suarez, M. J., Gelaro, R., Todling, R., Bacmeister, J., Liu, E., . . . Woollen, J. (2011). MERRA: NASA's modern-era retrospective analysis for research and applications. *Journal of Climate*, 24(14), 3624-3648. doi:10.1175/JCLI-D-11-00015.1.
- Rouse, W.R., Douglas, M.S., Hecky, R.E., Hershey, A.E., Kling, G.W., Lesack, L., Marsh, P., McDonald, M., Nicholson, B.J., Roulet, N.T. & Smol, J.P. (1998). Effects of climate change on the freshwaters of Arctic and Subarctic North America. *Hydrological Processes*, 11(8), 873–902. doi: [https://doi.org/10.1002/\(SICI\)1099-1085\(19970630\)11:8<873::AID-HYP510>3.0.CO;2-6](https://doi.org/10.1002/(SICI)1099-1085(19970630)11:8<873::AID-HYP510>3.0.CO;2-6).

- Serreze, M. C., & Barry, Roger G. (Roger Graham). (2014). *The Arctic climate system* (Second edition. ed.). New York, NY: Cambridge University Press.
- Shiklomanov, A. I., Lammers, R. B., & Vörösmarty, C. J. (2002). Widespread decline in hydrological monitoring threatens pan-arctic research. *Eos, Transactions American Geophysical Union*, 83(2), 13-17. doi: <https://doi.org/10.1029/2002EO000007>.
- Smith, C. D., Yang, D., Ross, A., & Barr, A. (2019). The environment and climate change Canada solid precipitation intercomparison data from Bratt's Lake and Caribou Creek, Saskatchewan. *Earth System Science Data*, 11(3), 1337-1347. doi: <https://doi.org/10.5194/essd-11-1337-2019>.
- Szeto, K. K. (2008). On the extreme variability and change of cold-season temperatures in northwest Canada. *Journal of Climate*, 21(1), 94-113. doi:10.1175/2007JCLI1583.1.
- Szeto, K. K., Tran, H., MacKay, M., Crawford, R., & Stewart, R. E. (2008). Assessing water and energy budgets for the Mackenzie River basin. (pp. 269-296).-Springer, Berlin Heidelberg. doi:10.1007/978-3-540-73936-4_16.
- Thompson, D. W. J., & Wallace, J. M. (1998). The Arctic oscillation signature in the wintertime geopotential height and temperature fields. *Geophysical Research Letters*, 25(9), 1297-1300. doi:10.1029/98GL00950.
- van de Poll, Willem H., Maat, D. S., Fischer, P., Visser, R. J. W., Brussaard, C. P. D., & Buma, A. G. J. (2021). Solar radiation and solar radiation driven cycles in warming and freshwater discharge control seasonal and inter-annual phytoplankton chlorophyll *a* and taxonomic

- composition in a high Arctic fjord (Kongsfjorden, Spitsbergen). *Limnology and Oceanography*, 66(4), 1221-1236. doi: <https://doi.org/10.1002/lno.11677>.
- Viglione, A., Borga, M., Balabanis, P., & Blöschl, G. (2010). Barriers to the exchange of hydrometeorological data in Europe: Results from a survey and implications for data policy. *Journal of Hydrology*, 394(1), 63-77. doi: <https://doi.org/10.1016/j.jhydrol.2010.03.023>.
- Vincent, L. A., Zhang, X., Brown, R. D., Feng, Y., Mekis, E., Milewska, E. J., . . . Wang, X. L. (2015). Observed trends in Canada's climate and influence of low-frequency variability modes. *Journal of Climate*, 28(11), 4545-4560. doi:10.1175/JCLI-D-14-00697.1.
- Wang, J., Zhang, J., Watanabe, E., Ikeda, M., Mizobata, K., Walsh, J. E., . . . Wu, B. (2009). Is the dipole anomaly a major driver to record lows in arctic summer sea ice extent? *Geophysical Research Letters* 36(5), L05706-n/a. doi:10.1029/2008GL036706.
- Weston, S. T., Bailey, W. G., McArthur, L. J. B., & Hertzman, O. (2007). Interannual solar and net radiation trends in the Canadian arctic. *Journal of Geophysical Research: Atmospheres*, 112 doi: <https://doi.org/10.1029/2006JD008000>.
- Whitfield, P. H., Hall, A. W., & Cannon, A. J. (2004). Changes in the seasonal cycle in the circumpolar arctic, 1976-95: Temperature and precipitation. *Arctic*, 57(1), 80-93. doi:10.14430/arctic485.
- Wilcox, E.J., Keim, D., de Jong, T., Walker, B., Sonntag, O., Sniderhan, A.E., Mann, P. & Marsh, P. (2019). Tundra shrub expansion may amplify permafrost thaw by advancing

snow- melt timing. *Arctic Science*, 5(4), 202–217. doi: <https://doi.org/10.1139/as-2018-0028>.

Woo, M., & Thorne, R. (2008). Analysis of cold season streamflow response to variability of climate in north-western north America. *Hydrology Research*, 39(4), 257-265.
doi:10.2166/nh.2008.102.

Zhang, X., Vincent, L. A., Hogg, W. D., & Niitsoo, A. (2000). Temperature and precipitation trends in Canada during the 20th century. *Atmosphere-Ocean*, 38(3), 395-429.
doi:10.1080/07055900.2000.9649654.

2 Evaluating the suitability of three gridded datasets and their impacts on hydrological simulation at Scotty Creek in the southern Northwest Territories, Canada

Chapter Status

Contents of this chapter were published in Hydrological Process

Persaud, B. D., Whitfield, P. H., Quinton, W. L., & Stone, L. E. (2020). Evaluating the suitability of three gridded-datasets and their impacts on hydrological simulation at Scotty Creek in the southern Northwest Territories, Canada. *Hydrological Processes*, 34(4), 898-913.
<https://doi.org/10.1002/hyp.13663>

2.1 Abstract

In the southern Northwest Territories (NWT) long time series of historical observations of climate and hydrology are scarce. Gridded datasets have been used as an alternative to *in situ* observations for climate analysis in this area, but not for driving models to understand hydrological processes in the southern NWT. The suitability of temperature and precipitation from three gridded datasets (ANUSPLIN, ERA-Interim and MERRA-2) as forcings for hydrological modelling in a small sub-catchment in the southern NWT are assessed. Multiple statistical techniques are used to ensure that structural and temporal attributes of the observational datasets are adequately compared. Daily minimum and maximum air temperatures in gridded datasets are more similar to observations than precipitation. The ANUSPLIN temperature time series are more statistically similar to observations, based on population statistics and temporal structure, than either ERA-Interim or MERRA-2. The gridded datasets capture the seasonal and annual seasonal variability of precipitation but with large biases. ANUSPLIN precipitation compares better with observations than either ERA-Interim or MERRA-2 precipitation. The biases in these gridded datasets affect runoff simulations. The biases in hydrological simulations are predictable from the statistical differences between gridded datasets and observations and can be used to make informed choices about their use.

2.2 Introduction

The Canadian subarctic, including the southern NWT, has limited long-term historical hydrometeorological observations in both space and time (Rouse et al., 1997; Vincent et al., 2015). Interpolated and reanalysis hydrometeorological products (gridded datasets) can be a complement to the existing sparse data network. Gridded datasets have been used to characterize the variability and trends of hydroclimate systems where observations are sparse or do not exist (e.g., Woo & Rouse, 2008; Snauffer et al., 2016; Way et al., 2017), to assess the outputs of global and regional climate models (e.g., Field, et al., 2012; Diaconescu, et al., 2018), and to study hydro-ecological responses to changing climate (e.g., Price et al., 2013).

If significant differences exist between observations and gridded datasets, climatological or hydrological interpretations will likely be misleading (Crout et al., 2008). Gridded datasets have the potential to be used as alternative inputs to force hydrological models for large watersheds (Chen & Brissette, 2017); however, it is important to consider possible biases that such datasets might introduce in hydrograph outputs (Crout et al., 2008). Errors or biases in climate inputs are known to affect hydrological fluxes (Essou et al., 2016; Snauffer et al., 2016; Chen & Brissette, 2017). While the assimilation and interpolation methods used to produce gridded datasets have improved (e.g. Dee et al., 2011a; Bosilovich et al., 2015), the suitability of gridded datasets as inputs for environmental modelling remains a concern (Crout et al., 2008; Bennett et al., 2013; Mo et al., 2014). Seasonal biases in gridded precipitation lead to biased simulations of river flow (Essou et al., 2016; Islam & Déry, 2017). For example, a cold bias in the ERA-40 temperature and precipitation gridded dataset resulted in models with a late start to snowmelt (Woo & Thorne, 2006).

Several studies have evaluated gridded datasets across Canada; ERA-Interim, and MERRA were the most consistent with observed data (Lindsay et al., 2014) and interannual variability (Rapačić et al., 2015). Summer biases in gridded precipitation were consistently the lowest in ANUSPLIN (Wong et al., 2017). Before supplementing, or replacing, observations with gridded datasets, gridded datasets should be thoroughly verified against existing observations to understand their limits (Crout et al., 2008; Mo et al., 2014). Obtaining long-term independent observations to validate gridded datasets in the southern NWT remains difficult. A comparison of reanalysis-to-station comparison should consider two issues; 1) use of truly independent station data; and 2) how to treat the gap in scales between the reanalysis and the point locations (Trubilowicz, et al., 2016). In the southern NWT the only truly independent data readily available was the short record from Scotty Creek.

Smoothing of daily data to monthly and seasonal means can reduce the effect of biases and outliers (Zhang et al., 2011) at the cost of lost temporal resolution. Many studies have focused on seasonal or annual means of climate variables (e.g. Zhang et al., 2011; Wong et al., 2017) but means alone may not reflect variability that is important hydrologically. While identifying changes in mean climate is important, the entire distribution is known to have climatological and hydrological impacts (Field et al., 2012; Cornes & Jones, 2013). Multiple metrics should be used to compare datasets so as to reflect all aspects of a time series and to offset existing bias that may be inherent in a particular metric (Bennett et al., 2013; Mo et al., 2014; Wilby et al., 2017). Using only a few statistical methods to understand uncertainty may lead researchers to incorrectly infer the suitability of gridded datasets (Crout et al., 2008; Jain & Sudheer, 2008; Bennett et al., 2013). A systematic and comprehensive assessment of gridded temperature and precipitation datasets is

needed to clarify the magnitudes of uncertainty and bias of gridded datasets over data-sparse regions (Lindsay et al., 2014).

In Northwestern Canada, older versions of gridded datasets have been used in hydrological studies. The Mackenzie GEWEX (Global Energy and Water Cycle Experiment) Study (MAGS) characterized the hydroclimatology of the Mackenzie River Basin (MRB), using a combination of gridded datasets and numerical model data from the Canadian Regional Climate Model (Liu et al. 2002; Louie et al., 2002; Woo & Rouse, 2008). By combining data from several gridded datasets, the MRB water budget was within 10% of the observed runoff (Szeto et al., 2008).

The present study assesses currently available gridded datasets discussed in Section 2.4.1 and has two objectives; 1) assess the similarity of three daily gridded datasets to daily climate station temperature and precipitation observations over a spatial domain in the southern NWT subarctic Canada; and 2) evaluate the impacts of using gridded temperature and precipitation datasets instead of observations as inputs to an operational hydrological model. One interpolated gridded dataset (ANUSPLIN) and two reanalysis gridded datasets (ERA-Interim and MERRA-2) are assessed for acceptable similarity against observations using: 1) population statistics, which compare the entire distributions; 2) temporal structure which determines whether differences are random or introduce a signal not present in the observations; and 3) differences in outputs from hydrological models driven by gridded datasets and observations which translate into biases that originate in the dataset. These three comparisons complement previous studies and provide a more detailed investigation of accuracy and biases in gridded datasets that could be used where observational data are limited.

2.3 Study Area

The southern Northwest Territories (NWT) is one of the most rapidly warming areas of Canada (Vincent *et al.*, 2015); with air temperatures rising at twice the rate of other regions (Richter-Menge *et al.*, 2017). Accelerated warming in this region has resulted in widespread permafrost thaw (Beilman & Robinson, 2003), including changes to landcover and hydrological patterns (Whitfield & Cannon, 2000; St. Jacques & Sauchyn, 2009). Understanding the impacts of these changes in air temperature is important from ecological, social, and economic perspectives (Rowland *et al.*, 2010).

The boreal forest that dominates the landscape of the southern NWT (Figure 2.1) is underlain by discontinuous permafrost (Beilman & Robinson, 2003) and has a continental climate with long cold winters and short summers. Monthly air temperature typically ranges from -29°C (January) to 24°C (July) (Phillips, 1990). Air temperatures in the NWT have risen by 1.5 to 3.0°C between 1948 and 2012, with the last decade being the warmest (Vincent *et al.*, 2015). Climate stations within the southern NWT have similar seasonal patterns of temperature and precipitation, and decadal change patterns (Whitfield *et al.*, 2004). The average total annual precipitation ranges between 200 and 400 mm, with approximately 40-80% falling as snow (Rouse *et al.*, 1997) between November and March (Phillips, 1990). Total annual precipitation generally decreases with increasing latitude in the NWT (Phillips, 1990). Changes in the southern NWT include permafrost thaw (Beilman & Robinson, 2003), landcover (Quinton *et al.*, 2011), runoff generation (Connon *et al.*, 2014), and streamflow patterns (Whitfield & Cannon, 2000; St. Jacques & Sauchyn, 2009) that have been linked to climate warming (Rowland *et al.*, 2010).

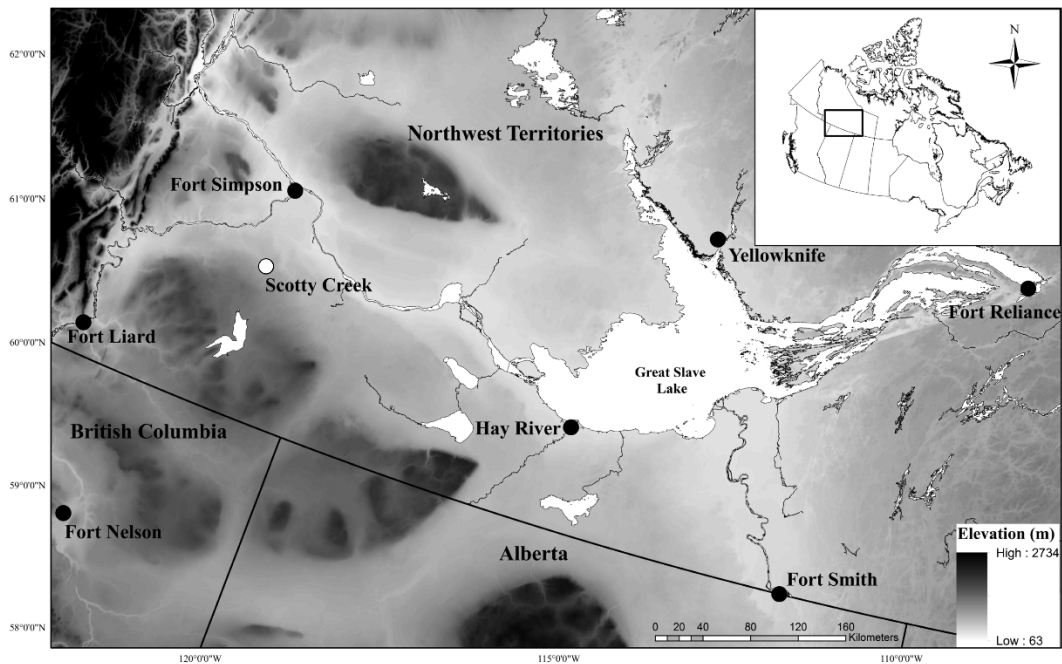


Figure 2.1 Topography of the southern NWT showing the location of the seven climate stations (black dots) and Scotty Creek Research Watershed (white dot) and of the study area in Canada

2.4 Data and Methods

2.4.1 Data and datasets

2.4.1.1 Station observations

Daily maximum and minimum temperatures and precipitation data were obtained from the Environment and Climate Change Canada (ECCC) database for the seven climate stations shown in Figure 2.1. These stations are part of the World Meteorological Organization (WMO) Global Climate Observing System and Regional Basic Climatological Networks, thus follow the WMO observation standards. Stations included in this study were selected based on their suitability in climate change and variability studies, and their length. ECCC data collection processes are described in Louie et al., (2002). A climate station at the Scotty Creek Research Basin, NWT was

also included for the period 2004-2013 to provide an independent set of observations, observations not included in the generation of the gridded datasets.

Scotty Creek is a peatland-dominated catchment typical of most of the southern NWT that consists of channel fens, bogs, and peat plateaus that are underlain by discontinuous permafrost (Quinton et al., 2011). Research at this basin seeks to improve the understanding of regional hydrological processes (Quinton et al., 2011). Methods for instrumentation and data collection for air temperature and precipitation at Scotty Creek Research Basin (Wright et al., 2013) conform to WMO practices. Climate observations were quality controlled using the methods of Klein Tank et al., (2009).

2.4.1.2 Gridded Datasets

Details of the three gridded datasets from 1980 to 2013 are provided in Table 2.1 and described in the preceding paragraphs. These gridded datasets replace older versions and benefit from i) increased spatial and temporal resolution, ii) improved assimilation methods (Dee et al., 2011a; Bosilovich et al., 2015), and iii) better representation of precipitation (Bosilovich et al., 2015). Interpolation of observations and gridded datasets to a common grid size before evaluation may introduce further uncertainties (Gervais et al., 2014).

Dataset Name	ANUSPLIN	ERA-Interim	MERRA-2
Data assimilation method	Spline interpolation of using station temperature and precipitation observations	4D-VAR using observations (e.g., satellite remote sensing, in situ, radio sounding, profilers and numerical weather forecasting	3D-VAR, now includes observation corrected precipitation forcing for land surface. Includes aerosol data in assimilation process
Time Period	1950-2013	1979-present	1980-present
Temporal Resolution	Daily	6 hourly and daily	3 hourly and daily
Model Output Spatial Resolution	10 km × 10 km	0.75° × 0.75° (~79 km) but user can select, down to 0.025° × 0.025° (~13km × 13km)	0.5° × 0.65° (~50 × 50 km)
Other data	-	Surface, upper air atmospheric and hydrological variables	Surface and upper air atmospheric and hydrological variables
Principle Reference	Hutchinson et al. 2009	Dee et al. 2011a	Bosilovich et al. 2015
Source	Natural Resources Canada https://cfs.nrcan.gc.ca/projects/3	http://apps.ecmwf.int/datasets/data/interim-full-daily/levtype=sfc/	https://disc.gsfc.nasa.gov/datasets?keywords=merra-2&page=1

Table 2.1 Summary of the characteristics of the three gridded datasets over study domain.

Hutchinson et al. (2009) developed a climate dataset of daily air temperature and precipitation over Canada using the Australian National University Spline (ANUSPLIN) model. The ANUSPLIN dataset uses station observations and the tri-variate thin-plate smoothing spline surface interpolation method to generate a dataset at a spatial resolution of ~10 km across Canada from 1950 to 2013 (Table 2.1) (Hutchinson et al., 2009). This gridded dataset, obtained from Natural Resources Canada, has yet to be thoroughly evaluated over the southern NWT.

ERA-Interim is the ECMWF global reanalysis atmospheric gridded dataset (Dee et al., 2011a) developed as a replacement of ERA-40 (Uppala et al., 2008). ERA-Interim used a four-dimensional variational data assimilation (4DVAR), which considers the time of an observation that occurs within the analysis window (Dee et al., 2011a) to improve the treatment of biases in observations and changes in the observing system, and better represent the hydrological cycle (Uppala et al., 2008; Dee et al., 2011a). ERA-Interim uses a spectral T255 (79 km) model grid for which the datasets are available since 1979.

The Modern-Era Retrospective Analysis for Research and Applications (MERRA), Version 2, is a gridded NASA product (Bosilovich et al., 2015). MERRA-2 (McCarty et al., 2016) includes ground and satellite-based precipitation observations to drive the land surface water budget and has not been widely evaluated against station observations in the NWT.

2.4.2 Statistical evaluation

There is no single satisfactory method for quantitatively evaluating similarity among datasets (Bennett et al., 2013). When comparing observed and gridded time series, the acceptable similarity should be based on the gridded time series having similar statistical and structural characteristics as the observed time series (Mo *et al.*, 2014). Metrics often used to assess the performance of gridded datasets include mean error (ME), root mean square error (RMSE), mean absolute error (MAE), correlation coefficients (R), regression slope (slope), and Nash-Sutcliffe model efficiency (NSE) (Rapaić et al., 2015; Essou et al., 2016; Islam & Déry, 2017). All statistical tests were performed at $p \leq 0.05$ using the R statistical language (R Development Core Team, 2016). A summary of statistical methods and the functions and packages used are provided in Table S2.1 (Supporting Information).

A simple test of gridded data suitability are population statistics; mean and standard deviation measure the location and spread of the distribution while skewness and kurtosis measure its shape (Wilks, 2006). Differences in these measures could identify biases that limit use. The two-sample Kolmogorov-Smirnov (KS) test was used to determine if the cumulative distribution of the time series of a grid point nearest to a climate station and the observation time series were different (Wilks, 2006), for each gridded dataset and each climate station. Duration curves compare magnitudes on an exceedance basis showing where biases exist (Cole et al., 2003). Pearson's correlation coefficient (R) indicates the strength and the direction (sign) of the relationship between observed and a gridded dataset (Mo et al., 2014). A linear regression between observations and a gridded dataset is expected to have a slope of one and an intercept of zero. In addition, the homogeneity of variances of the residuals of the regression errors were tested using the Breusch-Pagan test (Breusch & Pagan, 2006).

The utility of a gridded dataset also depends on the temporal structure being similar to observed data. Time series data have structure resulting from persistence, cycles, and/or trends. Whether local structural similarities of the observed data were represented in the gridded datasets was assessed with the Wang-Bovik (WB) index (Wang & Bovik, 2002) which penalizes the correlation for differences between means and variances of the two time series (Mo et al., 2014).

In the southern NWT, it is particularly important that gridded datasets capture the onset of melt and freezing periods; if the timing of these transitions is inaccurate, any subsequent hydrological analysis will be biased. The melt onset date is the first day when the mean daily air temperature is above 0°C, and follows last five-day period when the daily mean air temperature is below 0°C in spring (March to May) (Shi et al., 2015). Similarly, the freezing onset date is defined here as the

first day when the mean daily air temperature is below 0°C, following the last five-day period between when the daily mean air temperature is above 0°C in autumn (October to November).

2.4.3 Sensitivity analysis using Cold Regions Hydrological Model

The sensitivity of simulated runoff to inputs from different gridded datasets and an independent observation dataset was evaluated by comparing outputs from a Cold Regions Hydrological Modelling (CRHM) platform (Pomeroy et al., 2007) model for a 0.45 km² headwater sub-catchment of Scotty Creek, NWT. CRHM has been applied across many cold region studies (Pomeroy et al., 2007; Fang et al., 2010), including Scotty Creek (Quinton & Baltzer, 2013). CRHM is a physically based, lumped modelling platform designed to simulate cold regions hydrological processes in small to medium-sized basins (Pomeroy et al., 2007). CRHM has a limited need for calibration (Pomeroy et al., 2007). The input forcing dataset, used to simulate discharge for the sub-catchment, consisted of measured relative humidity, wind speed, incoming shortwave radiation, temperature, and precipitation at Scotty Creek from 2008 to 2013. Other model parameters for CRHM were transferred from similar basins or from field observations at Scotty Creek (Quinton & Baltzer, 2013; Stone et al., 2019). Since no discharge data exist at the sub-catchment level, model performance was determined to be acceptable by comparing observed and simulated snow depth, snow water equivalent, evapotranspiration, and water level in multiple hydrological response units against model output (Stone et al., 2019). Here, the same model was used changing only the input forcings using daily temperature and precipitation from ANUSPLIN, ERA-Interim, and MERRA-2 for the grid point nearest to Scotty Creek for the period from 2008 to 2013. The effects of each of the forcing datasets on simulated runoff were assessed by the methods outlined in Section 2.5.3 and are illustrated by the simulated hydrographs.

2.5 Results

2.5.1 Population statistics comparison

Gridded datasets have lower mean T_{\max} and generally higher mean T_{\min} than observations for all stations (Figure 2.2a & b). ANUSPLIN T_{\max} and T_{\min} aligned closely with observations, with a mean error less than 0.58 °C and 1.33 °C, respectively (Figure 2.2). Observed and ANUSPLIN T_{\max} and T_{\min} standard deviations were similar while ERA-Interim had smaller standard deviations (Figure 2.2d & e) and for most stations, MERRA-2 had larger standard deviations than observations. The skewness of T_{\max} and T_{\min} (Figure 2.2g & h) was negative at all stations, reflecting the lower variability of low temperatures. Kurtosis was similar to observations (Figure 2.2j & k) increasing from north to south.

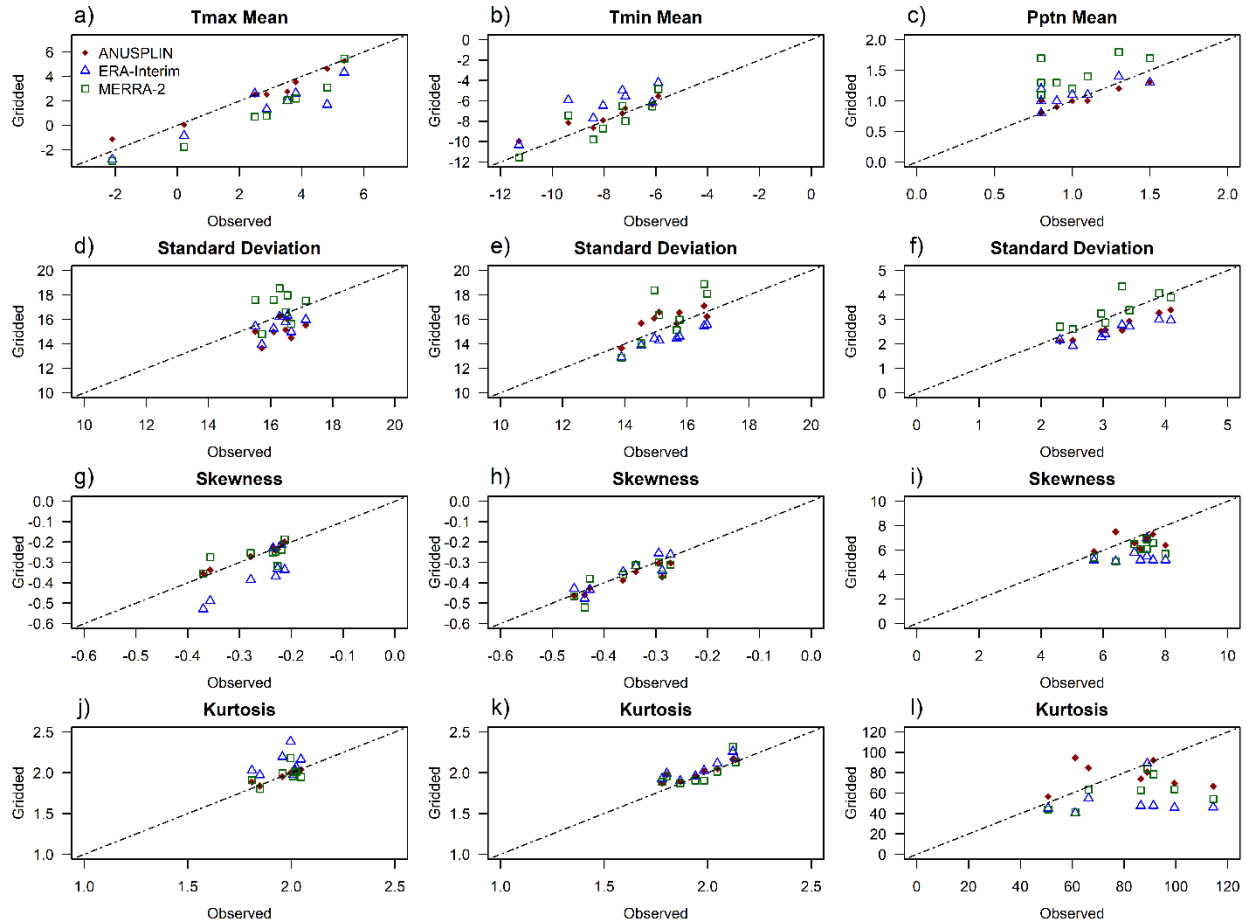


Figure 2.2 Statistical properties of gridded data against observations. Daily maximum temperature (a, d, g, j), daily minimum temperature (b, e, h, k) and daily precipitation (c, f, i, l); mean (central tendency), standard deviation (spread), skewness (symmetry) and kurtosis (peakedness) of the eight stations for observations, ANUSPLIN, ERA-Interim, and MERRA-2.

The daily mean precipitation for all three-gridded datasets were generally higher than observations (Figure 2.2c). The gridded datasets did not capture the variability present in the observed precipitation; the standard deviations of ANUSPLIN and ERA-Interim precipitation were smaller than those of observations, while MERRA-2 was generally higher (Figure 2.2f). The skewness (Figure 2.2i) and kurtosis (Figure 2.2l) were large and positive for all datasets and the observations, which are typical of precipitation data but were considerably smaller in the gridded datasets. The

skewness of gridded precipitation datasets was reflected in underestimation of the frequency where precipitation was lowest (< 0.1 mm), which accounts for the largest number of precipitation events. The frequencies of gridded datasets in higher precipitation intervals were generally overestimated. The KS test rejected the null hypothesis ($p \leq 0.05$) that gridded precipitation was the same as observations (Table 2.2).

Location	Dataset	Maximum Temperature	Minimum Temperature	Precipitation
	'best value'	> 0.05	> 0.05	> 0.05
Fort Reliance	ANUSPLIN	0.84	0.22	< 0.01
	ERA-INTERIM	< 0.01	< 0.01	< 0.01
	MERRA-2	< 0.01	< 0.01	< 0.01
Yellowknife	ANUSPLIN	0.81	<u>0.01</u>	< 0.01
	ERA-INTERIM	< 0.01	< 0.01	< 0.01
	MERRA-2	< 0.01	< 0.01	< 0.01
Fort Simpson	ANUSPLIN	0.26	0.51	< 0.01
	ERA-INTERIM	< 0.01	< 0.01	< 0.01
	MERRA-2	< 0.01	< 0.01	< 0.01
Scotty Creek	ANUSPLIN	0.74	< 0.01	< 0.01
	ERA-INTERIM	< 0.01	< 0.01	< 0.01
	MERRA-2	< 0.01	< 0.01	< 0.01
Hay River	ANUSPLIN	0.70	0.88	< 0.01
	ERA-INTERIM	< 0.01	< 0.01	< 0.01
	MERRA-2	< 0.01	< 0.01	< 0.01
Fort Smith	ANUSPLIN	0.54	0.97	< 0.01
	ERA-INTERIM	< 0.01	< 0.01	< 0.01
	MERRA-2	< 0.01	< 0.01	< 0.01
Fort Liard	ANUSPLIN	0.27	0.15	< 0.01
	ERA-INTERIM	< 0.01	< 0.01	< 0.01
	MERRA-2	< 0.01	< 0.01	< 0.01
Fort Nelson	ANUSPLIN	0.85	0.80	< 0.01
	ERA-INTERIM	< 0.01	< 0.01	< 0.01
	MERRA-2	< 0.01	< 0.01	< 0.01

Table 2.2 Kolmogorov-Smirnov test to assess the distributional similarity between the observations and gridded datasets. For values ≤ 0.05 , underlined, the null hypothesis is rejected, i.e., observations and gridded datasets do not represent the same continuous distribution.

Generally, the data for most stations in the study were similar; for brevity only the results for selected metrics from Fort Simpson are presented. The Fort Simpson climate station was chosen because, [1] it has consistent long term observations records, [2] the climate regime and the

peatland dominant landscape at Fort Simpson are representative of the southern NWT, [3] it is close to Scotty Creek, and [4] earlier studies, particularly the Mackenzie GEWEX, extensively used data and gridded datasets for Fort Simpson. The results for the other climate stations in Table 2.2, which had been used in producing the gridded datasets, and Scotty Creek, which is an independent dataset, were similar to Fort Simpson. At Fort Simpson, the probability distribution function (PDF) for T_{\max} and T_{\min} for ANUSPLIN, MERRA-2, and ERA-Interim generally took the same shape as the observations (Figure S2.1, Supporting Information). All PDFs had either two peaks and a shoulder or three peaks indicating a mixture of populations. Three peaks were evident in MERRA-2 T_{\max} , and further examination of the observations showed that they occurred between October and March and to a lesser extent during May and September on days when the T_{\max} was transitioning from colder to warmer temperatures (or vice versa). Differences in daily T_{\min} were most pronounced in the coldest part of the PDFs, where the ERA-Interim underestimated and MERRA-2 overestimated T_{\min} . The KS test statistic confirmed that ANUSPLIN T_{\max} and T_{\min} did not differ significantly from observations, but both ERA-Interim and MERRA-2 did (Table 2.3). Duration curves (Figure 2.3) confirmed that ANUSPLIN closely reproduced the behaviour of the observed temperatures and that ERA-Interim and MERRA-2 had lower values in the highest T_{\max} and MERRA-2 had lower T_{\max} in lowest T_{\max} values. MERRA-2 had higher T_{\min} in the lower range of T_{\min} values. ERA-Interim T_{\max} bias was greater above 0°C and the MERRA-2 bias below 0°C . ERA-Interim had a consistent T_{\min} positive bias below 0°C (Figure 2.3).

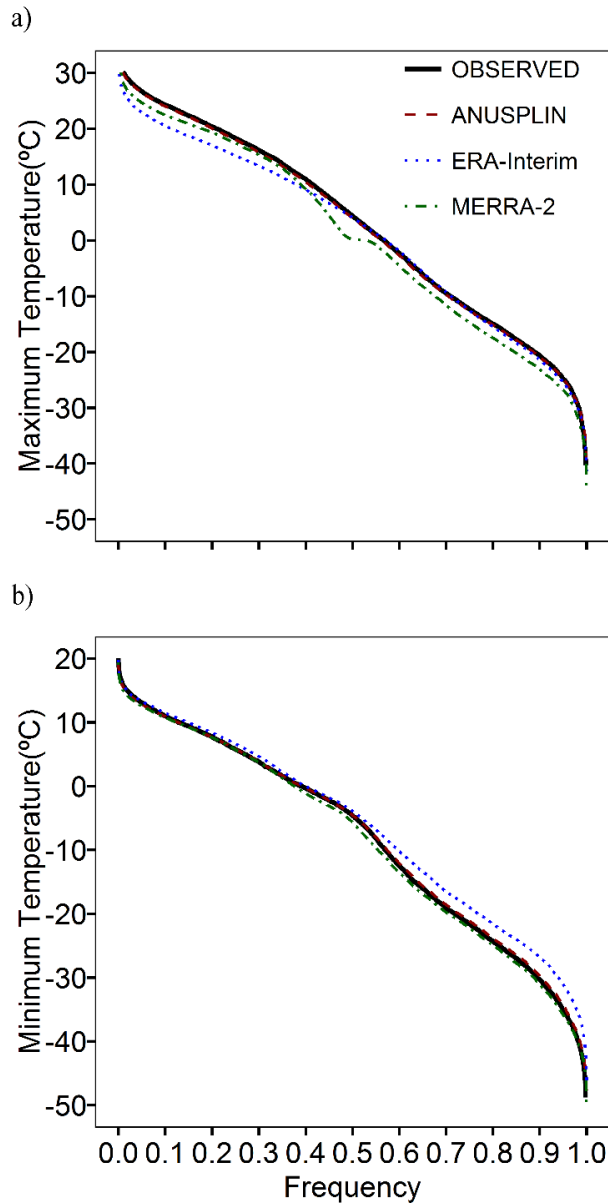


Figure 2.3 a) Daily maximum temperature and (b) daily minimum duration curves for observations, ANUSPLIN, ERA-Interim, and MERRA-2 for Fort Simpson, NWT, from 1980 to 2013.

The T_{\max} and T_{\min} for the observed and gridded datasets were linearly related (Figure 2.4) with slopes close to 1.0 (between 0.86 and 1.10, Table S2.2, Supporting Information). The slopes of the ERA-Interim and MERRA-2 regressions tended to either overpredict or underpredict

temperatures compared to ANUSPLIN (Figure 2.4). ANUSPLIN (Figure 2.4a & d) showed less scatter, consequently a smaller MAE, RSME, and a higher NSE and R (Table S2.2, Supporting Information) at all stations. ANUSPLIN underestimated T_{\max} and T_{\min} (small negative ME). ERA-Interim (Figures 2.4b & e) and MERRA-2 (Figure 4c & f) had more scatter and larger ME, MAE and RSME. The T_{\max} ME in the MERRA-2 was larger at all stations (Table S2.2). NSE, WB, R for the daily T_{\max} and T_{\min} were greater than 0.86 (Table S2.2) suggesting that the ERA-Interim and MERRA-2 had a temporal pattern similar to those of the observations.

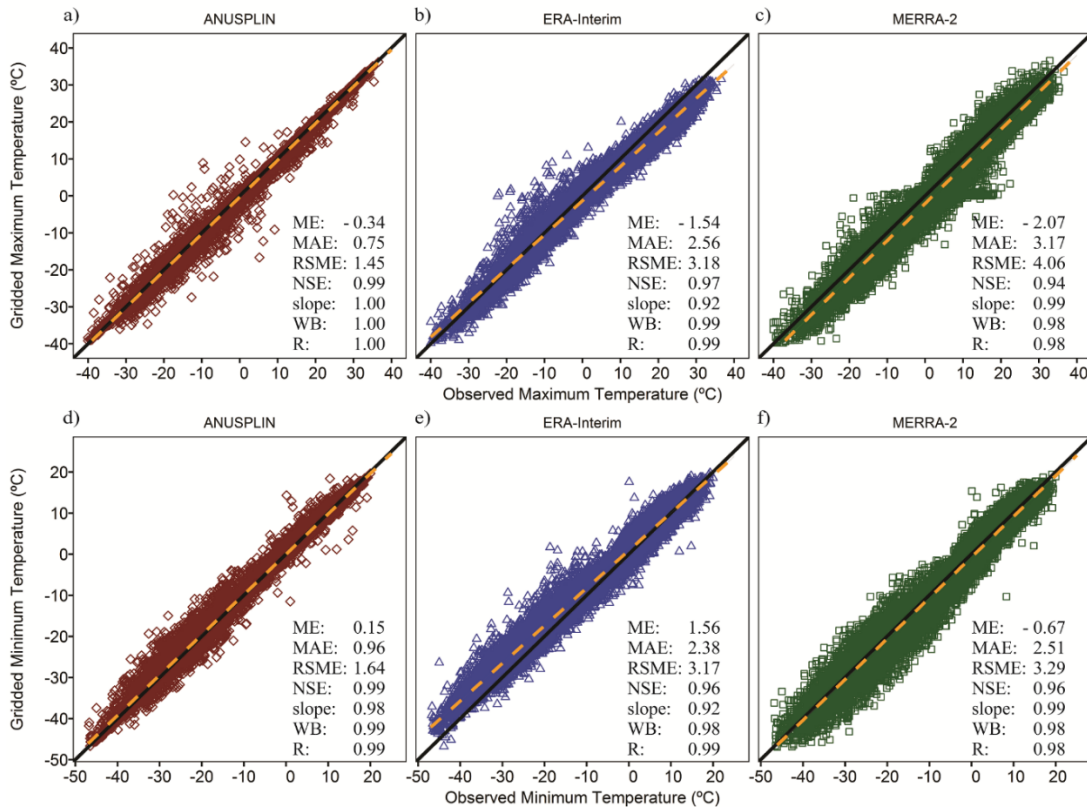


Figure 2.4 Example for Fort Simpson demonstrating the relationship of (a-c) observed maximum and (d-f) observed temperatures against the gridded data for ANUSPLIN (a & d), ERA-Interim (b & e), and MERRA-2 (c & f) from 1980 to 2013. In each case, the dashed line is the regression line of the gridded data to the observations, and the black line is the 1:1 line; also presented are the mean error (ME), mean absolute error (MAE), root mean square error (RSME), Nash-Sutcliffe model efficiency (NSE), and Wang-Bovick statistic (WB). The total number of observations N is $12000 < N \leq 12410$ between 1980 and 2013.

The magnitude of observed precipitation events was underestimated in gridded datasets as the linear relationship between observed and gridded precipitation datasets falls below the 1:1 line for all three datasets (Figure 2.5, Table S2.2). Across all stations, ANUSPLIN precipitation had the smallest MAE, RMSE, ME and NSE and the highest slope; therefore, was more similar to observed precipitation (Figure 2.5a) than either ERA-Interim (Figure 2.5b) or MERRA-2 (Figure 2.5c). Daily precipitation events were compared for 12 intervals for observation and gridded datasets (Figure 2.6); gridded datasets had fewer of the smallest events (< 0.1 mm) compared to observations and more of the larger events (> 0.1 mm). Overall, the consistency between the different datasets was stronger for daily maximum and minimum temperatures than for daily precipitation. These differences exist across a range of intensities (Figure 2.6) and the bias for ANUSPLIN was less than that for ERA-Interim and MERRA-2.

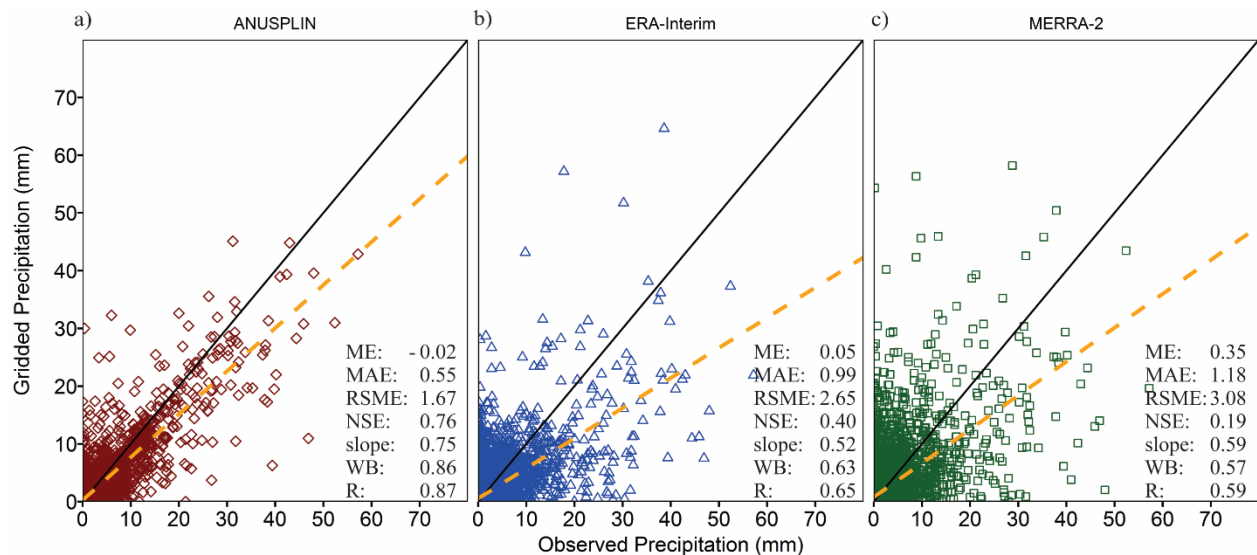


Figure 2.5 Daily observed precipitation against the daily gridded data at Fort Simpson, (a) ANUSPLIN, (b) ERA-interim and (c) MERRA-2. Dashed line is the regression line of the gridded data to the observations, and the black line is the 1:1 line; also presented are the mean error (ME), mean absolute error (MAE), root mean square error (RSME), Nash-Sutcliffe model efficiency (NSE), and Wang-Bovic statistic (WB). The total number of observations N is $12000 < N \leq 12410$ between 1980 and 2013.

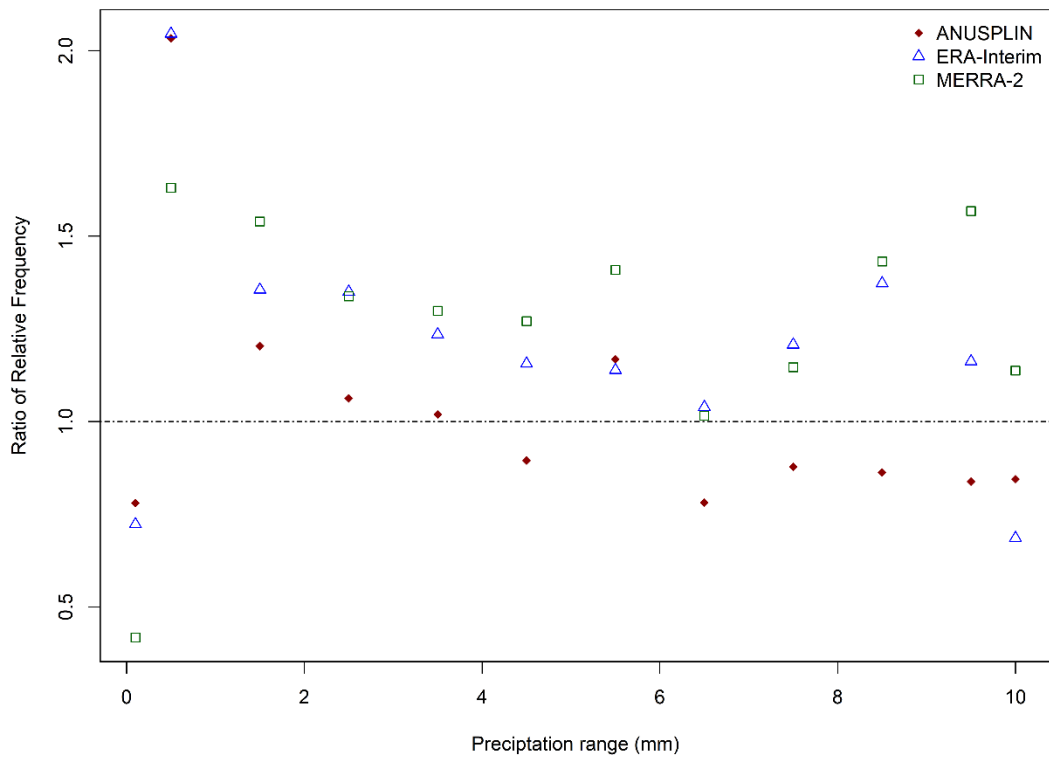


Figure 2.6 The ratio of the relative frequency ANUSPLIN/OBSERVED, ERA/OBSERVED, and MERRA-2/OBSERVED daily precipitation. The dashed line at 1.0 indicates the count per intensity category that would be expected if the gridded data were equal to the observed data.

2.5.2 Temporal structure

The differences between gridded datasets and observations were neither small nor random and had a seasonal structure (Figure 2.7). The MAE for ANUSPLIN T_{\max} and T_{\min} ranged from 0.5 to 1.5°C and were largest in the winter and smallest in the summer. ERA-Interim and MERRA-2 had colder T_{\max} temperatures than the observations (Figures 2.2-2.4) and the seasonal structure of MAE had the highest biases during winter (November to March) (Figure 2.7a). ERA-Interim and MERRA-2 T_{\min} had the highest MAE, which for MERRA-2 was largest during summer and smaller in winter (Figure 2.7a), while the MAE for T_{\min} from ERA-Interim was largest in March and April. The

ERA-Interim results for temperatures had abrupt changes unlike the smooth seasonal pattern of the other two gridded datasets.

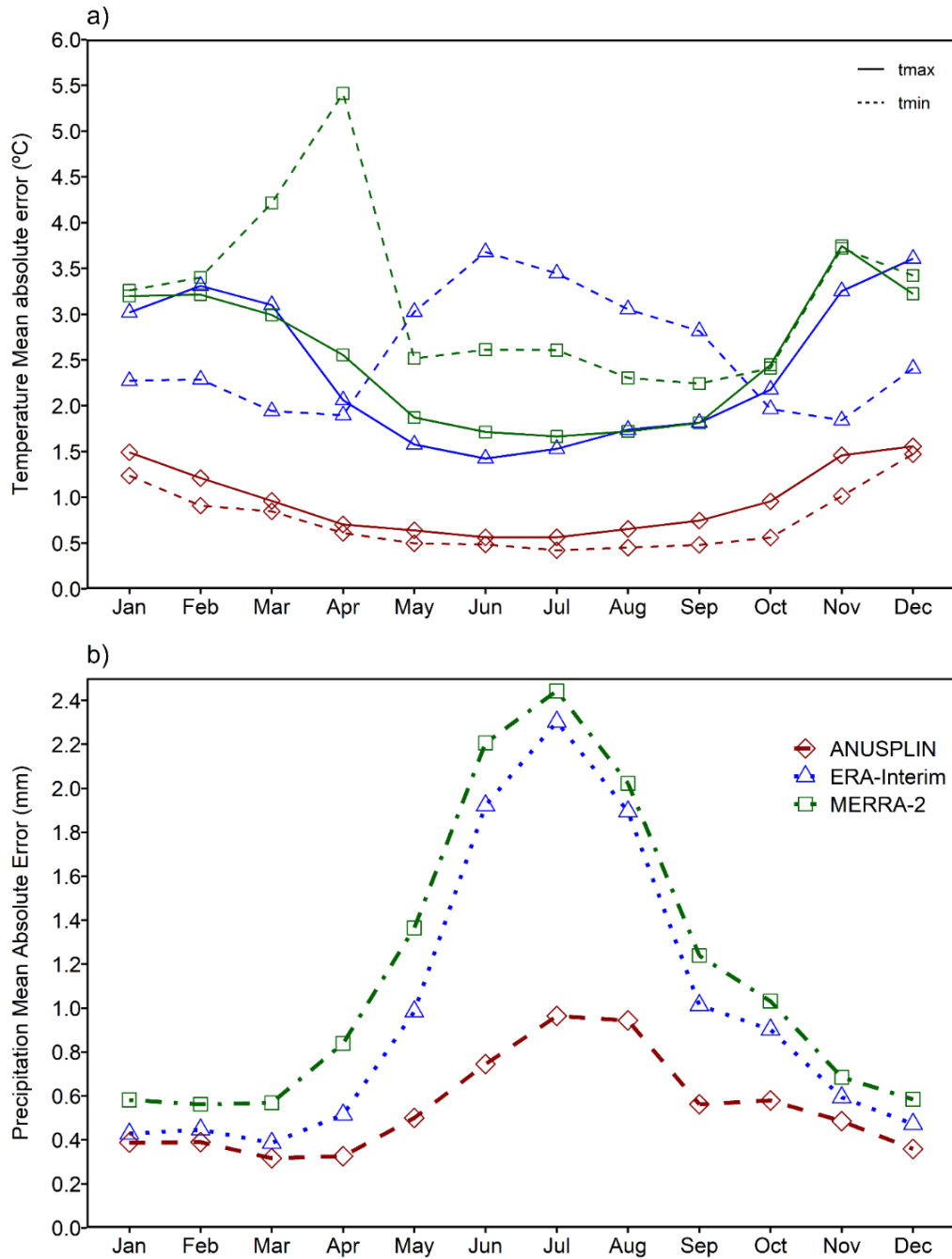


Figure 2.7 a) Example of monthly averaged daily mean absolute error between gridded and observed temperatures for ANUSPLIN, ERA-Interim and MERRA-2 at Fort Simpson, NWT. Maximum temperature (solid lines) and minimum (dashed lines), b) Example of monthly averaged mean absolute error between gridded and observed precipitation.

The temporal structure of the differences between observations and gridded datasets also existed at the daily level. At all climate stations, small but significant autocorrelations were found for ANUSPLIN in lags 1-20 (not shown), suggesting a difference in the daily temporal structure, that was more pronounced for ERA-Interim and MERRA-2 than ANUSPLIN. The Breusch-Pagan statistic confirmed homoscedasticity of residuals for ANUSPLIN T_{\max} , but not for ERA-Interim and MERRA-2, where during summer (Table 2.3) residuals were not homoscedastic. For T_{\min} , the homoscedasticity of residuals for ANUSPLIN in all months but July and October were confirmed by the Breusch-Pagan test; ERA-Interim and MERRA-2 failed this test in most months (Table 2.3) suggesting that the differences should not be attributed to random errors.

Month	Maximum Temperature			Minimum Temperature			Precipitation		
	ANUSPLIN	ERA-Interim	MERRA-2	ANUSPLIN	ERA-Interim	MERRA-2	ANUSPLIN	ERA-Interim	MERRA-2
'best value'	> 0.05	> 0.05	> 0.05	> 0.05	> 0.05	> 0.05	> 0.05	> 0.05	> 0.05
Jan	0.70	0.28	0.76	0.98	0.14	0.80	0.46	<0.01	0.90
Feb	0.61	0.25	0.64	0.51	0.11	0.45	<u>0.04</u>	<0.01	0.15
Mar	0.69	0.65	<0.01	0.44	<0.01	0.76	0.19	<u>0.03</u>	0.55
Apr	0.97	<0.01	<0.01	0.97	<0.01	0.07	0.39	0.20	0.44
May	0.93	<0.01	<0.01	0.66	<u>0.03</u>	0.38	0.28	0.07	<0.01
Jun	0.64	<0.01	<0.01	0.32	<u>0.01</u>	<u>0.02</u>	0.26	0.10	<0.01
Jul	0.69	<0.01	<0.01	<u>0.04</u>	<0.01	<0.01	0.65	0.13	<0.01
Aug	0.98	<0.01	<0.01	0.06	<0.01	<0.01	0.08	0.20	<0.01
Sep	0.39	<0.01	<0.01	0.39	0.08	<u>0.03</u>	0.66	0.49	<0.01
Oct	0.65	<0.01	0.15	<u>0.01</u>	<0.01	0.36	0.18	<u>0.01</u>	<u>0.05</u>
Nov	0.65	0.13	0.69	0.46	<0.01	0.06	0.14	<u>0.01</u>	<u>0.05</u>
Dec	0.85	<u>0.01</u>	0.22	0.31	0.08	0.45	0.44	<u>0.00</u>	0.13

Table 2.3 Berusch-Pagan test to assess for homoscedasticity of residuals of the regression of gridded against observations at Fort Simpson. For values ≤ 0.05 , underlined, the null hypothesis is rejected, i.e., observations and gridded residuals are not homoscedastic.

The difference between observed precipitation and gridded datasets was strongly seasonal (Figure 2.7b) with MAE being larger during the spring and summer, and, smaller in winter when precipitation amounts are smallest in the subarctic, for all gridded datasets. ANUSPLIN had the smallest precipitation bias (<1.0 mm/day MAE). ERA-Interim and MERRA-2 both had large spring and summer mean absolute errors (>2.0 mm/day) (Figure 2.7b). The systematic differences between observations and gridded datasets, especially from May to September, may explain the low correlations in Figure 2.5. The difference between observed precipitation and gridded datasets also had a temporal structure; all climate stations demonstrated significant autocorrelation at multiple time steps. ANUSPLIN exhibited homoscedasticity of residuals in all months while ERA-Interim failed the Breusch-Pagan test in winter and MERRA-2 in summer and autumn (Table 2.3).

Melt onset dates had large interannual variability (Figure 2.8a). ANUSPLIN and ERA-Interim were similar to station observations, but large differences occurred in some years. MERRA-2 consistently showed a later melt onset date than observations. Freezing onset dates for ANUSPLIN and ERA-Interim were similar to the observed onset dates, with large exceptions in the winters of 1992 and 2007 where they failed to capture observations at Fort Simpson (Figure 2.8b). MERRA-2 recorded earlier winter onset dates than observations, with exceptions, at Fort Simpson, in 2005 and 2010 (Figure 2.8b).

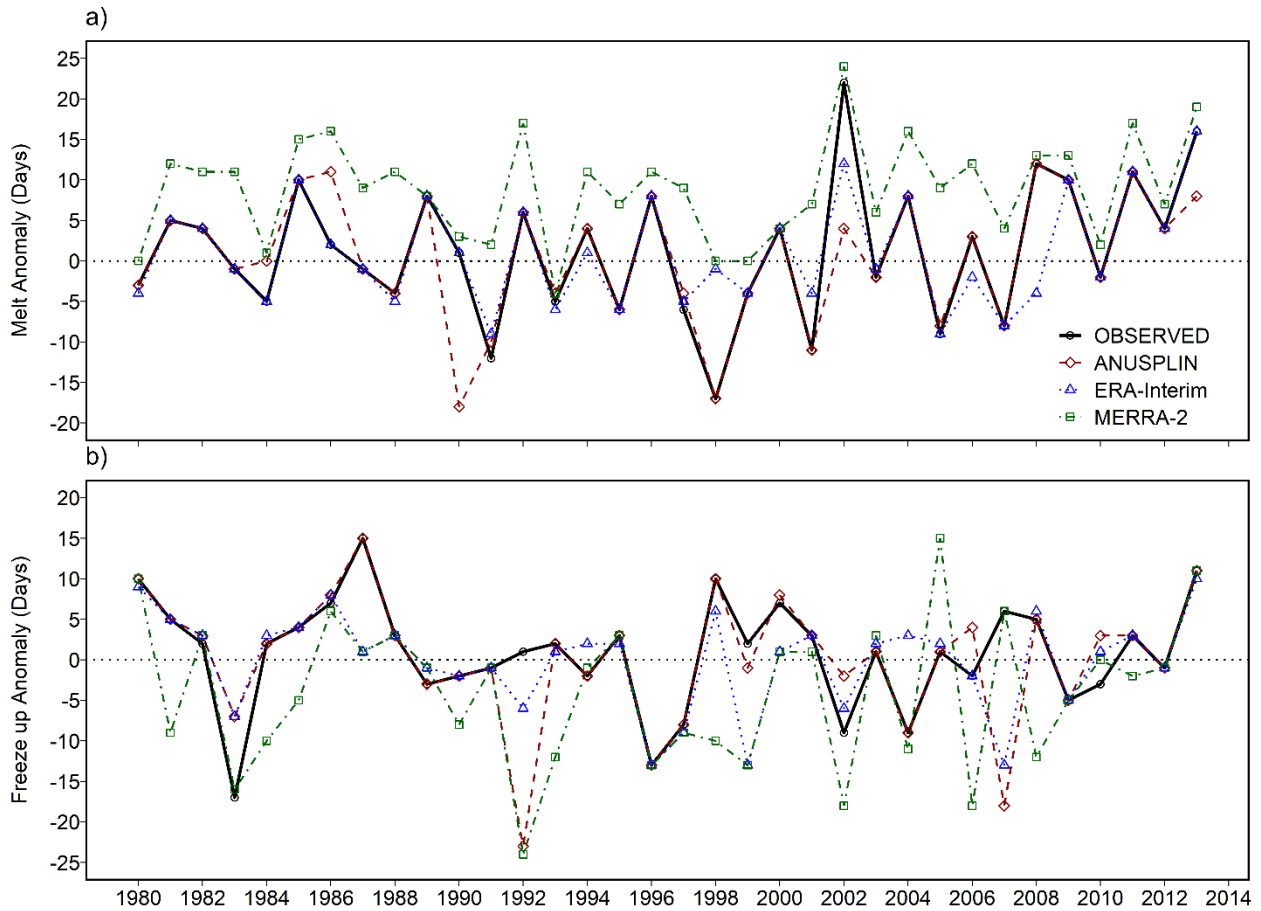


Figure 2.8 a) Deviation onset date of melt from long term average for Fort Simpson computed as the first day on which mean daily air temperature was above 0°C, following the last five-day period between March and April, when the daily mean air temperature was below 0°C; and b) deviation of onset date of freezing from long term average observed onset date. The onset date of freezing was defined as the first day on which mean daily air temperature was below 0°C following the last five-day period between October and November when daily mean air temperature was above 0°C.

2.5.3 Hydrological sensitivity to differences in gridded datasets

Simulated runoffs generated by CHRM, driven by either observations or gridded datasets, were evaluated with reference to a 1:1 line in a plot of observation data-driven and gridded dataset-driven runoff (Figure 2.9). The performance of CRHM for the 0.45 km² sub-basin when forced with ANUSPLIN temperature and precipitation was closer to simulated runoff using observed data

when compared to forcing with either ERA-Interim or MERRA-2. The metrics (Figure 2.9) for ANUSPLIN forced simulated runoff had a smaller ME (-0.25), MAE (0.41), RSME (1.35), but also a higher NSE (0.46), WB (0.60), and R (0.70).

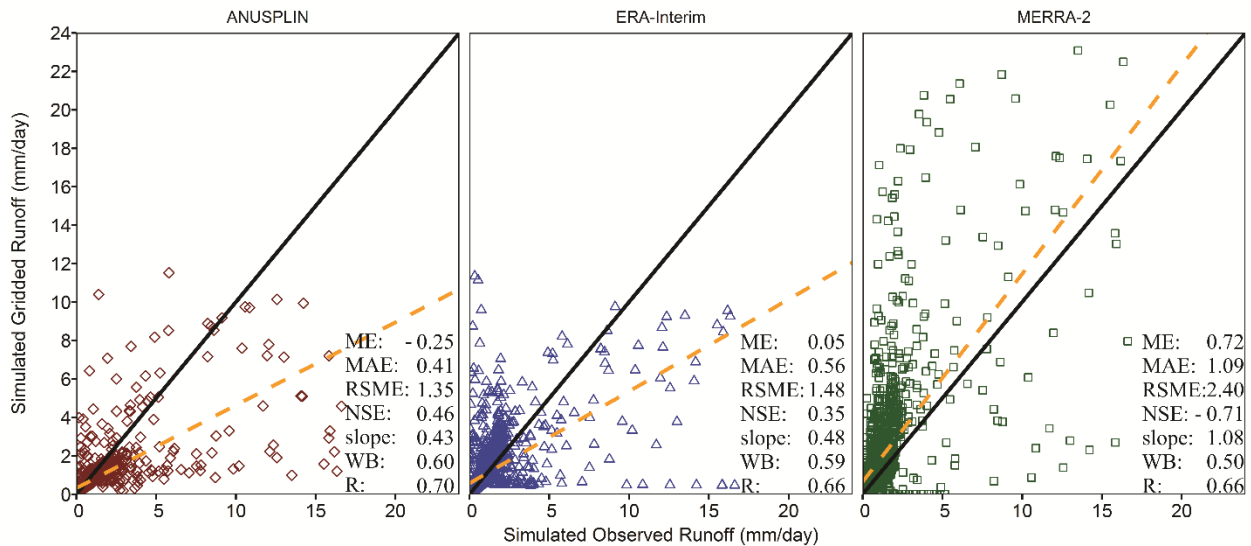


Figure 2.9 Comparing daily simulated runoff forced by observations against forces by gridded data. Dashed line is the regression line of the gridded data to the observations, and the black line is the 1:1 line; also presented are the mean error (ME), mean absolute error (MAE), root mean square error (RSME), Nash-Sutcliffe model efficiency (NSE), and Wang-Bovic statistic (WB). The total number of observations is 1825.

Runoff simulations forced by gridded datasets were different ($KS\ p \leq 0.05$) from simulations using observations. Simulated hydrographs driven with the three gridded dataset captured events that are typical for Scotty Creek (Figure 2.10) (Quinton *et al.*, 2011), spring freshet in April/May, and baseflow-dominated runoff during October to March. But, considerable variability existed among the hydrographs driven by the three types of gridded precipitation and air temperature datasets (Figure 2.10). While the population statistics for ERA-Interim were similar to those for ANUSPLIN forcing (Figure 2.9), the simulated ERA-Interim hydrograph showed an earlier freshet

date and a lower peak runoff (Figure 2.10). The MERRA-2 driven hydrograph had the greatest difference from observations; the peak generated by snowmelt was the most delayed but was also nearly three-times higher than the peak simulated with observations (Figure 2.10). MERRA-2 forcings also produced further runoff events during the summer period. The hydrograph forced by ANUSPLIN was most similar to that forced by observations in terms of both timing and magnitude. The fluctuations of the ERA-Interim hydrograph were greater than the relatively muted ANUSPLIN hydrograph but not as great as those produced using MERRA-2 forcings. Flow duration curves (Figure 2.10 inset) showed that ANUSPLIN and ERA-Interim forcings resulted in flows quite similar in probability to observations. MERRA-2 systemically overestimated high runoff and consistently underestimated low runoff (Figure 2.10 inset).

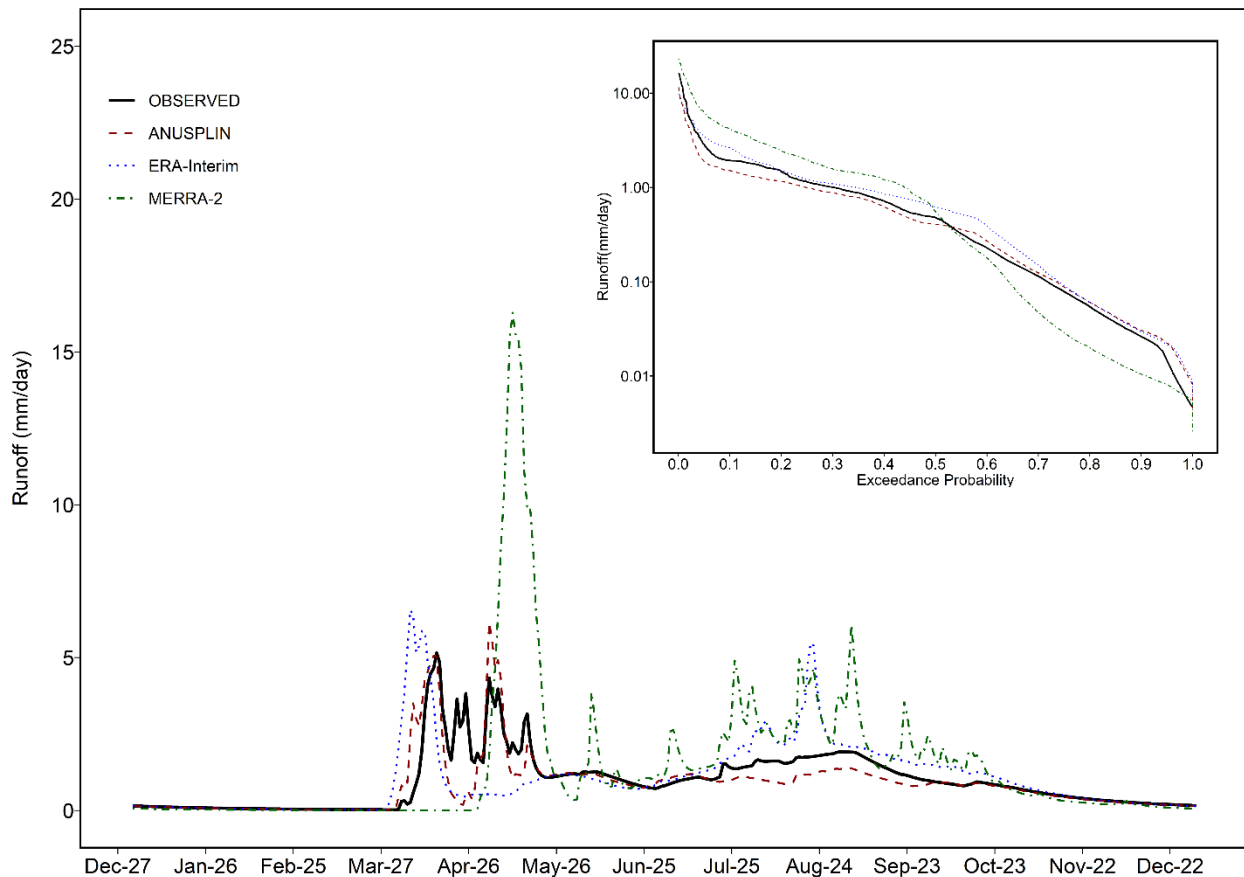


Figure 2.10 Daily simulated runoff using Cold Region Hydrological Model (CRHM) for a 0.45 km² drainage area at Scotty Creek for 2011 when driven by temperature and precipitation input from observations, and ANUSPLIN, ERA-Interim and MERRA-2 datasets. Inset: Flow duration curves for runoff (on a log scale) simulated using CRHM driven by four different input forcing datasets (temperature and precipitation): observations and three different gridded datasets.

2.6 Discussion

Gridded datasets are a reasonable alternative source of surface meteorological forcings (e.g., Essou et al., 2016; Islam & Déry, 2017; Ledesma & Futter, 2017; Way et al., 2017), but it is important to evaluate and assess gridded products at the specific scale at which they will be used (Wong et al., 2017). In hydrological applications, such as watershed modelling, biases in forcing data at any scale have the potential to affect the results. Population statistics alone (mean and variance) may

be relevant when considering annual differences and trends, but are not sufficient evidence that the dataset will be suitable for use at finer time scales as is done in hydrological simulations. Observations and gridded datasets can differ in fundamental statistical characteristics such as their shape, skewness, and tail behaviour (Director & Bornn, 2015). Systematically evaluating gridded datasets is essential (Lindsay et al., 2014) not only to determine their suitability for a specific use but to quantify uncertainties (Crout et al., 2008; Jain & Sudheer, 2008; Bennett et al., 2013; Mo et al., 2014). If gridded datasets are to be used to strengthen knowledge of hydroclimatic and extreme processes, their biases and uncertainties should be made available (Dee et al., 2011b).

Ideally, truly independent station observations would be used to validate gridded datasets. Trubilowicz *et al.* (2016) bridged the gap in scales between a reanalysis product and point locations in mountainous terrain using observations from a short temporal period (<3 years) and a different gridded dataset. In the absence of a sufficiently dense hydrometeorological observing network in the NWT, options for assessing the different gridded products with independent stations observations are limited. Scotty Creek data were not included in the ANUSPLIN interpolation model or ERA-Interim/MERRA-2 assimilation models, but the data from this location were similar to those from Fort Simpson and other stations.

Biases that might exist in gridded products intended for use in hydrological modelling, were assessed here using three complementary approaches. If gridded products do not retain fidelity to the local scale observations it is unlikely that hydrological model performance driven by such products will be satisfactory (Ledesma & Futter, 2017). Local conditions are often not captured in the gridding process, but are integral to the observed series. ANUSPLIN interpolates between surface observations to minimize overall interpolation error, so observation points are not changed

(Hutchinson *et al.*, 2009), and local conditions are largely captured. ERA-Interim and MERRA-2 use additional information, such as remote sensing data, that captures regional scale information and might not retain the local conditions of observations.

While gridded datasets are biased, they are not necessarily worse than observations in representing the spatiotemporal distribution of temperature and precipitation at larger scales over the southern NWT. The quality of gridded products is directly linked to the number of observation stations and quality of observations used in the interpolation processes (Haylock *et al.*, 2008) and assimilation processes (Dee *et al.*, 2011a; Reichle *et al.*, 2017). For example, observations collected using various types of instruments and applying different correction methods may also lead to different results (Taskinen & Söderholm, 2016). Some differences between observations and gridded products can be attributed to the challenges in measuring solid precipitation in northern Canada (Bonsal & Kochtubajda, 2009). The biases in ANUSPLIN are not as large as would be expected given that the observation data in northern Canada are approximately 20 times sparser than in southern Canada (Hutchinson *et al.*, 2009). The biases in MERRA-2 may be attributed to the fact that the precipitation correction in MERRA-2 did not extend into high latitudes (Reichle *et al.*, 2017).

Previous studies evaluated the mean and variance of individual gridded datasets on coarse time scales, such as annual, seasonal, and monthly (Rapaić *et al.*, 2015; Henn *et al.*, 2018). That approach is insufficient for applications such as hydrological modelling, where daily or hourly scales are important. In many applications, understanding how well-gridded datasets mimic the statistical properties of observations, particularly the temporal structure and the tails of the distributions, can their appropriateness be determined. The larger set of metrics used here provides

a thorough, but not exhaustive, characterization of how well or how poorly these gridded datasets compare to the observational record in the time domain. High values of similarity metrics such as correlation coefficients or Nash-Sutcliffe Efficiency do not necessarily imply high distributional or temporal structure similarity (Mo et al., 2014). The results here are consistent with the general findings of Wong et al. (2017) and Diaconescu et al. (2018); however, the graphical techniques presented provide additional insight into the shortcomings of gridded datasets which may not be evident in statistical performance measures (Crout et al., 2008). For example, in MERRA-2 T_{\max} (Figure 2.4c) there is a clear discontinuity where the gridded temperatures are near 0°C .

Air temperature and snow depth are two important climatic variables that determine the existence of permafrost in the NWT (Rouse et al., 1997). Datasets with systematic biases in T_{\max} near 0°C (e.g., Figure 2.4c) should be avoided in process based studies since feedbacks in permafrost terrain at these latitudes are often poorly simulated (Hagemann et al., 2016). The extent and the timing of near-surface permafrost degradation is sensitive to biases in forcing datasets and could affect the understanding of future behaviour (Slater & Lawrence, 2013).

Using different input forcings for CRHM simulations, at Scotty Creek, demonstrated the impacts on streamflow simulations of using gridded temperature and precipitation datasets as a substitute for observations. CRHM runoff simulations forced by ANUSPLIN, and ERA-Interim are generally encouraging; they match reasonably well the freshet timing and baseflow magnitude (Figure 2.10). Small biases in forcing will not necessarily mean that models will unrealistically simulate all details in a hydrological regime (Essou *et al.*, 2016). Simulated hydrographs for the Fraser River Basin using ANUSPLIN forcings (Islam & Déry, 2017) are similar to observed hydrographs; as are those for Scotty Creek. Adequately representing temperature and precipitation seasonality is

important. The precipitation biases during spring and summer (Figure 2.7b), suggest that the liquid phase precipitation is over estimated and that these biases from gridded datasets cascade into the simulated runoff for Scotty Creek. For example, the seasonal biases identified in MERRA-2 temperature and precipitation (Figures 2.7) result in overestimated runoff and poor matching of the timing and magnitude of peaks (Figure 2.10).

The differences between gridded datasets and observations limit how temperature and precipitation can be incorporated into hydrological modelling. Part of these differences is the result of averaging precipitation over a single ($>1000 \text{ km}^2$) grid cell as opposed to a single point observation at Scotty Creek, capturing regional scales at the cost of local scales. Interpolated distance and the spatial resolution of the gridded product may not be detailed enough to drive a hydrologic model for small-scale catchments (e.g. MERRA-2). There are also concerns about the representativeness of using point precipitation observations as an input to support hydrological models that represent a large basin. Statistical interpolation of station-point observations to create locally relevant high-resolution gridded datasets over the conterminous United States resulted in averages that were unchanged across grid scales from 500 m to 32 km (Thornton et al., 1997). Comparing the statistical characteristics of daily precipitation time series from station observations with those time-series from areal-mean sources is difficult (Osborn & Hulme, 1997); precipitation responses tend to be small scale processes which can be sometimes less than the size of the grid boxes so anomalies can occur. When data are interpolated to represent a larger area, smoothing can produce variables which have statistical characteristics that are different from those of the station observations (Haylock et al., 2008; Diaconescu et al., 2018). Spatial matching between gridded datasets and station observations will never be perfect (Sapiano & Arkin, 2009). Using forcing

datasets from large grid cells may reduce local information important in small subcatchments (such as Scotty Creek) as could using gridded land use, soil, and slope information in such a model. Where gridded datasets are used in place of observations, these types of biases need to be recognized and acknowledged. The reasons behind these potentially correlated errors between gridded dataset and CRHM are left as a subject for future research.

The day on which melt and freezing start in the gridded dataset does not always match observations (Figure 2.8) and led to incorrect timing of freshet. These differences are a critical concern for peak flow in a small watershed and subsequent hydroclimatic analysis that without correction will be biased. Despite this, the timing of peak runoff performance was notably better here when compared with the findings of the Mackenzie GEWEX Study (Szeto et al., 2008) where modelled peak runoff occurred two months earlier than the observed peak over MRB using the ERA-40 gridded dataset. At Scotty Creek, ERA-Interim forced hydrograph had earlier peak flows (~ 2 weeks) during the spring freshet (Figure 2.10) highlighting an improvement made in ERA-Interim. This improvement maybe also attributed other factors such as the differences in spatial scales used in the hydrological simulations; in this study, simulations were done at microscale ($< 1\text{km}^2$) while simulations for MRB were done at large scale ($>1000\text{km}^2$) (Szeto et al., 2008). Future studies should replicate MAGs using different hydrological models and gridded datasets that have improved spatial and temporal resolution and assimilation schemes such as the recently released ERA5 global reanalysis dataset from ECMWF, which succeeds ERA-Interim (Hersbach et al., 2018).

The evaluation undertaken here does not diagnose sources of uncertainty of individual gridded dataset and model performance, but demonstrates a robust analysis to provide qualitative

information about how biases in daily temperatures and precipitation may impact simulated runoff at Scotty Creek. Since the means and standard deviations of the distributions of precipitation in gridded datasets (ERA-interim and MERRA-2) are different than observations, the results of models using those datasets will contain bias. The differences in moments between the gridded data and observations suggests that CRHM model results will differ from those driven by observations and will depend upon the differences between these moments. For example, none of the gridded datasets were able to robustly reproduce the observed daily precipitation skewness and kurtosis. This also led to bias in simulated runoff suggesting the assimilation/interpolation schemes are failing to represent the some of the non-linear and/or temporal aspects of gridded precipitation. Higher order moments comparisons are often neglected (Maeda et al., 2013; Director & Bornn, 2015), and should be either point-level to point-level distributions, or gridded to gridded distributions to reduce the inherent bias (Director & Bornn, 2015).

While there is no measured hydrograph for the 0.45km² subcatchment at Scotty Creek to compare hydrographs simulated by CRHM; a simulated hydrograph using observations was similar to the observed hydrograph for another sub-catchment within Scotty Creek (Connon et al., 2015). Small catchments, such as Scotty Creek, are widely used for studying hydrological processes across the NWT (e.g., Connon et al., 2014; Shi et al., 2015) and in other regions globally (Ledesma & Futter, 2017) but historical climate data are generally limited. Downscaling temperature and precipitation from gridded datasets to the Scotty Creek catchment may introduce additional errors or uncertainties (Gervais et al., 2014). Despite the scaling issues, understanding the model sensitivities to differences in gridded products are necessary. Until more long-term observation

data become available, understanding the limitations of gridded datasets is important when used in process-based hydrological studies.

2.7 Conclusions

Attributes of temperature and precipitation from ANUSPLIN, ERA-Interim, and MERRA-2 were compared to station observations using population statistics and temporal structure of the entire distribution for the period between 1980 and 2013. The feasibility of using these datasets as hydrological model inputs within the southern NWT was explored. The main findings are summarised as follows:

1. Overall, despite some limitations, the gridded datasets have strong skill in simulating daily T_{\max} and T_{\min} observations over southern NWT and have potential for use as proxies as surface observations in data-sparse NWT. Precipitation datasets perform more poorly. ANUSPLIN, a gridded interpolation between stations, is most consistent with observations, while ERA-Interim and MERRA-2 showed promising performance.
2. The existing hydrometeorological network in the NWT does not have sufficient detail to understand the implications of current climate warming on the NWT water resources; hence, gridded datasets can be a source of information to strengthen our knowledge on the climate processes across the region. ANUSPLIN can be used as input forcing to understand current and future climate processes across the NWT, but the biases of ERA-Interim and MERRA-2 temperature and precipitation demand a thorough examination of the impacts

those biases would introduce before they are used in hydroclimate analysis in the data-sparse southern NWT.

3. This study demonstrated that when comparing two hydroclimate datasets, it is important to use multiple statistical techniques, to ensure that the structural attributes of the datasets are adequately understood by users. Results show that while similarity performance measures are good on comparing the means, they may mask discrepancies in the variance. By using PDF and other evaluation metrics, this research highlighted the presence of systematic biases in certain parts of the distribution for all three gridded datasets. Users are encouraged to do a robust evaluation using multiple assessment methods to assess their use in hydroclimate applications as continuing improvements in gridded datasets are expected to reduce the biases reported here.

While gridded datasets are no substitute for high-quality long time series observations, they may be useful where there are limited long-term observational data both spatially and temporally. These gridded datasets, despite their limitations in capturing local conditions, are useful for broad-scale and regional assessments and can be applied to improve understanding in hydrometeorological processes in data-sparse regions if used with caution. This information, used with understanding of its limitations, can aid improving and developing reliable hydrometeorological models that will assist NWT communities to understand current and future hydrometeorological scenarios assess future impacts.

2.8 Acknowledgements

Funding for this work was provided by Wilfrid Laurier University, the Government of the Northwest Territories and the Natural Sciences and Engineering Research Council of Canada. We appreciate Environment and Climate Change Canada, NASA and ECMWF for making climate data, MERRA-2, and ERA-interim datasets freely available via their respective websites. The authors thank Drs. Daniel McKenny and Pia Papadopol from Natural Resources Canada for providing ANUSPLIN daily gridded temperature and precipitation datasets for the study domain. The efforts of the R Development Core Team and authors of the packages in Table S2.1 are appreciated. We thank Drs. Justin Adams, Ryan Connon and Kristine Hayes for useful comments that have helped to improve earlier versions of this manuscript. Two anonymous reviewers and the handling and associate editors provided constructive comments that greatly improved the paper.

2.9 Data Availability Statement

Gridded datasets used in this study can be obtained from public sources provided in Table 2.1 With the exception of Scotty Creek, all observations are available from Environment and Climate Change Canada website. Scotty Creek datasets are available upon request by contacting the Dr William Quinton at Wilfrid Laurier University.

2.10 References

- Beilman, D. W., & Robinson, S. D. (2003). Peatland permafrost thaw and landform type along a climatic gradient. In S. & A. Permafrost, Phillips (Ed.), *Proceedings of the 8th International Conference on Permafrost* (pp. 61–65). Retrieved from https://www.arlis.org/docs/vol1/ICOP/55700698/Pdf/Chapter_012.pdf.
- Bennett, N. D., Croke, B. F. W., Guariso, G., Guillaume, J. H. A., Hamilton, S. H., Jakeman, A. J., ... Andreassian, V. (2013). Characterising performance of environmental models. *Environmental Modelling and Software*, *40*, 1–20. doi: <https://doi.org/10.1016/j.envsoft.2012.09.011>.
- Bonsal, B. R., & Kochtubajda, B. (2009). An assessment of present and future climate in the Mackenzie Delta and the near-shore Beaufort Sea region of Canada. *International Journal of Climatology*, *29*(12), 1780–1795. doi: <https://doi.org/10.1002/joc.1812>.
- Bosilovich, M., Akella S., Coy L., Cullather, R., Draper. C., Gelaro R., ... Suarez, M. (2015). *MERRA-2: Initial evaluation of the climate Technical Report Series on Global Modeling and Data Assimilation* (Vol. 43). NASA/TM–2015-104606. Available online at <https://gmao.gsfc.nasa.gov/pubs/docs/Bosilovich803.pdf>.
- Breusch, T. S., & Pagan, A. R. (2006). A simple test for heteroscedasticity and random coefficient variation. *Econometrica*, *47*(5), 1287. doi: <https://doi.org/10.2307/1911963>.
- Chen, J., & Brissette, F. P. (2017). Hydrological modelling using proxies for gauged precipitation and temperature. *Hydrological Processes*, *31*(22), 3881–3897. doi: <https://doi.org/10.1002/hyp.11304>.

- Cole, R. A. J., Johnston, H. T., & Robinson, D. J. (2003). The use of flow duration curves as a data quality tool. *Hydrological Sciences Journal*, 48(6), 939–952. doi: <https://doi.org/10.1623/hysj.48.6.939.51419>.
- Connon, R. F., Quinton, W. L., Craig, J. R., Hanisch, J., & Sonnentag, O. (2015). The hydrology of interconnected bog complexes in discontinuous permafrost terrains. *Hydrological Processes*, 29(18), 3831–3847. doi: <https://doi.org/10.1002/hyp.10604>.
- Connon, R. F., Quinton, W. L., Craig, J. R., & Hayashi, M. (2014). Changing hydrologic connectivity due to permafrost thaw in the lower Liard River valley, NWT, Canada. *Hydrological Processes*, 28(14), 4163–4178. doi: <https://doi.org/10.1002/hyp.10206>.
- Cornes, R. C., & Jones, P. D. (2013). How well does the ERA-Interim reanalysis replicate trends in extremes of surface temperature across Europe? *Journal of Geophysical Research: Atmospheres*, 118(18), 10,262–10,276. doi: <https://doi.org/10.1002/jgrd.50799>.
- Crout, N., Kokkonen, T., Jakeman, A. J., Norton, J. P., Newham, L. T. H., Anderson, R., ... & Whitfield P. (2008). Chapter 2: Good modelling practice. In: *Environmental Modelling, Software and Decision Support*, A. J. Jakeman, A. A. Voinov, A. E. Rizzoli, and S. H. Chen. (eds). Amsterdam. Elsevier. pp 15-31.
- Dee, D. P., Uppala, S. M., Simmons, a. J., Berrisford, P., Poli, P., Kobayashi, S., ... Vitart, F. (2011a). The ERA-Interim reanalysis: Configuration and performance of the data assimilation system. *Quarterly Journal of the Royal Meteorological Society*, 137(656), 553–597. doi: <https://doi.org/10.1002/qj.828>.

- Dee, D. P., Källén, E., Simmons, A. J., & Haimberger, L. (2011b). Reanalyses suitable for characterizing long-term trends. *Bulletin of the American Meteorological Society*. doi: <https://doi.org/10.1175/2010BAMS3070.1>.
- Diaconescu, E. P., Mailhot, A., Brown, R., & Chaumont, D. (2018). Evaluation of CORDEX-Arctic daily precipitation and temperature-based climate indices over Canadian Arctic land areas. *Climate Dynamics*, *50*(5–6), 2061–2085. doi: <https://doi.org/10.1007/s00382-017-3736-4>.
- Director, H., & Bornn, L. (2015). Connecting point-level and gridded moments in the analysis of climate data. *Journal of Climate*, *28*(9), 3496–3510. doi: <https://doi.org/10.1175/JCLI-D-14-00571.1>.
- Essou, G. R. C., Sabarly, F., Lucas-Picher, P., Brissette, F., & Poulin, A. (2016). Can precipitation and temperature from meteorological reanalyses be used for hydrological modeling? *Journal of Hydrometeorology*, *17*(7), 1929–1950. doi: <https://doi.org/10.1175/jhm-d-15-0138.1>.
- Fang, X., Pomeroy, J. W., Westbrook, C. J., Guo, X., Minke, A. G., & Brown, T. (2010). Prediction of snowmelt derived streamflow in a wetland dominated prairie basin. *Hydrology and Earth System Sciences*, *14*(6), 991–1006. doi: <https://doi.org/10.5194/hess-14-991-2010>.
- Field, C. B., Barros, V., Stocker, T. F., & Dahe, Q. (Eds.). (2012). Managing the risks of extreme events and disasters to advance climate change adaptation: special report of the intergovernmental panel on climate change. *Cambridge University Press*.

- Hagemann, S., Blome, T., Ekici, A., & Beer, C. (2016). Soil-frost-enabled soil-moisture-precipitation feedback over northern high latitudes. *Earth System Dynamics*, 7(3), 611–625. doi: <https://doi.org/10.5194/esd-7-611-2016>.
- Haylock, M. R., Hofstra, N., Klein Tank, A. M. G., Klok, E. J., Jones, P. D., & New, M. (2008). A European daily high-resolution gridded data set of surface temperature and precipitation for 1950-2006. *Journal of Geophysical Research-Atmospheres*, 113(20). doi: <https://doi.org/10.1029/2008JD010201>.
- Henn, B., Newman, A. J., Livneh, B., Daly, C., & Lundquist, J. D. (2018). An assessment of differences in gridded precipitation datasets in complex terrain. *Journal of Hydrology*, 556, 1205–1219. doi: <https://doi.org/10.1016/j.jhydrol.2017.03.008>.
- Hersbach, H., de Rosnay, P., Bell, B., Schepers, D., Simmons, A., Soci, C.,... & Zuo, H. (2018). Operational global reanalysis: progress, future directions and synergies with NWP, ERA Report Series 27, European Centre for Medium Range Weather Forecasts, Reading, UK. Doi: doi: <https://doi.org/10.21957/tkic6g3wm>.
- Hutchinson, M. F., McKenney, D. W., Lawrence, K., Pedlar, J. H., Hopkinson, R. F., Milewska, E., & Papadopol, P. (2009). Development and testing of Canada-wide interpolated spatial models of daily minimum-maximum temperature and precipitation for 1961-2003. *Journal of Applied Meteorology and Climatology*, 48(4), 725–741. doi: <https://doi.org/10.1175/2008JAMC1979.1>.

- Islam, S., & Déry, S. J. (2017). Evaluating uncertainties in modelling the snow hydrology of the Fraser River Basin, British Columbia, Canada. *Hydrology and Earth System Sciences*, 21(3), 1827–1847. doi: <https://doi.org/10.5194/hess-21-1827-2017>.
- Jain, S. K., & Sudheer, K. P. (2008). Fitting of hydrologic models: a close look at the Nash–Sutcliffe index. *Journal of Hydrologic Engineering*, 13(10), 981–986.
[https://doi.org/10.1061/\(ASCE\)1084-0699\(2008\)13:10\(981\)](https://doi.org/10.1061/(ASCE)1084-0699(2008)13:10(981)).
- Klein Tank, A. M. G., Zwiers, F. W., & Zhang, X. (2009). *Guidelines on analysis of extremes in a changing climate in support of informed decisions for adaptation. Climate Data and Monitoring* (WMO/TD-No). World Meteorological Organization (WMO). Retrieved from https://library.wmo.int/index.php?lvl=notice_display&id=138#.XL3ug-hKguV.
- Ledesma, J. L. J., & Futter, M. N. (2017). Gridded climate data products are an alternative to instrumental measurements as inputs to rainfall–runoff models. *Hydrological Processes*, 31(18), 3283–3293. doi: <https://doi.org/10.1002/hyp.11269>.
- Lindsay, R., Wensnahan, M., Schweiger, A., & Zhang, J. (2014). Evaluation of seven different atmospheric reanalysis products in the Arctic. *Journal of Climate*, 27(7), 2588–2606. doi: <https://doi.org/10.1175/JCLI-D-13-00014>.
- Liu, J., Cho, H., & Stewart, R. E. (2007). Characteristics of the water vapour transport over the Mackenzie River basin during the 1994/95 water year. *Atmosphere-Ocean*, 40(2), 101–111. doi: <https://doi.org/10.3137/ao.400202>.

- Louie, P. Y. T., Hogg, W. D., MacKay, M. D., Zhang, X., & Hopkinson, R. F. (2002). The water balance climatology of the Mackenzie basin with reference to the 1994/95 water year. *Atmosphere - Ocean*, 40(2), 159–180. doi: <https://doi.org/10.3137/ao.400206>.
- Maeda, E. E., Arevalo Torres, J., & Carmona-Moreno, C. (2013). Characterisation of global precipitation frequency through the L-moments approach. *Area*, 45(1), 98-108. doi: <https://doi.org/10.1111/j.1475-4762.2012.01127>.
- McCarty, W., Coy, L., Gelaro, R., Huang, A., Merkova, D., Smith, E. B., ... Wargan, K. (2016). MERRA-2 Input observations: Summary and assessment. *Technical Report Series on Global Modeling and Data Assimilation*, 46(October). Retrieved from <https://gmao.gsfc.nasa.gov/pubs/docs/McCarty885.pdf>.
- Mo, R., Ye, C., & Whitfield, P. H. (2014). Application potential of four nontraditional similarity metrics in hydrometeorology. *Journal of Hydrometeorology*, 15(5), 1862–1880. doi: <https://doi.org/10.1175/jhm-d-13-0140.1>.
- Nash, J. E., & Sutcliffe, J. V. (1970). River flow forecasting through conceptual models part I — A discussion of principles. *Journal of Hydrology*, 10(3), 282–290. doi: [https://doi.org/10.1016/0022-1694\(70\)90255-6](https://doi.org/10.1016/0022-1694(70)90255-6).
- Osborn, T. J., & Hulme, M. (1997). Development of a relationship between station and grid-box rainday frequencies for climate model evaluation. *Journal of Climate*, 10(8), 1885–1908. doi: [https://doi.org/10.1175/1520-0442\(1997\)010<1885:DOARBS>2.0.CO;2](https://doi.org/10.1175/1520-0442(1997)010<1885:DOARBS>2.0.CO;2).
- Phillips, D. (1990). The Climates of Canada, Catalogue No. En56-1/1990E ISSN 0-660-13459-4. Minister of Supply and Services Canada, Ottawa, Canada. 176 pp.

- Pomeroy, J. W., Gray, D. M., Brown, T., Hedstrom, N. R., Quinton, W. L., Granger, R. J., & Carey, S. K. (2007). The cold regions hydrological model: A platform for basing process representation and model structure on physical evidence. *Hydrological Processes*, *21*(19), 2650–2667. doi: <https://doi.org/10.1002/hyp.6787>.
- Price, D. T., Alfaro, R. I., Brown, K. J., Flannigan, M. D., Fleming, R. A., Hogg, E. H., ... Venier, L. A. (2013). Anticipating the consequences of climate change for Canada's boreal forest ecosystems. *Environmental Reviews*, *21*(4), 322–365. doi: <https://doi.org/10.1139/er-2013-0042>.
- Quinton, W. L., & Baltzer, J. L. (2013). The active-layer hydrology of a peat plateau with thawing permafrost (Scotty Creek, Canada). *Hydrogeology Journal*, *21*(1), 201–220. doi: <https://doi.org/10.1007/s10040-012-0935-2>.
- Quinton, W. L., Hayashi, M., & Chasmer, L. E. (2011). Permafrost-thaw-induced land-cover change in the Canadian subarctic: implications for water resources. *Hydrological Processes*, *25*(1), 152–158. doi: <https://doi.org/10.1002/hyp.7894>.
- R Development Core Team. 2016. R: A language and environment for statistical computing: R Foundation for Statistical Computing. <https://www.R-project.org/>.
- Rapaić, M., Brown, R., Markovic, M., & Chaumont, D. (2015). An evaluation of temperature and precipitation surface-based and reanalysis datasets for the Canadian Arctic, 1950-2010. *Atmosphere - Ocean*, *53*(3), 283–303. doi: <https://doi.org/10.1080/07055900.2015.1045825>.

- Reichle, R. H., Liu, Q., Koster, R. D., Draper, C. S., Mahanama, S. P., & Partyka, G. S. (2017). Land surface precipitation in MERRA-2. *Journal of Climate*, 30(5), 1643-1664. doi: <https://doi.org/10.1175/JCLI-D-16-0570.1>.
- Richter-Menge, J., Overland, J. E., & Mathis, J. T. (2017). *Arctic Report Card, 2017*. <https://arctic.noaa.gov/Report-Card/Report-Card-2017>.
- Rienecker, M. M., Suarez, M. J., Gelaro, R., Todling, R., Bacmeister, J., Liu, E., ... Woollen, J. (2011). MERRA: NASA's Modern-Era Retrospective Analysis for Research and Applications. *Journal of Climate*, 24(14), 3624–3648. doi: <https://doi.org/10.1175/JCLI-D-11-00015.1>.
- Rouse, W. R., Douglas, M. S., Hecky, R. E., Hershey, A. E., Kling, G. W., Lesack, L., ... & Smol, J. P. (1997). Effects of climate change on the freshwaters of arctic and subarctic North America. *Hydrological Processes*, 11(8), 873–902. [https://doi.org/10.1002/\(SICI\)1099-1085\(19970630\)11:8<873::AID-HYP510>3.0.CO;2-6](https://doi.org/10.1002/(SICI)1099-1085(19970630)11:8<873::AID-HYP510>3.0.CO;2-6).
- Rowland, J. C., Jones, C. E., Altmann, G., Bryan, R., Crosby, B. T., Geernaert, G. L., ... Wilson, C. J. (2010). Arctic landscapes in transition: Responses to thawing permafrost. *Eos*, 91(26), 229–230. doi: <https://doi.org/10.1029/2010EO260001>.
- Sapiano, M. R. P., & Arkin, P. A. (2008). An intercomparison and validation of high-resolution satellite precipitation estimates with 3-hourly gauge data. *Journal of Hydrometeorology*, 10(1), 149–166. doi: <https://doi.org/10.1175/2008jhm1052.1>.

- Shi, X., Marsh, P., & Yang, D. (2015). Warming spring air temperatures, but delayed spring streamflow in an Arctic headwater basin. *Environmental Research Letters*, 10(6). doi: <https://doi.org/10.1088/1748-9326/10/6/064003>.
- Slater, A. G., & Lawrence, D. M. (2013). Diagnosing present and future permafrost from climate models. *Journal of Climate*, 26(15), 5608–5623. doi: <https://doi.org/10.1175/JCLI-D-12-00341.1>.
- Snauffer, A. M., Hsieh, W. W., & Cannon, A. J. (2016). Comparison of gridded snow water equivalent products with *in situ* measurements in British Columbia, Canada. *Journal of Hydrology*, 541, 714–726. doi: <https://doi.org/10.1016/j.jhydrol.2016.07.027>.
- St. Jacques, J. M., & Sauchyn, D. J. (2009). Increasing winter baseflow and mean annual streamflow from possible permafrost thawing in the Northwest Territories, Canada. *Geophysical Research Letters*, 36(1), 1–6. doi: <https://doi.org/10.1029/2008GL035822>.
- Stone, L.E., Fang, F., Haynes, K.M., Helbig, M., Pomeroy, J.W., Sonnentag, O., & Quinton, W.L. (2019) Modelling the effects of permafrost loss on discharge from a wetland-dominated basin in the discontinuous permafrost zone in northwestern Canada. *Hydrological Processes*. doi: <https://doi.org/10.1002/hyp.13546>.
- Szeto, K. K., Tran, H., MacKay, M., Crawford, R., & Stewart, R. E. (2008). *Assessing water and energy budgets for the Mackenzie River Basin*. (M.-K. Woo, Ed.), *Cold Region Atmospheric and Hydrologic Studies. The Mackenzie GEWEX Experience: Volume 1: Atmospheric Dynamics*. Springer Berlin Heidelberg. doi: https://doi.org/10.1007/978-3-540-73936-4_16.

- Taskinen, A., & Söderholm, K. (2016). Operational correction of daily precipitation measurements in Finland. *Boreal Environment Research*, 21(1–2), 1–24. Retrieved from doi: <http://hdl.handle.net/10138/225261>.
- Thornton, P. E., Running, S. W., & White, M. A. (1997). Generating surfaces of daily meteorological variables over large regions of complex terrain. *Journal of Hydrology*, 190(3–4), 214–251. doi: [https://doi.org/10.1016/S0022-1694\(96\)03128-9](https://doi.org/10.1016/S0022-1694(96)03128-9).
- Trubilowicz, J. W., Shea, J. M., Jost, G., & Moore, R. D. (2016). Suitability of North American Regional Reanalysis (NARR) output for hydrologic modelling and analysis in mountainous terrain. *Hydrological Processes*, 30(13), 2332–2347. doi: <https://doi.org/10.1002/hyp.10795>.
- Uppala, S. M., Kållberg, P. W., Simmons, A. J., Andrae, U., da Costa Bechtold, V., Fiorino, M., ... Woollen, J. (2005). The ERA-40 re-analysis. *Quarterly Journal of the Royal Meteorological Society*, 131(612), 2961–3012. doi: <https://doi.org/10.1256/qj.04.176>.
- Vincent, L. A., Zhang, X., Brown, R. D., Feng, Y., Mekis, E., Milewska, E. J., ... Wang, X. L. (2015). Observed trends in Canada's climate and influence of low-frequency variability modes. *Journal of Climate*, 28(11), 4545–4560. doi: <https://doi.org/10.1175/JCLI-D-14-00697.1>.
- Wang, Z., & Bovik, A. C. (2002). A universal image quality index. *IEEE Signal Processing Letters*, 9(3), 81–84. doi: <https://doi.org/10.1109/97.995823>.
- Way, R. G., Oliva, F., & Viau, A. E. (2017). Underestimated warming of northern Canada in the Berkeley Earth temperature product. *International Journal of Climatology*, 37(4), 1746–1757. doi: <https://doi.org/10.1002/joc.4808>.

- Whitfield, P. H., & Cannon, A. J. (2000). Recent variations in climate and hydrology in Canada. *Canadian Water Resources Journal*, 25(1), 19–65. doi: <https://doi.org/10.4296/cwrj2501019>.
- Whitfield, P. H., Hall, A. W., & Cannon, A. J. (2004). Changes in the seasonal cycle in the circumpolar Arctic, 1976-95: Temperature and precipitation. *Arctic*, 57(1), 80–93. doi: <https://doi.org/10.14430/arctic485>.
- Wilby, R. L., Clifford, N. J., De Luca, P., Harrigan, S., Hillier, J. K., Hodgkins, R., ... Wood, P. J. (2017). The ‘dirty dozen’ of freshwater science: detecting then reconciling hydrological data biases and errors. *Wiley Interdisciplinary Reviews: Water*, 4(3), e1209. doi: <https://doi.org/10.1002/wat2.1209>.
- Wilks, D.S. (2006). *Statistical Methods in the Atmospheric Sciences*, 2nd edition. Academic Press: San Diego US.
- Wong, J. S., Razavi, S., Bonsal, B. R., Wheeler, H. S., & Asong, Z. E. (2017). Inter-comparison of daily precipitation products for large-scale hydro-climatic applications over Canada. *Hydrology and Earth System Sciences*, 21(4), 2163–2185. doi: <https://doi.org/10.5194/hess-21-2163-2017>.
- Woo, M. K., & Thorne, R. (2006). Snowmelt contribution to discharge from a large mountainous catchment in subarctic Canada. *Hydrological Processes*, 20(10), 2129–2139. doi: <https://doi.org/10.1002/hyp.6205>.
- Woo M., & Rouse W.R. (2008) MAGS contribution to hydrologic and surface process research. In: Woo M. (eds) Cold Region Atmospheric and Hydrologic Studies. The

Mackenzie GEWEX Experience (Vol.2). Springer, Berlin, Heidelberg. doi:
https://doi.org/10.1007/978-3-540-75136-6_2.

Wright, N., Hayashi, M., & Quinton, W. L. (2009). Spatial and temporal variations in active layer thawing and their implication on runoff generation in peat-covered permafrost terrain. *Water Resources Research*, 45(5), 1–13. doi: <https://doi.org/10.1029/2008WR006880>.

Zhang, X., Alexander, L., Hegerl, G. C., Jones, P., Tank, A. K., Peterson, T. C., ... Zwiers, F. W. (2011). Indices for monitoring changes in extremes based on daily temperature and precipitation data. *Wiley Interdisciplinary Reviews: Climate Change*, 2(6), 851–870. doi: <https://doi.org/10.1002/wcc.147>.

3 Sensitivity of seasonal air temperature and precipitation, and onset of snowmelt, to Arctic dipole modes across the Taiga Plains, Northwest Territories, Canada

Chapter status

Contents of this chapter were published in International Journal of Climatology

Persaud, B. D., Chasmer, L. E., Quinton, W. L., Wolfe, B.B., & English, M.C., (2022). Sensitivity of seasonal air temperature and precipitation, and onset of snowmelt, to Arctic dipole modes across the Taiga Plains, Northwest Territories, Canada, *International Journal of Climatology* <https://doi.org/10.1002/joc.7810>

3.1 Abstract

Northern high latitudes are experiencing some of the greatest increases in air temperatures on Earth. Air temperatures (along with other modulating variables including precipitation and the onset of snowmelt) are influenced by atmospheric-oceanic circulation patterns, some of which are persistent and recurrent. One pattern in particular, the Arctic Dipole (AD) anomaly, is a persistent sea-level pressure teleconnection pattern between the Canadian Archipelago and Barents Sea that has unknown impacts on local climate variability. These patterns may be important, especially in hydro-ecologically sensitive areas such as Northwest Territories (NWT), Canada, where permafrost thaw and ecosystem changes are influenced by interannual climate variability. The goal of this research is to determine the impacts of the AD on local climate (air temperature, precipitation, snowmelt) for a 66-year period (1950–2015) spanning both latitudinal and longitudinal gradients across NWT from north to south and foothills to plains. Deviations during strong positive and negative modes of the AD index were calculated in reference to the complete 66-year record. Results showed considerable year-to-year variability in the AD pattern, with more frequent strong negative modes during the 2000s. During 1950-2015, there were 64 and 56 occurrences of strong positive and strong negative AD modes, respectively, across all seasons. Spring and summer strong AD modes led to local air temperature anomalies of greater than 0.8°C compared with the long-term (66 years) mean. Earlier onset of snowmelt, by an average of 3-5 days, was also noted during positive AD modes. Despite strong connectivity between the AD and local air temperature, we found less correspondence between the AD and seasonal precipitation. These findings improve understanding of the impacts of the AD on local weather and climate in NWT and suggest implications for ecosystem change, such as drying and shrubification of northern boreal peatlands and possible connectivity to teleconnection impacts on wildland fire.

3.2 Introduction

Global air temperatures have increased during the past century and are projected to increase in the coming decades (IPCC, 2021). High-latitude regions have been especially prone to both increases and greater range of variability in air temperatures (IPCC, 2021). The surface climate of northern Canada is largely influenced by synoptic scale atmospheric circulation patterns. The strength and location of mid-tropospheric troughs and ridges drive the movement and persistence of air masses across the region (Klock et al., 2001; Newton et al., 2014). For example, rapid warming in northern Canada, resulting in earlier snowmelt in spring and later onset of snow in autumn, impacts permafrost thaw and ecosystem change (e.g., Chasmer & Hopkinson, 2017; Connon et al., 2021). These observations have also led to increased interest in atmospheric circulation patterns and the influences that these may have on inter- and intra-annual climate variability. Climate anomalies can have numerous implications, including ecosystem threshold responses, changing hydrological processes, and ecosystem services (Newton et al., 2014; Vincent et al., 2015; Chasmer & Hopkinson, 2017; Tan et al., 2019). The combined effects of atmospheric circulations and climate change in northern Canada are not well-understood, thereby creating uncertainties in our understanding of the long-term impacts of these changes on ecosystems, water resources, and northern communities (Woo et al., 2008; Serreze & Barry, 2014; Shi et al., 2015; Vincent et al., 2015; DeBeer et al., 2016).

Variations in air temperature are driven by global atmospheric circulation, modified by recurrent and persistent atmospheric–oceanic patterns (specifically sea surface temperature–atmosphere relationships), referred to as teleconnection patterns (Wallace & Gutzler, 1981; Barnston & Livezey, 1987). Teleconnection patterns are recognized for their opposing centre of action (dipole)

of atmospheric pressures and/or sea surface air temperature anomalies, with dipoles typically located between 2,000 and 6,000 km apart. As such, these patterns influence weather and climate across various temporal and spatial scales, which are driven, in part, by phase (positive or negative) and strength. The phase and strength of the patterns vary temporally and can impact air temperature and precipitation to greater or lesser amounts, depending on location (Jiang et al., 2014; Vincent et al., 2015). The influence and magnitude of the opposing dipole systems are typically described using a teleconnection index (Barnston & Livezey, 1987).

The Arctic Oscillation (AO) is one of the dominant atmospheric circulation modes in the Northern Hemisphere and is characterized by a north–south dipole structure of the sea level pressure (SLP) pattern with one sign in the Arctic and the opposite sign at $\sim 45^\circ$ latitude (Thompson & Wallace, 1998). The positive mode of the AO index has lower SLP anomalies in the Arctic and higher SLP anomalies in the Northern Hemisphere mid-latitudes, resulting in strengthened westerlies, northward shift in the jet stream, and fewer periods of cold air outbreaks, while during the negative mode in the AO, the opposite occurs (Thompson & Wallace, 1998). Previous studies also explored the relationship between the AO and Canada's weather and climate across various temporal and spatial scales (Déry & Wood, 2004; Fleming et al., 2006; Déry et al., 2009; Bonsal & Shabbar, 2011; Tan et al., 2019). Positive AO index was associated with consistently higher spring and summer air temperatures in southwestern Yukon and northwestern British Columbia (Fleming et al., 2006), while Déry & Wood (2004) noted that between 1964 and 2000, positive AO index was associated with cooler and drier conditions over northern Canada. While the impacts of the AO are known, there may be other northern teleconnection patterns that also influence climate variability in northern high latitudes (Déry et al., 2009).

Another, lesser-known teleconnection pattern in the Arctic is the Arctic Dipole (AD) (Wu et al., 2005; Watanabe et al., 2006; Wang et al., 2009; Overland et al., 2012). The AD pattern is associated with a SLP dipole between the Canadian Archipelago and northern Siberia/ Barents Sea (Wang et al., 2009; Overland et al., 2012). Overland et al. (2012) stated when there are positive SLP anomalies in the Canadian Archipelago/Beaufort Sea and negative SLP anomalies in the northern Siberia/Barents Sea (negative AD), a strong meridional wind is observed from the western to eastern Arctic. This wind pattern has led to the movement of sea ice out of the Arctic and into the northern Atlantic Ocean via the Trans-Polar Drift Stream, resulting in warming of the Arctic (Wang et al., 2009; Overland et al., 2012). This SLP anomaly strengthens local southerly winds and promotes northward movement of warm water in the Pacific Ocean, resulting in increased oceanic heat flux into the Arctic Ocean via the Bering Strait (Wang et al., 2009; Overland et al., 2012). This impacts sea ice by accelerating melt and amplifying ice–albedo feedback (Wang et al., 2009; Lei et al., 2016; Heo et al., 2021). Overland et al. (2012) found that enhanced negative mode of the AD was coincident with dramatic ice loss in the Arctic Ocean beginning in 2007. The opposite occurs during the positive AD phase. The prominence of the AD as a driver of ice loss has raised questions pertaining to its influence on northern continental regions (Zhang et al., 2008; Wang et al., 2009; Tang et al., 2014; Choi et al., 2019; Xiao et al., 2020). These include the Northwest Territories (NWT) Canada, as sea ice reduction can influence changes of local climate extending inland (Budikova, 2009).

The AD has also been linked to various weather patterns in many regions in the Northern Hemisphere (Wu et al., 2009; Matsumura et al., 2014; Cai et al., 2018; Fazel-Rastgar, 2020; Horvath et al., 2021). For instance, Cai et al. (2018) used European Centre for Medium-Range

Weather Forecasts Reanalysis (ERA-Interim reanalysis) data and showed that for North America, higher SLP is associated with positive air temperature anomalies (greater than long-term average temperature) during summer months, while both negative and positive precipitation anomalies prevailed. Using 30 models from CMIP5 (Coupled Model Intercomparison Project Phase 5) to determine the impacts AD will have on climate from 2006 and 2100, Cai et al. (2018) predicted that atmospheric circulation patterns associated with the AD will have a larger impact on summer precipitation variability over the Arctic in the future. The heatwaves during summer 2007, 2012, and 2016 in the Canadian Arctic were also attributed to the AD (Fazel-Rastgar, 2020) indicating that severe weather anomalies may be associated with these patterns. There is also evidence to suggest that the dipole pattern has become more pronounced since the 2000s with stronger high and low SLP anomalies and high AD index values (Overland et al., 2012). This has been linked to earlier spring snowmelt between 1988 and 2011 in Eurasia and associated with positive SLP anomaly over the Arctic and negative SLP anomaly over Eurasia (Matsumura et al., 2014). Horvath et al. (2021) also found earlier melt onset during positive SLP dipole over the Arctic over a longer temporal period (1979–2018). In Canada, increasing temperature and decreasing snow cover indices are only partly explained by other teleconnections (Vincent et al., 2015). These authors concluded that anthropogenic forces were responsible for most of the observed changes in climate variables in Canada (Vincent et al., 2015). However, these authors did not examine the influence of AD circulation on Canada's weather and climate.

Here, we examine the seasonal impacts of the AD oscillation on local weather across a latitudinal gradient of sites in the Taiga Plains ecozone, NWT, Canada from 1950 to 2015. The objectives of this study are to (a) quantify relationships between strong seasonal modes of the AD and coincident

surface climate variables (air temperature, precipitation, and the onset of snowmelt); (b) explore physical mechanisms, including pressure dipoles associated with these relations, which could alter local weather; and (c) discuss the implications of these changes on terrestrial ecosystems in Taiga Plains. The findings presented provide greater understanding of the historical impacts of AD on surface climate variables and mechanisms responsible and provide a framework for more detailed investigations, which can lead to better models used in weather and climate forecasting across NWT communities.

3.3 Data and Methods

3.3.1 Study Area

The study sites are located between 60°–70°N latitude and 101°–130°W longitude, spanning mainly the Taiga Plains, NWT (Figure 3.1). All sites include long-term meteorological records collected by Environment and Climate Change Canada and have been included in earlier regional research initiatives (e.g., the Mackenzie GEWEX study; Woo et al., 2008). The Taiga Plains is Canada's sixth largest ecozone, with distinct ecological, climatic, and landscape features (Phillips, 1990). Drained by Canada's largest river, the Mackenzie, approximately 90% of the Taiga Plains, is located within the western NWT, with small extensions into northeastern British Columbia and northern Alberta. For this study, the Taiga Plains was subdivided into northern, foothills, lake, and southern regions based on geography, latitude, and proximity to mountains, lakes, and other landforms, which may be differentially affected by climate (Ecosystem Classification Group, 2009). The Taiga Plains is bounded to the east by the Taiga Shield including Great Slave Lake and Great Bear Lake, to the west by the foothills of the Mackenzie Mountains, to the north by the

Mackenzie Delta, and to the south by a mix of black spruce dominated peatlands and upland mixedwood of the Boreal Plains (Ecosystem Classification Group, 2009).

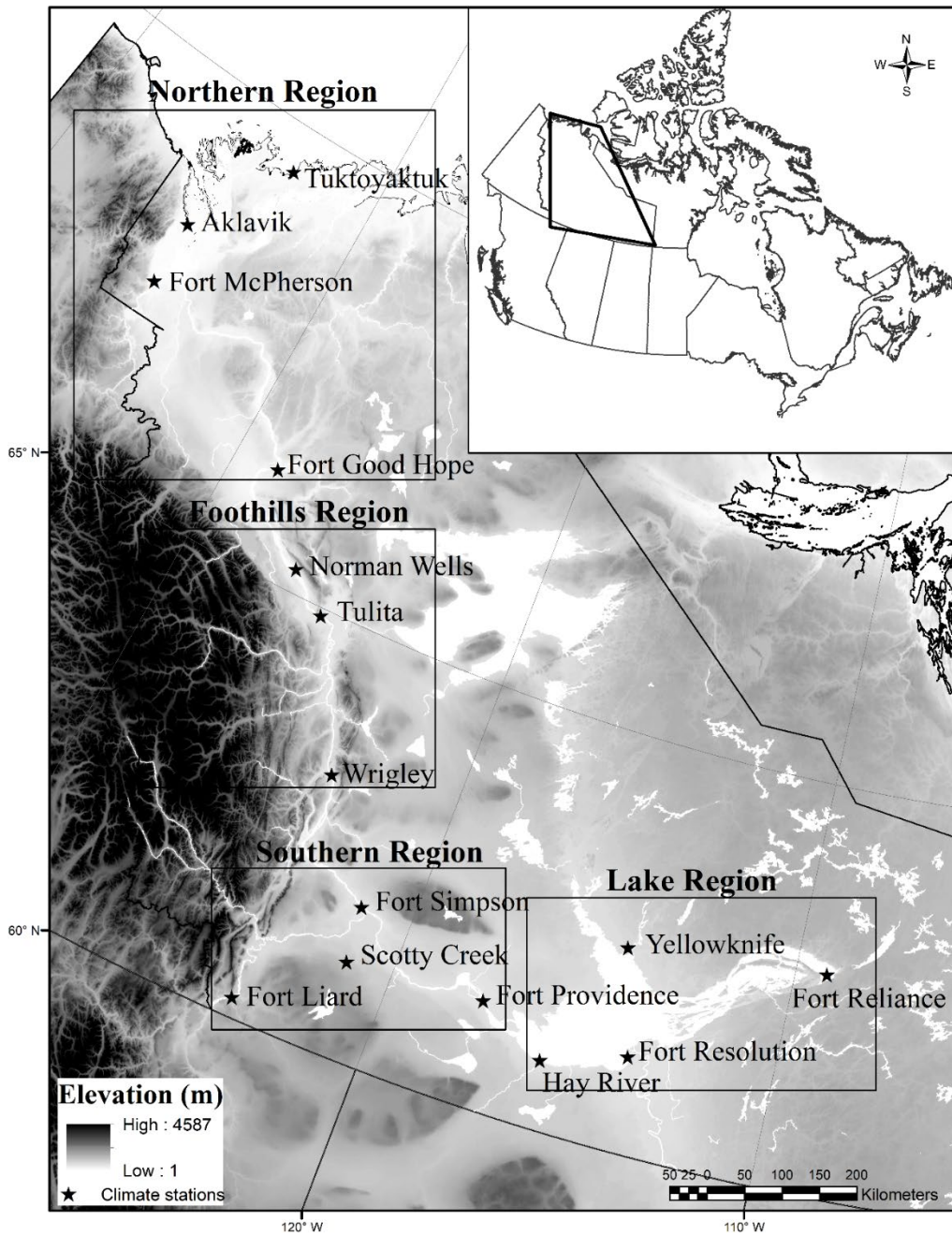


Figure 3.1 Locations of the study domain (inset map) and study sites (black stars) within the four regions.

The climate of the Taiga Plains includes long cold winters and short, cool summers (Phillips, 1990). Winters are characterized by the dominance of cold, dry high Arctic high-pressure systems. During spring, summer, and autumn, weak low-pressure systems originating in the Beaufort Sea and Gulf of Alaska bring moist air to the region. Occasionally, low-pressure systems originating from the Pacific Ocean generate substantial precipitation (Dyke & Brooks, 2000). Mean annual air temperature varies from -10.1°C to -2.6°C , while mean annual precipitation ranges from 160 to 388 mm (Ecosystem Classification Group, 2009), with highest cumulative precipitation occurring in the Cordillera and southern NWT (Phillips, 1990). Rainfall accounts for nearly half of precipitation (Phillips, 1990). Snowmelt typically commences in early April to mid-May (Dyke & Brooks, 2000).

3.3.2 Arctic Dipole index

The AD index, derived by Overland et al. (2012), is the second leading principal component of the mean SLP north of 70°N. Although the literature agrees on the existence of the SLP dipole and calculation of the AD index (Wu et al., 2005; Wang et al., 2009; Overland et al., 2012), there are opposing definitions of negative and positive AD. Unless otherwise indicated, in this study, the negative (positive) AD mode circulation is defined as positive (negative) sea level pressure (SLP) anomalies in the Canadian Archipelago and negative (positive) SLP anomalies in the northern Siberia/Barents Sea (Figure 3.2) (Overland et al., 2012; Choi et al., 2019). The standardized AD index is defined for each season as the AD principal component index value per year subtracted from the 1950–2015 long-term mean divided by the standard deviation (Overland et al., 2012). The seasonal standardized AD index from 1950 to 2015 was downloaded from the NOAA Bering Climate website (NOAA, 2021). Meteorological seasons were defined as winter (December–February), spring (March–May), summer (June–August), and autumn (September–November). To the best of the authors' knowledge, there is no consensus on the quantitative strength thresholds for AD classifications. For this study, standardized AD index (herein refer to AD index) values exceeding ± 0.5 were classified as strong positive or strong negative modes, following methods applied to other teleconnection pattern classifications (Trenberth, 1997).

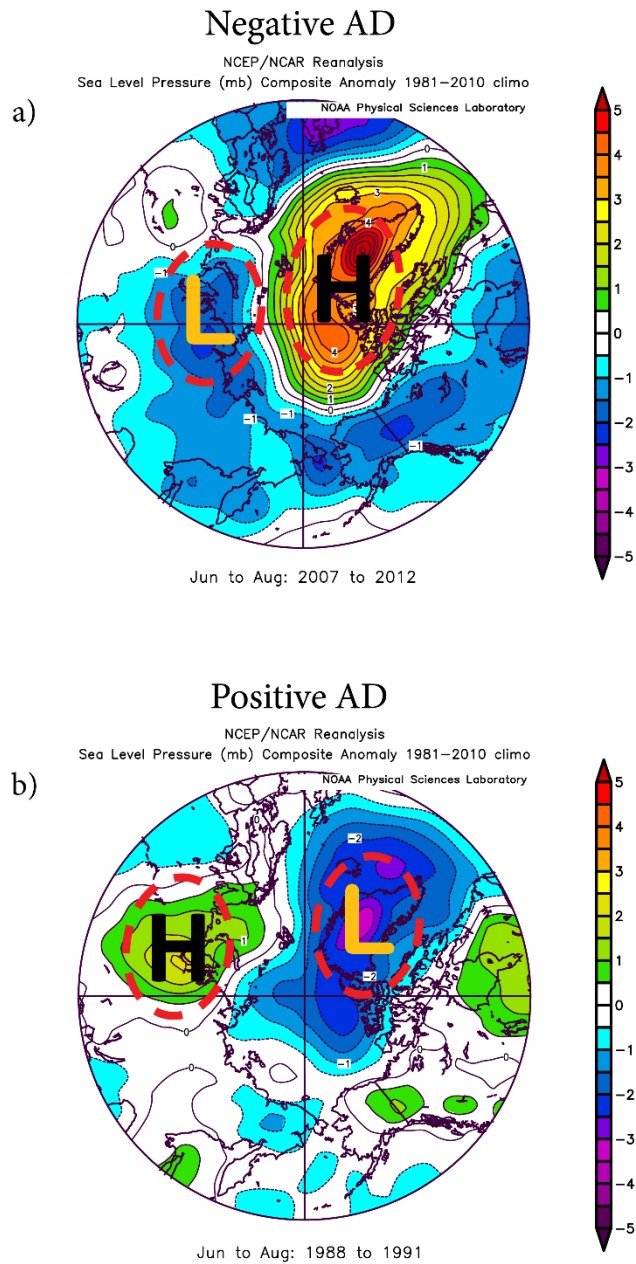


Figure 3.2 Example multi-year composite sea level pressure (SLP) anomaly patterns, that is SLP deviation from long term averages, in Summer (June-July-Aug) during a) the strong negative AD mode from 2007 to 2012 and b) the strong positive AD mode from 1988 to 1991. Data are from the NCEP–NCAR Reanalysis through the NOAA/Earth Systems Research Laboratory (NOAA, 2020).

3.3.3 Climate data

Daily interpolated air temperature and precipitation data were obtained from National Resources Canada (Hutchinson et al., 2009; NRCAN, n.d.). These air temperature and precipitation data were

interpolated using Australian National University Spline (ANUSPLIN), using a thin plate smoothing spline methodology (Hutchinson et al., 2009; McKenney et al., 2011) and applied by National Resources Canada at a cell resolution of approximately 10 km² from 1950 to 2015 (McKenney et al. 2011). Interpolated data from ANUSPLIN have been used as an alternative to *in situ* data in areas where data consistency may be limited and gaps in data collection may occur and uncertainty over northern regions is high due to the low spatial coverage of *in situ* climate stations. Exploring of teleconnection impacts, such as AD and AO, on northern Canada's climate has received little attention because there are very few *in situ* stations with long-term consistent records. However, evaluation of ANUSPLIN interpolated data has low bias compared with *in situ* observation data across northwestern Canada (Wong et al., 2017; Persaud et al., 2020).

Daily air temperature and precipitation data were obtained from nearest interpolated cells at each location (Figure 3.1). Average air temperatures were aggregated for each season from interpolated daily maximum and minimum air temperature. Seasonal air temperature and precipitation anomalies for each site were computed as the difference between the annual seasonal value and the 66-year (1950–2015) average. A positive anomaly indicates that the observed air temperature (precipitation) was warmer (wetter) than the long-term seasonal average, while a negative anomaly indicates that the observed temperature (precipitation) was cooler (drier) than the long-term average. The date of sustained snowmelt was defined as the first day in which the mean daily air temperature was higher than 0°C following the final consecutive 5-day period between March and May when the daily mean air temperature was less than 0°C (Shi et al., 2015). Air temperature and precipitation anomalies and onset date of snowmelt were compared to the positive and negative modes of the AD.

To explore mechanistic understanding between air temperature, snowmelt onset, and precipitation, and positive and negative modes of the AD, this study adapted an approach utilized by Overland et al. (2012). Geopotential height from National Centres for Environmental Prediction/National Centre for Atmospheric Research (NCEP/NCAR) reanalysis data (Kalnay et al., 1996) were accessed and visualized using the NOAA Climate Analysis and Plotting tool (NOAA, 2020). Geopotential heights at 850–500 mb were selected for this exploratory analysis because they are relatively free from atmospheric boundary layer influences, while describing upper-level tropospheric patterns (Francis & Vavrus, 2015). To provide insights on the implications of the AD on NWT terrestrial ecosystem climate, this study incorporated findings from the literature.

3.3.4 Statistical Analysis

All statistical analyses were undertaken using R 3.5.3 Project software (R Development Core and Team, 2016). The nonparametric Kruskal–Wallis test *kruskal.test* function in R was used to evaluate relationships among climate variables (air temperature, precipitation, and onset of snowmelt) and the two AD modes at each site. Here, the null hypothesis states that there was no difference among climate variables during the two modes (strong positive and strong negative) of the AD at sites. Nonparametric tests were chosen because climate variables often demonstrated a skewed distribution (Helsel & Hirsch, 1992). Additionally, Tukey honest significant differences (HSD) post hoc tests were used to assess the statistical significance of differences among site means during positive and negative AD modes. Post hoc analysis provides insight into the similarities/ differences between specific groups and is, therefore, an essential step in data analysis (Tukey, 1949). In all cases, differences were considered statistically significant when $p < 0.05$.

3.4 Results

3.4.1 Temporal distribution of the seasonal Arctic Dipole index

The AD index displays considerable annual variability in magnitude with few clear temporal trends from 1950-2015 (Figure 3.3). Some years and seasons exhibit periods of strong positive ($AD \geq 0.5$) modes and others display strong negative AD modes ($AD \leq -0.5$). The AD index varied from -1.75 (summer 1958) to 1.28 (summer 1994), illustrating the range of variability during the past 66 years. Analysis of the AD index time series data for all seasons indicate a total of 64 (24%) and 56 (21%) occurrences were in the strong positive and strong negative AD modes, respectively. In winter, mostly strong positive values occurred from 1953 to early 1957 (0.59 to 1.01), and strong negative AD index (ranged from -0.54 to -1.01) between 1958 and 1977 (Figure 3.3a). Between 1990 and the early 2000s, AD index values remained negative but were also of smaller magnitude (from -0.24 to -0.54). There has not been another strong negative AD mode in winter since 2004. The spring AD index is largely characterised by frequent strong positive modes (from 0.55 to 1.21) occurring during the early 1970s to 1995 (Figure 3.3b). This was followed by a period (late 1990s to mid-2000s) of consistently strong negative AD values, ranging from -0.55 to -1.04. During summer between mid-1965 and 2000, the AD index was characterised by mostly positive values, with strong positive values (from 0.63 to 0.81) between 1988 and 1991 (Figure 3.3c). A noticeable feature in the summer AD index is the abrupt change to more persistent, and the strongest recorded, negative AD index between 2002 and 2007, which ranged from -0.79 to -1.5. The autumn AD index (Figure 3.3d) pattern is similar to summer during strong modes, but with reduced magnitude.

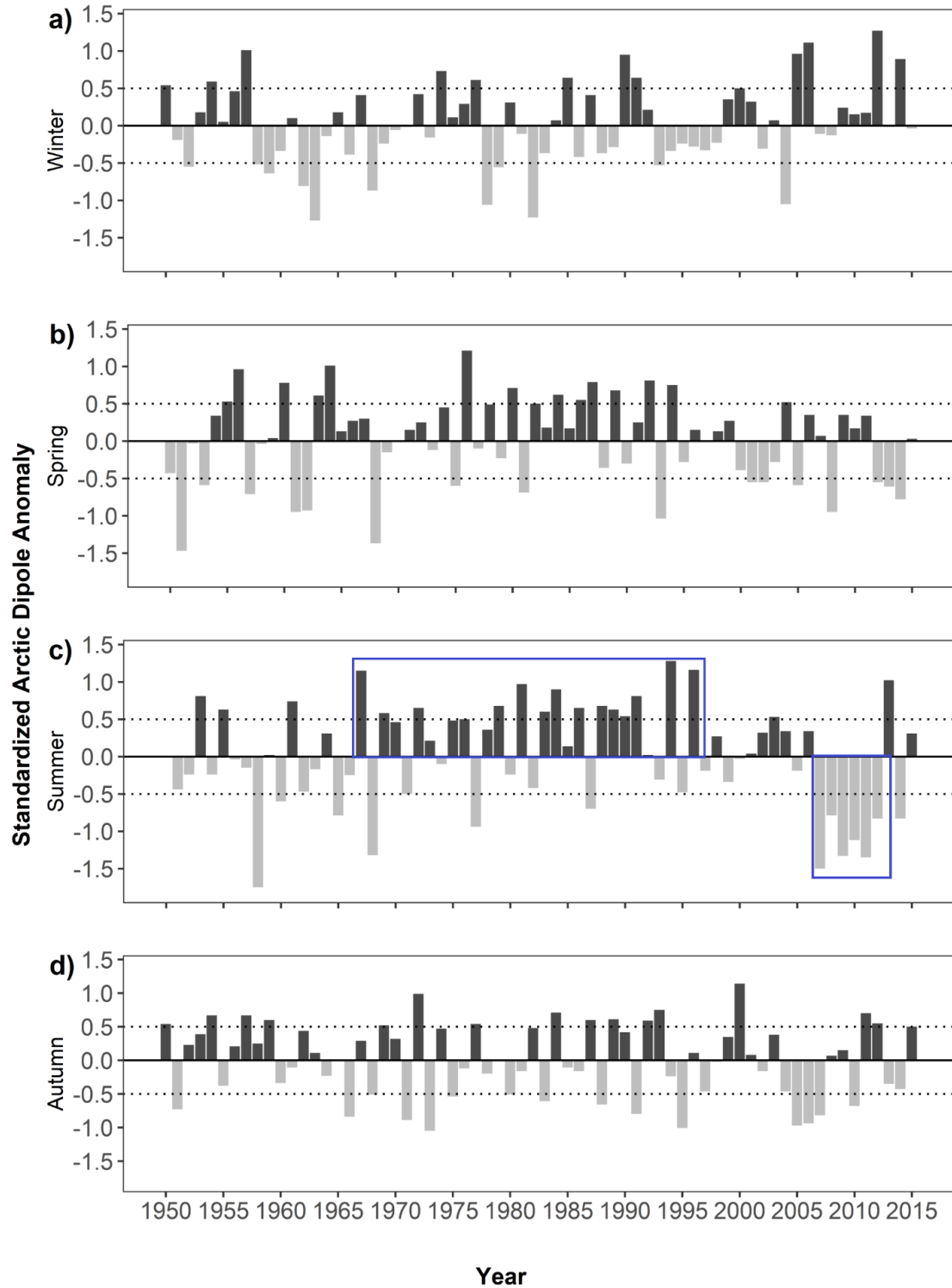


Figure 3.3 Standardized AD for a) winter, b) spring, c) summer and d) autumn. Grey bars are negative AD anomalies and black bars are positive AD anomalies. Indices exceeding ± 0.5 threshold (dashed lines) are defined as strong \pm AD modes. The blue boxes highlight areas mentioned in the text.

3.4.2 Geopotential height patterns during periods of strong negative and positive AD mode

To explore mechanistic understanding of atmospheric circulation patterns during strong AD modes, variations in middle- to upper-level geopotential height patterns over the NWT during strong negative AD mode (2007-2012, Figure 3.4a, b) and positive AD mode (1988-1991, Figure 3.4c, d) were examined. When compared with the long-term average for 2007-2012 period, greater geopotential heights (ranges from 3020 to 3060 m) and therefore, greater geopotential anomalies (Figure 3.4b) were observed near Southern and Lake sites in the negative AD mode. In contrast during the same period, the Northern sites showed that the ridge had reduced amplitude, lower geopotential heights (ranges from 2980 to 3010 m) and lower geopotential height anomalies (Figure 3.4a). Whilst in the positive AD summers of 1988-1991, there was a broad region of high geopotential heights prevalent over continental Canada combined with a mid-level ridge over NWT, whose axis appears more elongated and amplified northwards (over Alaska/Yukon and southern NWT; Figure 3.4b). The elongated high amplitude ridge observed during summer positive AD (Figure 3.4b) suggests advection of stronger southwesterly warm air masses (Overland et al., 2012) toward NWT from the warmer Pacific Ocean, potentially contributing to positive air temperature anomalies. A similar anomaly pattern, with reduced variability, existed from 850 hPa to 500 hPa geopotential height fields (not shown) during these two same periods.

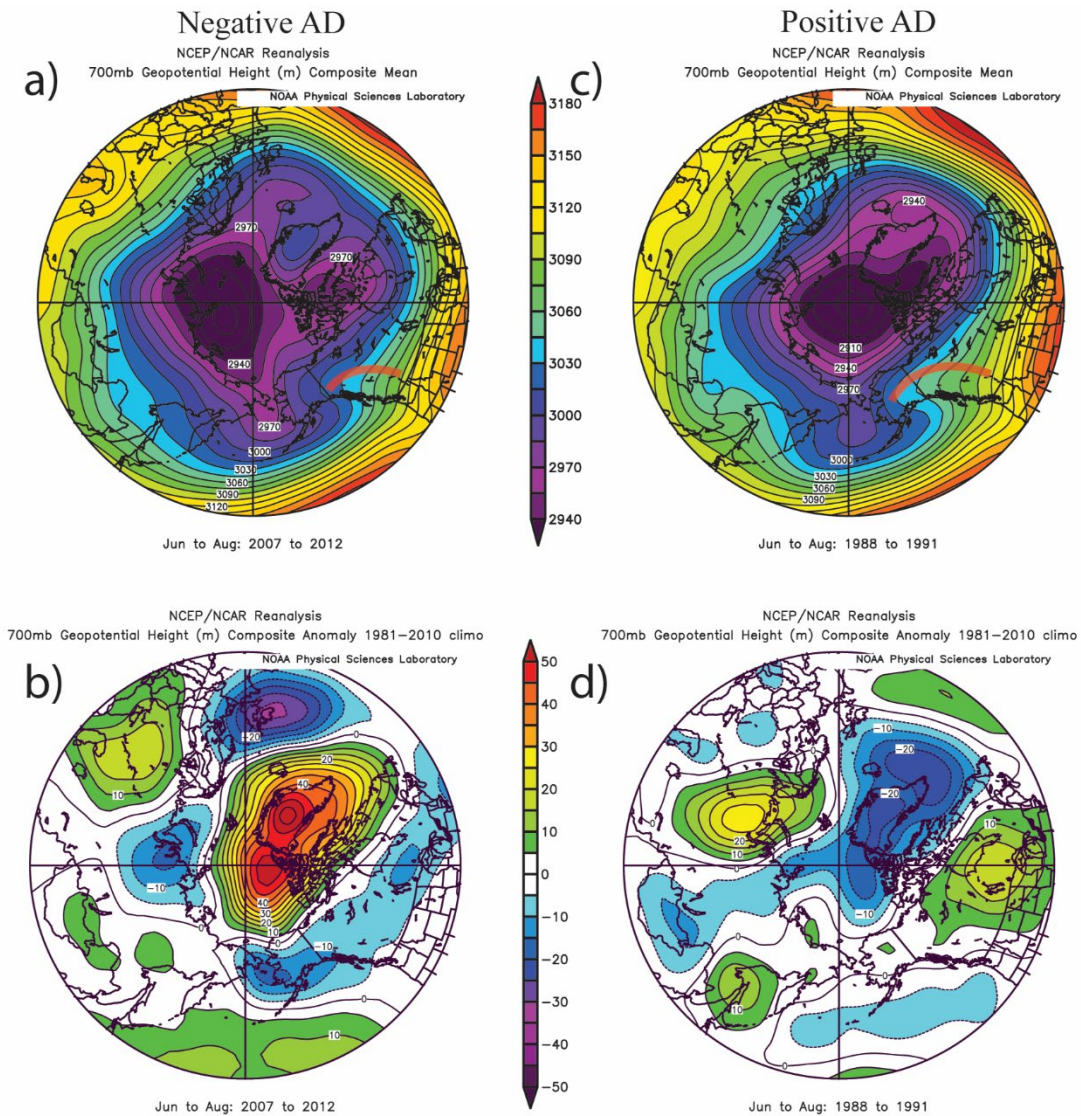


Figure 3.4 Summer multi-year composite during a period strong negative AD modes 2007 to 2012 for the a) 700 hPa geopotential height mean and b) 700 hPa geopotential height anomaly and during a strong positive AD mode (1988 to 1991) c) mean 700 hPa geopotential height and d) 700 hPa geopotential height anomaly. Data and plotting tool used for data are from the NCEP–NCAR Reanalysis through the NOAA/Earth Systems Research Laboratory (NOAA, 2020). Solid red lines on figures represent the ridge axis.

3.4.3 Positive and negative modes of the AD index and air temperature

The seasonal distribution of air temperature anomalies in strong positive and negative AD modes showed some consistent patterns across a latitudinal gradient in the NWT, illustrated in Figure 3.5.

Air temperature anomalies correspond with strong positive and negative mode AD anomalies across 73% of sites ($p < 0.05$; Figure 3.5, Table 3.1). Air temperature anomalies vary less in winter (standard deviation (σ) ranges from 1.8 to 3.1 °C) compared with air temperature anomalies in other seasons. Further, these shift towards cooler temperature anomalies (between -0.9 to -2.5 °C) during both modes of the AD. In spring, air temperature anomalies show an emerging response to AD modes (Figure 5b). During strongly positive AD mode, the σ of spring air temperature anomaly is low, with σ ranging from 1.8 to 2.2 °C, while during strong negative AD mode the σ spring air temperature anomaly increases ($\sigma = 2.5$ to 3.3 °C), illustrating greater magnitude, especially in Southern, Lake, and Foothill regions (Figure 3.1). Similar AD-air temperature patterns were observed in summer for both modes (Figure 3.5c and Table 3.1). During positive AD modes, significantly greater median summer air temperature anomalies were observed ($p < 0.05$): Southern (1.1 °C), Lake (1.1 °C), and Foothill (1.0 °C) regions. Similarly, there was also an observed decrease in standard deviation ($\sigma \approx 1.5$ °C) of air temperature anomalies across all regions. During the negative AD mode, increased variance in the range of temperatures occurred across all regions (Figure 3.5c and Table 3.1). During the negative AD mode, greater variability in air temperature anomalies were observed in the Southern ($\sigma = 2.4$ °C), Lake ($\sigma = 1.5$ °C), Foothill ($\sigma = 2.6$ °C), Northern regions ($\sigma = 1.9$ °C) when compared with air temperature variance in the positive AD modes in summer. Despite larger variability in spring and summer air-temperature anomalies, these tended to be dampened during the autumn (Figure 3.4d) when air temperature anomalies did not deviate significantly from the long-term average. Of note, during autumn, there was less variability among sites during the strong negative (median = 0.3 to -0.04°C; $\sigma = 1.3$ to 1.5°C) and strong positive modes of the AD (median = -0.4 to -0.7 °C; $\sigma = 1.3$ to 2.2°C).

In summary, the AD was a source of intra-seasonal variability of air temperature over the NWT during summer. Results indicate that summer AD modes elicited the strongest response in air temperature, predominantly across Southern, Lake and Foothill regions. The influence of AD on air temperatures began in spring, intensified during summer, and was dampened during autumn. A clear spatial and gradual latitudinal response was displayed in the dataset, given the less evident AD-temperature relations at the Northern region.

Location	Air Temperature				Precipitation			Snowmelt	
	winter	Spring	summer	fall	winter	spring	summer	fall	onset
Tuktoyaktuk	0.43	0.30	0.42	0.43	0.26	0.10	0.27	0.32	0.14
Aklavik	0.79	0.29	0.25	0.53	0.58	0.43	0.27	0.87	0.91
Fort McPherson	0.79	0.36	0.30	0.64	0.62	0.32	0.22	0.21	0.66
Fort Good Hope	0.37	0.87	0.09	0.36	0.98	0.55	0.80	0.78	0.28
Norman Wells	0.71	0.69	<u>0.09</u>	0.94	0.54	0.30	0.63	0.61	<u>0.04</u>
Tulita	0.75	0.72	<u>0.03</u>	0.97	0.54	0.25	0.77	0.17	0.51
Wrigley	0.54	0.69	<u>0.00</u>	0.97	0.58	0.41	0.58	<u>0.05</u>	0.08
Fort Reliance	0.66	0.58	<u>0.01</u>	0.25	0.34	0.29	0.58	0.61	0.43
Yellowknife	0.98	0.48	<u>0.01</u>	0.24	0.58	0.61	0.53	0.69	<u>0.02</u>
Fort Simpson	0.51	0.48	<u>0.00</u>	0.94	0.93	0.38	0.77	0.12	0.32
Fort Providence	0.58	0.45	<u>0.00</u>	0.94	0.75	0.48	0.85	0.97	0.26
Fort Resolution	0.84	0.27	<u>0.00</u>	0.48	0.54	0.48	0.29	0.53	0.08
Scotty Creek	0.43	0.50	<u>0.00</u>	0.97	0.98	0.27	0.51	0.08	0.11
Hay River	0.54	0.27	<u>0.00</u>	0.72	0.79	0.81	0.61	0.78	<u>0.04</u>
Fort Liard	0.21	0.48	<u>0.03</u>	0.97	0.84	1.00	0.27	<u>0.03</u>	0.20

Table 3.1 p-values the Kruskal–Wallis test for AD events exceeding the ± 0.5 AD index thresholds were examined to quantify whether the mean climate variables anomalies (air temperature, precipitation, and onset date of sustained snowmelt) were significantly different during these positive and negative AD modes For p values ≤ 0.05 (bold and underlined) the null hypothesis is rejected (i.e., there is no change in the mean of climate variables anomaly (air temperature, precipitation and onset date of sustained snowmelt) during the positive and negative AD modes.

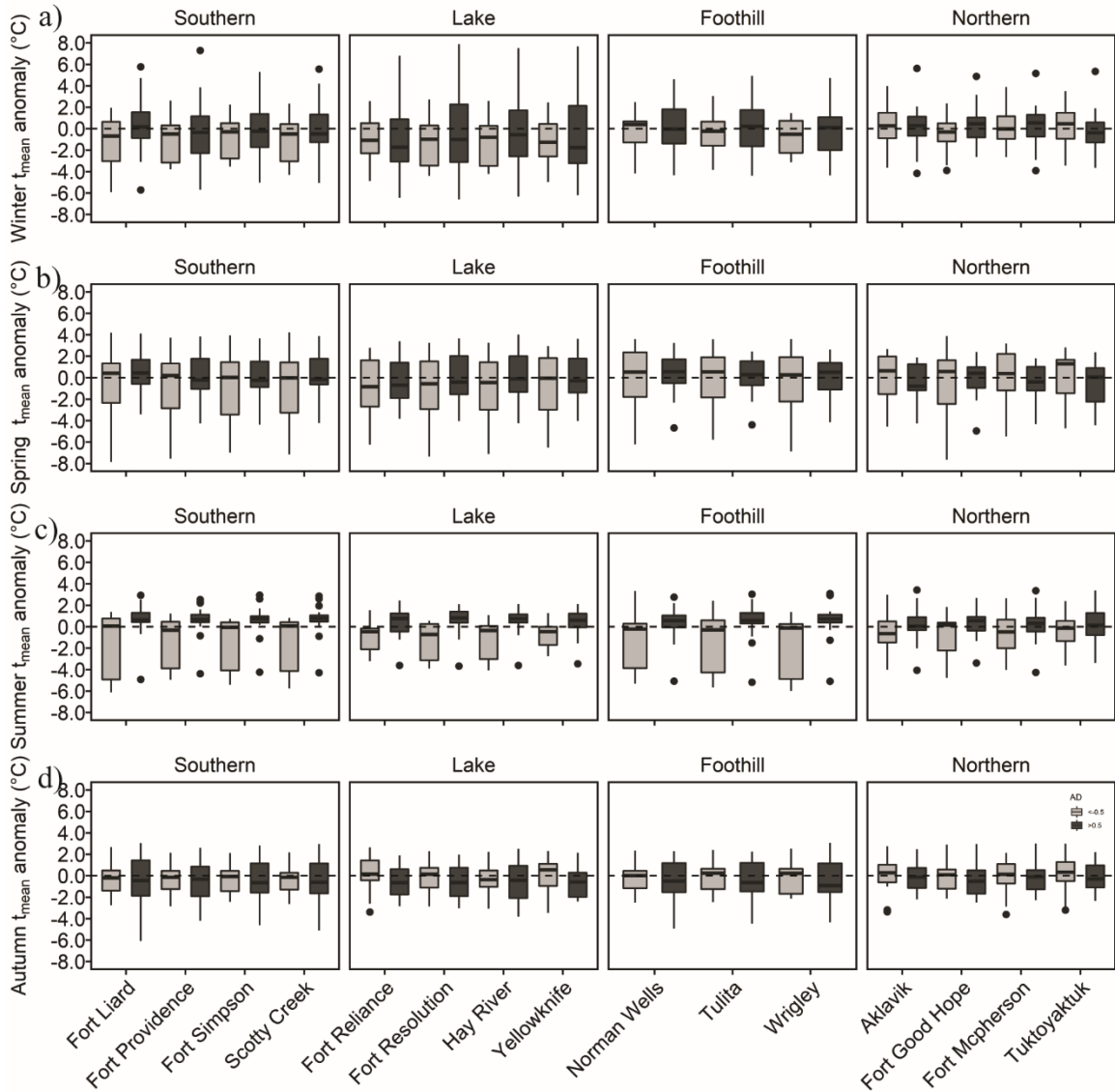


Figure 3.5 Boxplots showing the distribution of winter, spring, summer and autumn AD modes exceeding the ± 0.5 threshold and its corresponding mean temperature anomaly. Anomalies are departures from 1950 to 2015 seasonal mean air temperatures. Black boxes represent positive AD mode while grey boxes represent negative AD mode, while black dots represent outliers.

3.4.4 Positive and negative modes of the AD index and precipitation amount

The amount of precipitation that falls during positive and negative modes of the AD varied across the Taiga Plains (Figure 3.6; Table 3.1). There were few observable variations (from average) in total seasonal precipitation during strongly positive and negative modes of the AD. For example,

during positive mode, winter precipitation anomalies were less variable ($\sigma = 14.8$ mm) than during negative modes ($\sigma = 19.8$ mm) (Figure 3.6b). These observed patterns in winter precipitation were not statistically significant ($p > 0.05$). In spring, across all regions, median precipitation anomalies remained near the long-term average during both AD modes (Figure 3.6b). In summer, median precipitation anomalies in the Southern (median = -15.3 mm), Lake (median = -10.1 mm), and Northern regions (median = -3.2 mm), during negative modes of the AD were often lower than the long-term average. Further, summer precipitation anomalies had slightly greater variance during the positive mode of the AD ($\sigma = 39.3$ mm) compared with the negative AD mode ($\sigma = 32.0$ mm) across all regions (Figure 3.6c). However, there was no significance difference between the positive and negative AD mode across regions. During autumn, the Southern (median = -9.1 mm), Foothill (median = -9.2 mm) and Northern (median = -3.9 mm) region precipitation anomalies were less than the long-term mean in the positive AD mode. In the negative AD mode, Southern (median = 3.4 mm) and Lake (median = 6.3 mm) regions, precipitation anomalies tend to be above the long-term mean with little difference to total seasonal precipitation in Northern (median = 1.5 mm) and Foothill regions (median = 1.6 mm) (Figure 3.6d). There were no significance differences ($p > 0.05$) in the distribution of precipitation anomalies during the two AD modes in autumn across the Taiga Plains. Although no distinct and persistent relations could be detected between strong AD modes and precipitation, statistical significance responses were dependent on specific locations and seasons. For instance, in autumn, Fort Liard (in Southern region) Wrigley (in Foothill region) experience significant difference in total seasonal precipitation during positive and negative modes of AD (Table 3.1).

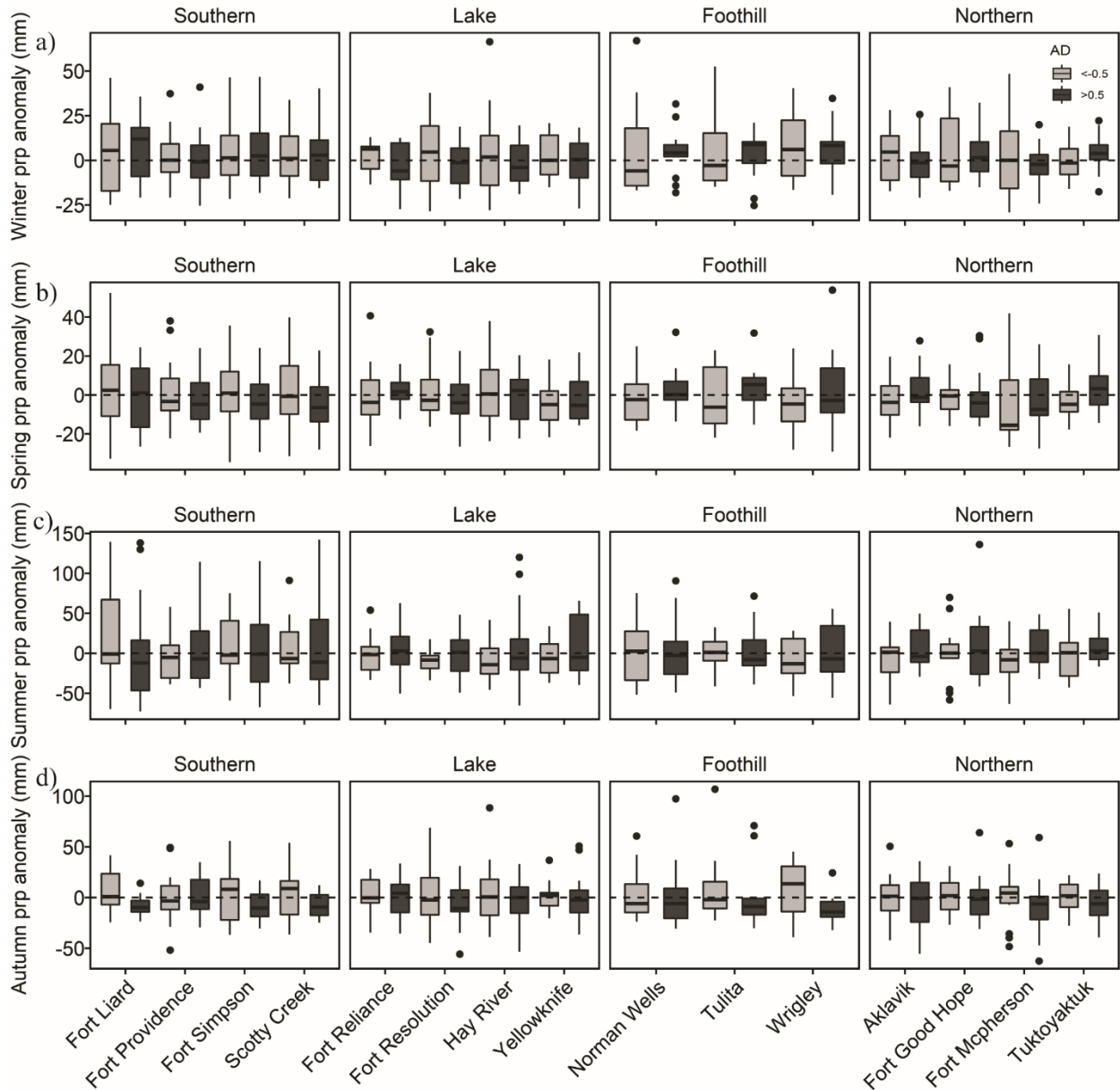


Figure 3.6 Boxplots displaying precipitation anomalies during positive (black boxes) and negative (grey boxes) modes of the AD index in winter, spring, summer, and fall. Anomalies are departures from 1950 to 2015 seasonal total precipitation. A positive anomaly indicates the observed precipitation was greater than the long-term total average while a negative anomaly indicates the observed precipitation was less than the long-term average. Black dots represent outliers.

3.4.5 Positive and negative modes of the AD index and onset of snowmelt

Comparison between modes of AD and onset of snowmelt reveals consistent patterns across Southern, Lake, and Foothill regions (Figure 3.7). Earlier onset of snowmelt occurred during years that also had positive mode of the AD in spring. In comparison, delays of snowmelt onset date for Southern, Lake, and Foothills sites tended to occur during the negative mode of the AD (Figure 3.7). Further, all regions except farthest north (Northern region) had greater variability in the timing of onset of snowmelt ($\sigma \sim 10\text{-}13$ days; 6 days at Northern sites) during the negative mode of the AD. During the positive mode of the AD, there was a southern latitudinal shift towards progressively earlier onset dates of snowmelt, by an average of 3 to 5 days. The greatest difference in variability in onset snowmelt date occurred in Southern ($\sigma = 10$ days) and Lake sites ($\sigma = 11$ days), when compared with Foothills ($\sigma = 8$ days) and Northern sites ($\sigma = 6$ days). Despite the variability, snowmelt onset was significant ($p < 0.05$) at some Foothills and Lake sites, specifically Norman Wells, Yellowknife, and Hay River (Table 3.1).

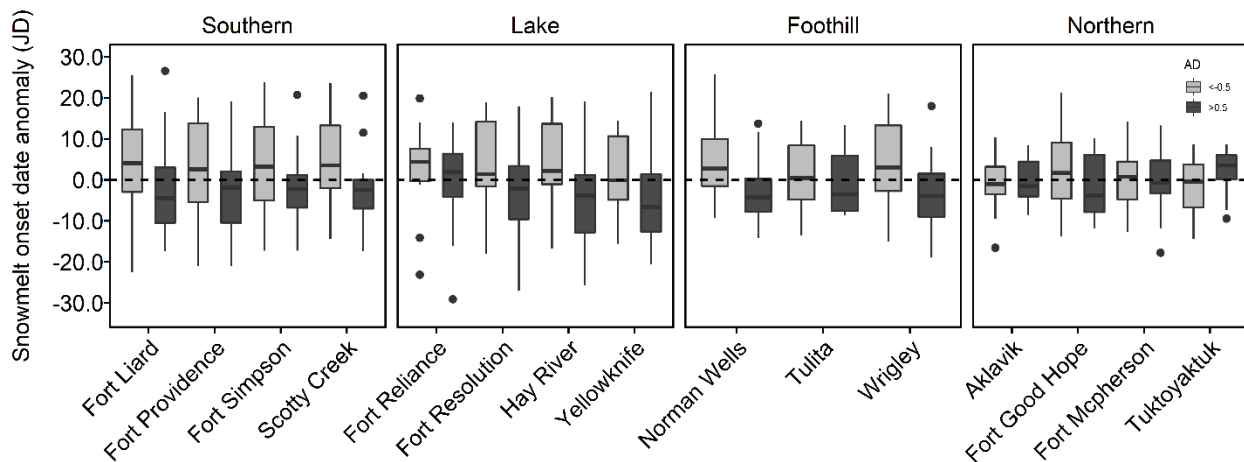


Figure 3.7 Deviation in the timing of snowmelt (in days) from the mean date of snowmelt during spring AD modes exceeding an index threshold of ± 0.5 . Black boxes represent positive AD mode and grey boxes represent negative AD mode. Black dots represent outliers. Positive anomaly on y axis = later snowmelt; negative anomaly on y axis = earlier snowmelt.

3.5 Discussion

The results of this study indicate that when compared with long-term averages, greater magnitudes and higher summer air temperature anomalies occur during positive modes of the AD in southern, foothills, and lake sites (Figure 3.4). Air temperatures anomalies during positive modes of the AD tended to be greatest at southern sites, becoming more similar to the long-term average (less significantly different) with increasing latitude. Earlier onset of snowmelt by at least 5-11 days in the spring seasons also occurred during positive modes of the AD (Figure 3.7). Results indicate significant differences between snowmelt onset in spring and mean air temperatures in summer. However, there were no significantly large deviations in air temperature in winter during positive and negative modes of the AD. Further, there were no significant variations in total precipitation from the median during any of the seasons or regions studied. The results suggest that the variability of AD index values may be increasing in latter years (Figure 3.3). These results are consistent with Cai et al. (2018), who utilized ERA-Interim and CMIP5 model across the Arctic during the summer season between 1979 and 2016. They found that positive AD impacts summer air temperatures, while the influence of AD on total precipitation varied depending on the location (Cai et al., 2018). These results noted for NWT also elicit the following questions: How do pressure differentials during the AD enhance positive temperature anomalies and changes in snowmelt onset? Why are precipitation anomalies during the AD difficult to discern or are nonexistent? Should we expect a warmer, possibly drier climate associated with increasing periodicity of the AD? This discussion will explore answers to some of these questions and will also provide insights on the implications of the AD on NWT terrestrial ecosystem climate.

3.5.1 Mechanistic interactions between the AD and climate in the Taiga Plains

Inter- and intra-annual surface climate variability across Arctic and sub-Arctic regions may be explained by numerous atmospheric phenomena observed in the literature and described here. For example, the location, magnitude, and persistence of ridges and troughs influence weather and climate in northwestern Canada (Skinner et al., 1999). During normal conditions, summer climate tends to be relatively dry in northwestern Canada (Skinner et al., 1999). Occasionally, stagnant or slow-moving ridges over western North America lead to warmer and drier conditions (Skinner et al., 1999). Increased geopotential heights and ridging may be associated with the positive mode of the AD and results in sustained high pressure, reduced cloud cover and enhanced shortwave radiation receipt, and atmospheric warming (e.g., Figure 3.4) (Newton et al., 2014; Bezeau et al., 2015; Fazel-Rastgar, 2020). During the summers of 2000–2012, warm surface air temperature anomalies were also observed over the Arctic Ocean, which were likely driven by meridional movement of warm air masses from the south (Wang et al., 2009; Overland et al., 2012). In addition to and associated with these anomalies, Lackmann & Gyakum (1996) also noted elevated moisture transport to mid-level atmospheric layers (500, 700, and 800 mb) from the northern Pacific Ocean, thereby modulating weather and climate across the Taiga Plains by increasing the precipitation over the region. With regards to springtime onset of snowmelt (Figure 3.7), which is also related to warmer than average air temperatures, a recent study by Horvath et al. (2021) reported that the timing of melt onset in the Arctic was strongly influenced by atmospheric circulation patterns. Horvath et al. (2021) showed that prevailing pressure patterns associated with early melt onset in the Arctic were initiated by low SLP over Eurasia and high SLP over the Canadian Arctic Archipelago. This study noted similar pattern with SLP, and it is hypothesized that the onset of snowmelt in NWT (Figure 3.7) could have also been triggered or delayed by

dipole circulation pattern prevalent during AD modes, but this requires additional investigation. During autumn at Wrigley and Fort Laird, there were some notable differences in precipitation during the strong positive and negative modes of AD, but these relations did not persist across all regions. The lack of a significant relationship between the AD and precipitation patterns could be because precipitation was likely influenced by local factors including topography, latitude, and proximity to land- forms such as large lakes and mountains (Phillips, 1990). Thus, it may be more difficult to identify correspondence with synoptic-scale precipitation patterns and large-scale teleconnection anomalies.

Another hypothesis that may be responsible for mechanistic relations between the AD and air temperature (Figure 3.4) in NWT may be associated with the sea ice–albedo feedback (Watanabe et al., 2006; Wang et al., 2009; Tang et al., 2014; Choi et al., 2019; Xiao et al., 2020). Sea ice modulates the connection between the atmosphere and the ocean by influencing heat and moisture exchanges at the air–sea interface (Watanabe et al., 2006; Wang et al., 2009; Tang et al., 2014; Francis & Vavrus, 2015; Xiao et al., 2020). As sea-ice extent decreases, surface albedo also decreases; thus, there is more open water and absorption of solar radiation increases, thereby accelerating warming (Serreze & Barry, 2014; Bezeau et al., 2015; Lei et al., 2016). Arctic sea ice has been declining since the 1980s, with amplification of these trends especially during the past decade (Wang et al., 2009; Overland et al., 2012). It has been suggested that the decline of Arctic sea ice has become sufficient to have a noticeable impact on large-scale atmospheric circulation (Zhang et al., 2008; Overland & Wang, 2010; Serreze et al., 2016). The negative AD has resulted in enhanced sea ice melt in the Arctic (Overland et al., 2012; Choi et al., 2019; Heo et al., 2021). Lei et al. (2016) and Choi et al. (2019) found that positive SLP anomalies in most of the Arctic

Basin and negative SLP anomalies over the northern Siberia/Barents Sea (Figure 3.2a) were associated with strong southerly winds from the northern Pacific, which bring in relatively warm air masses. These warm air masses enhance oceanic heat flux into the Arctic Ocean and results in increased sea ice melt, thereby further amplifying the ice–albedo feedback (Lei et al., 2016; Choi et al., 2019). Also, reduced sea ice is coincident with negative zonal wind anomalies at high latitudes, along with increased meridional flow in upper atmospheric layers (Tang et al., 2014; Francis & Vavrus, 2015). These effects may lead to an enhanced meridional gradient in near-surface air temperature, resulting in the movement of air masses from southern to northern latitudes (Wang et al., 2009; Overland et al., 2012; Lei et al., 2016). Warmer open water in the Arctic Ocean also warms the overlying atmosphere (Lei et al., 2016; Heo et al., 2021). Similarly, Overland et al. (2012) postulated that sea ice decline may have resulted in positive feedback associated with the movement of warmer air masses into the Arctic from the south. This movement of warmer air masses may have contributed to warmer than long-term average air temperature and earlier onset of snowmelt during the positive modes of the AD in spring in the NWT (Figure 3.5).

3.5.2 Implications of AD and surface climate variability on terrestrial ecosystem in the Taiga Plains

The CMIP5 climate model predicts that the impacts of the AD in the Arctic will be enhanced during the 2006– 2100 period, with higher-than-average air temperature and greater variability in cumulative precipitation during summer (Cai et al., 2018). Increases in air temperature are known to induce permafrost thaw via a warmer ground and energy exchange at the surface, which has had significant impacts on changing water resources and terrestrial ecosystems in NWT (Wright et al.,

2009; Quinton et al., 2011; Cannon et al., 2015; DeBeer et al., 2016). Changes in surface climate variables alter local energy balance and changes albedo, which could exacerbate or reduce snowmelt in NWT (Chapin et al., 2005; Helbig et al., 2017). A shortened snow-covered season (Serreze & Barry, 2014; Chasmer & Hopkinson, 2017) and early snowmelt leads to exposure of the ground surface and litter to atmospheric warming and drying, which not only enhances permafrost thaw, but also increases the availability of fuels for wildland fire (Westerling, 2016), especially as depth to frost table increases (Sniderhan & Baltzer, 2016). For example, the severe wildland fire year in 2014, when the largest areas burned occurred (Kochtubajda et al., 2019), also corresponds with strong negative AD mode in spring and summer which was preceded by a strong positive AD mode during winter periods. With earlier snowmelt onset, there is also increased energy available for photosynthesis, lengthening of the growing season period (Lafleur & Humphreys, 2008; IPCC, 2021), and enhanced shrub growth (Chapin et al., 2005; Baltzer et al., 2014; Wilcox et al., 2019). It is expected that shrubification in Arctic tundra regions and southern NWT may be amplified (Chasmer & Hopkinson, 2017; Mekonnen et al., 2021). Bhatt et al. (2021) also illustrated that summer positive AD circulation, higher SLP over the Canadian Archipelago (defined as negative AD in this study), can influence local climate, which can have competing effects during the same AD mode on Arctic tundra vegetation across scales. For example, in the pan Arctic during the positive AD circulation in summer, open water in the Kara–Barents Seas was linked with below the long-term average vegetation greenness, indicated by maximum Normalized Difference Vegetation Index (MaxNDVI), and above the long-term average summer precipitation amounts between 1982 and 2019. However, the same positive AD circulation system in the Laptev Sea corresponded with above long-term average vegetation greenness (MaxNDVI), total summer precipitation amounts, and summer warmth index on adjacent lands (Bhatt et al.,

2021). The present study found that the positive mode of the AD in spring resulted in earlier onset of snowmelt, while the opposite occurred during negative modes of the AD, especially in southern, lake, and foothill regions (Figure 3.7). Thus, the results observed here, across the NWT during positive AD, may be associated with amplified landcover changes during AD circulation (Figure 3.4).

We hypothesize that the ridging pattern that is associated with the AD (Figure 3.4) could have also been a potential precursor to dry conditions and terrestrial ecosystem changes observed in NWT. For example, several studies have examined the influence of mid-atmospheric circulation to the presence of an anomalously strong ridge with coincident periods of warm and dry conditions, and the potential for increased severity and intensity of wildland fire in Canada (Skinner et al., 1999; Skinner et al., 2002; Serreze & Barry, 2014; Kochtubajda et al., 2019; Jain & Flannigan, 2021). The presence of these strong ridges over the NWT may be related to positive AD modes. Increased tundra fires across the North Slope of Alaska, summer 2007, were attributed to the presence of a high- pressure circulation pattern over the Beaufort Sea (Alexeev et al., 2015), a feature typical of the negative mode of the AD (Figure 3.2a). The atmospheric circulation linked negative AD modes may modulate the location and magnitude of ridges in the troposphere over the NWT, enhancing wildland fire in southern sites through the presence of an amplified ridge. For instance, the summer 2014 wildfire was attributed to the presence of slow moving ridges across the Canadian north in the NWT (Kochtubajda et al., 2019). At the same time, the AD was in its negative mode (Figure 3.3). Additionally, wildland fires enable climate warming by accelerating active layer deepening and talik expansion in the boreal region (Gibson et al., 2018). The latitudinal effect on the proportion of thaw in permafrost peatland (Gibson et al., 2021), along with a coincident strong

positive AD mode which elicited warmer temperature, also is indicative of the potential for continued widespread and amplified thawing throughout the discontinuous permafrost zone in western Canada. Permafrost thaw can also have significant implications for climate change over broad areas associated with increased microbial decomposition of unfrozen organic material and enhanced greenhouse gas emissions to the atmosphere (Turetsky et al., 2007). Warming of soils and permafrost thaw stimulate microbial activity and decomposition of organic materials, thereby increasing respiration, carbon dioxide, and methane production (Helbig et al., 2017).

3.5.3 Recommendations for future study

The analysis presented here lays the groundwork for hypotheses on AD influences on local meteorology and the hydroecology of changing ecosystems in the NWT. However, an implicit assumption is the presence of a contemporaneous relationship between AD modes and surface climate variables. Here, it is assumed that atmospheric circulations associated with both AD modes operate independently to impact surface climate in the NWT. In some years this may not necessarily be a valid assumption since a lag/lead relationship between AD and surface climate variables are possible. This lag/lead linkage between atmospheric anomalies and impacts on local meteorology/climate is not uncommon for other teleconnections (e.g., El Niño–Southern Oscillation) across various regions (Shabbar et al., 1997; McCabe & Dettinger, 1999). This study also acknowledges that teleconnections are not always independent, and feedbacks on climatology and weather patterns found in the NWT may be due to nonlinear, positive and negative teleconnection pattern interactions (Jiang et al., 2014; Heo et al., 2021). The effects of coupled teleconnections (e.g., AO and AD) on NWT hydroclimate will also require investigation. Although this research offered some insights into potential linkages between AD and surface climate for the

NWT, additional research into the robustness of some of the physical mechanisms explored here should be further investigated. This is important as future climate AD is predicted to drive greater variability of air temperature and precipitation (Cai et al., 2018). For example, literature (e.g., Alexeev et al., 2015; Déry et al., 2009) indicates that drivers could exist between AD, hydroclimatology, and the potential for accelerated ecosystem changes observed in the Taiga Plains, but this requires further exploration. While these additional investigations are beyond scope of this research, the results of this analysis provides numerous avenues and hypotheses for improved understanding of the interactions between atmospheric teleconnection patterns, local meteorology, and ecosystem change.

3.6 Conclusion

This study explored the relationship of strong positive and negative AD modes on seasonal air temperature, precipitation, and snowmelt onset anomalies in the Taiga Plains, NWT (Canada), during the past 66 years (1950-2015). The three main findings were (a) local air temperature increased during strong AD modes, which is intensified from southern, lake, foothill regions and to the northern regions of the Taiga Plains during summer; (b) local surface air temperature responses to AD were evident, but the coincident impact of AD on local total precipitation were not; and (c) when AD is in its positive (negative) strong mode, earlier (later) onset date of snowmelt is observed when compared with the long- term average for southern, lake, and foothill regions and is more extreme in the southern and lakes regions. These results suggest that the strong AD modes could be a precursor for certain characteristic mid- to upper-level geopotential heights/pressure patterns and surface climate responses, which has implications for rapidly changing ecosystems in the NWT especially across southern regions which have more sensitive patches of ecosystem (Rouse et al., 1997). The air temperature/snowmelt onset north–south

response to the AD maybe linked to the position and intensity of the geopotential heights ridge axis over the NWT and sea-ice feedback as previous studies identified similar characteristic mid-to upper-level geopotential heights/pressure patterns known to persist in the northwestern Canada (e.g., Kochtubajda et al., 2019). This requires further exploration.

Although there is much to learn about the interactions between a rapidly warming NWT and large-scale teleconnection patterns, this study identified notable association between surface climate variables and strong AD modes. This has direct relevance to NWT communities, especially as these communities are among the most vulnerable in Canada to climate-induced environmental change. This study also implies that if a developing strong AD mode were to be detected early enough, threats like heatwaves and wildland fires, as well as their ecological consequences, could be better anticipated, hence enabling northern governments to be better prepared for wildland fire seasons. This work also provides insights for hydrometeorological modellers in their efforts to improve weather and climate models. Furthermore, NWT population that resides in the Taiga Plains will also benefit as these findings may help strengthen climate adaptation and mitigation policies in the NWT at the local level.

3.7 Acknowledgements

We thank Natural Resources Canada, especially Drs. Daniel McKenny and Pia Papadopol, for making available ANUSPLIN daily temperature and precipitation data. Thanks to Julie Grant for her help with the figures. Funds for this work were partially provided by Wilfrid Laurier University and ArcticNet Programme. The analyses were performed using research facilities made available via the Canada First Research Excellence Fund's Global Water Futures Programme. We also thank the two anonymous reviewers and editors for their helpful insights and suggestions that contributed towards the final version of manuscript.

3.8 Data availability statement

The Arctic dipole index data were downloaded from the United States National Oceanic and Atmospheric Administration <https://www.beringclimate.noaa.gov/data/>. ANUSPLIN daily temperature and precipitation data for Canada were provided by Natural Resources Canada staff via this link ftp://ftp.nrcan.gc.ca/pub/outgoing/canada_daily_grids data last accessed in 2019.

3.9 References

- Alexeev, V.A., Euskirchen, E.S., Cherry, J.E. & Busey, R.C. (2015). Tundra burning in 2007— Did sea ice retreat matter? *Polar Science*, 9(2), 185–195. doi: <https://doi.org/10.1016/j.polar.2015.02.002>.
- Baltzer, J.L., Veness, T., Chasmer, L.E., Sniderhan, A.E. & Quinton, W.L. (2014). Forests on thawing permafrost: fragmentation, edge effects, and net forest loss. *Global Change Biology*, 20(3), 824–834. doi: <https://doi.org/10.1111/gcb.12349>.
- Barnston, A.G. & Livezey, R.E. (1987). Classification, seasonality and persistence of low-frequency atmospheric circulation patterns. *Monthly Weather Review*, 115(6), 1083–1126. doi: [https://doi.org/10.1175/1520-0493\(1987\)1152.0.CO;2](https://doi.org/10.1175/1520-0493(1987)1152.0.CO;2).
- Bezeau, P., Sharp, M. & Gascon, G. (2015). Variability in summer anticyclonic circulation over the Canadian Arctic Archipelago and West Greenland in the late 20th/early 21st centuries and its effect on glacier mass balance. *International Journal of Climatology*, 35(4), 540–557. doi: <https://doi.org/10.1002/joc.4000>.
- Bhatt, U.S., Walker, D.A., Raynolds, M.K., Walsh, J.E., Bieniek, P. A., Cai, L., Comiso, J.C., Epstein, H.E., Frost, G.V., Gersten, R. & Hendricks, A.S. (2021). Climate drivers of Arctic tundra variability and change using an indicators framework. *Environmental Research Letters*, 16(5), 055019. doi: <https://doi.org/10.1088/1748-9326/abe676>.
- Bonsal, B. & Shabbar, A. (2011). Large-scale climate oscillations influencing Canada, 1900–2008. Canadian biodiversity: ecosystem status and trends 2010. Ottawa, ON: Canadian

Councils of Resource Ministers. Technical thematic report no. 4. Available at:
<http://www.biodivcanada.ca/default.asp?lang=En&n=137E1147-0>.

Budikova, D. (2009). Role of Arctic sea ice in global atmospheric circulation: A review. *Global and Planetary Change*, 68(3), 149-163. doi:
<https://doi.org/10.1016/j.gloplacha.2009.04.001>.

Cai, L., Alexeev, V.A., Walsh, J.E. & Bhatt, U.S. (2018). Patterns, impacts, and future projections of summer variability in the Arctic from CMIP5 models. *Journal of Climate*, 31(24), 9815–9833. doi: <https://doi.org/10.1175/JCLI-D-18-0119.1>.

Chapin III, F.S., Sturm, M., Serreze, M.C., McFadden, J.P., Key, J. R., Lloyd, A.H., McGuire, A.D., Rupp, T.S., Lynch, A.H., Schimel, J.P. & Beringer, J. (2005). *Role of land-surface changes in Arctic summer warming*. *Science*, 310(5748), 657– 660. doi:
<https://www.science.org/doi/10.1126/science.1117368>.

Chasmer, L. & Hopkinson, C. (2017). Threshold loss of discontinuous permafrost and landscape evolution. *Global Change Biology*, 23(7), 2672–2686. doi:
<https://doi.org/10.1111/gcb.13537>.

Choi, N., Kim, K., Lim, Y. & Lee, M. (2019). Decadal changes in the leading patterns of sea level pressure in the Arctic and their impacts on the sea ice variability in boreal summer. *Cryosphere*, 13(11), 3007–3021. doi: <https://doi.org/10.5194/tc-13-3007-2019>.

Connon, R.F., Chasmer, L., Haughton, E., Helbig, M., Hopkinson, C., Sonnentag, O. & Quinton, W.L. (2021). The implications of permafrost thaw and land cover change on snow water

equivalent accumulation, melt and runoff in discontinuous permafrost peatlands. *Hydrological Processes*, 35(9), e14363. doi: <https://doi.org/10.1002/hyp.14363>.

Connon, R.F., Quinton, W.L., Craig, J.R., Hanisch, J. & Sonnentag, O. (2015). The hydrology of interconnected bog complexes in discontinuous permafrost terrains. *Hydrological Processes*, 29(18), 3831–3847. doi: <https://doi.org/10.1002/hyp.10604>.

DeBeer, C.M., Wheeler, H.S., Carey, S.K. & Chun, K.P. (2016). Recent climatic, cryospheric, and hydrological changes over the interior of western Canada: a review and synthesis. *Hydrology and Earth System Sciences*, 20(4), 1573–1598. doi: <https://doi.org/10.5194/hess-20-1573-2016>.

Déry, S.J., Hernandez-Henríquez, M.A., Burford, J.E. & Wood, E.F. (2009). Observational evidence of an intensifying hydrological cycle in northern Canada. *Geophysical Research Letters*, 36(13), L13402. doi: <https://doi.org/10.1029/2009GL038852>.

Déry, S.J. & Wood, E.F. (2004). Teleconnection between the Arctic Oscillation and Hudson Bay River discharge. *Geophysical Research Letters*, 31(18), L18205. doi: <https://doi.org/10.1029/2004GL020729>.

Dyke, L.D. & Brooks, G.R. (2000). *The Physical Environment of the Mackenzie Valley, Northwest Territories: A Base Line for the Assessment of Environmental Change*. Ottawa, ON: Geological Survey of Canada.

Ecosystem Classification Group. (2009). *Ecological regions of the Northwest Territories, Taiga Plains*. Yellowknife, NT: Department of Environment and Natural Resources, Government

of the Northwest. Available at: https://www.enr.gov.nt.ca/sites/enr/files/resources/taiga_plains_ecological_land_classification_report.pdf.

Fazel-Rastgar, F. (2020). Synoptic climatological approach associated with three recent summer heatwaves in the Canadian Arctic. *Journal of Water and Climate Change*, 11(S1), 233–250. doi: <https://doi.org/10.2166/wcc.2020.281>.

Fleming, S.W., Moore, R.D. & Clarke, K.C. (2006). Glacier- mediated streamflow teleconnections to the Arctic Oscillation. *International Journal of Climatology*, 26(5), 619–636. doi: <https://doi.org/10.1002/joc.1273>.

Francis, J.A. & Vavrus, S.J. (2015). Evidence for a wavier jet stream in response to rapid Arctic warming. *Environmental Research Letters*, 10(1), 014005. doi: <https://doi.org/10.1088/1748-9326/10/1/014005>.

Gibson, C., Cottenie, K., Gingras-Hill, T., Kokelj, S.V., Baltzer, J.L., Chasmer, L. & Turetsky, M.R. (2021). Mapping and understanding the vulnerability of northern peatlands to permafrost thaw at scales relevant to community adaptation planning. *Environmental Research Letters*, 16(5), 055022. doi: <https://doi.org/10.1088/1748-9326/abe74b>.

Gibson, C.M., Chasmer, L.E., Thompson, D.K., Quinton, W.L., Flannigan, M.D. & Olefeldt, D. (2018). Wildfire as a major driver of recent permafrost thaw in boreal peatlands. *Nature Communications*, 9(1), 3041. doi: <https://doi.org/10.1038/s41467-018-05457-1>.

Helbig, M., Chasmer, L.E., Kljun, N., Quinton, W.L., Treat, C.C. & Sonntag, O. (2017). The positive net radiative greenhouse gas forcing of increasing methane emissions from a

thawing boreal forest-wetland landscape. *Global Change Biology*, 23(6), 2413–2427. doi: <https://doi.org/10.1111/gcb.13520>.

Helsel, D.R. & Hirsch, R.M. (1992). *Statistical Methods in Water Resources*. Amsterdam: Elsevier.

Heo, E., Sung, M., An, S. & Yang, Y. (2021). Decadal phase shift of summertime Arctic Dipole pattern and its nonlinear effect on sea ice extent. *International Journal of Climatology*, 41(9), 4732–4742. doi: <https://doi.org/10.1002/joc.7097>.

Horvath, S., Stroeve, J., Rajagopalan, B. & Jahn, A. (2021). Arctic sea ice melt onset favored by an atmospheric pressure pattern reminiscent of the north American Eurasian Arctic pattern. *Climate Dynamics*, 57(7), 1771–1787. doi: <https://doi.org/10.1007/s00382-021-05776-y>.

Hutchinson, M.F., Mckenny, D.W., Lawrence, K., Pedlar, J.H., Hopkinson, R.F., Mileweska, E. & Papadopol, P. (2009). Development and testing of Canada-wide interpolated spatial models of daily minimum–maximum temperature and precipitation for 1961–2003. *Journal of Applied Meteorology and Climatology*, 48(4), 725–741. doi: <https://doi.org/10.1175/2008JAMC1979.1>.

IPCC. (2021). In: Masson-Delmotte, V., Zhai, P., Pirani, A., Connors, S.L., Péan, C., Berger, S., Caud, N., Chen, Y., Goldfarb, L., Gomis, M.I., Huang, M., Leitzell, K., Lonnoy, E., Matthews, J.B.R., Maycock, T.K., Waterfield, T., Yelekçi, O., Yu, R. and Zhou, B. (Eds.) *Climate Change 2021: The Physical Science Basis. Contribution of Working Group I to the*

Sixth Assessment Report of the Intergovernmental Panel on Climate Change. Cambridge: Cambridge University Press.

Jain, P. & Flannigan, M. (2021). The relationship between the polar jet stream and extreme wildfire events in North America. *Journal of Climate*, 34(15), 6247–6265. doi: <https://doi.org/10.1175/JCLI-D-20-0863.1>.

Jiang, R., Gan, T.Y., Xie, J. & Wang, N. (2014). Spatiotemporal variability of Alberta's seasonal precipitation, their teleconnection with large-scale climate anomalies and sea surface temperature. *International Journal of Climatology*, 34(9), 2899–2917. doi: <https://doi.org/10.1002/joc.3883>.

Kalnay, E., Kanamitsu, M., Kistler, R., Collins, W., Deaven, D., Gandin, L. & Woollen, J. (1996). The NCEP/NCAR 40-year reanalysis project. *Bulletin of the American Meteorological Society*, 77(3), 437–472. doi: [https://doi.org/10.1175/1520-0477\(1996\)077<0437:TNYRP>2.0.CO;2](https://doi.org/10.1175/1520-0477(1996)077<0437:TNYRP>2.0.CO;2).

Kochtubajda, B., Stewart, R.E., Flannigan, M.D., Bonsal, B.R., Cuell, C. & Mooney, C.J. (2019). An assessment of surface and atmospheric conditions associated with the extreme 2014 wild- fire season in Canada's Northwest Territories. *Atmosphere- Ocean*, 57(1), 73–90. doi: <https://doi.org/10.1080/07055900.2019.1576023>.

Lackmann, G.M. & Gyakum, J.R. (1996). The synoptic- and planetary-scale signatures of precipitating systems over the Mackenzie River basin. *Atmosphere-Ocean*, 34(4), 647–674. doi: <https://doi.org/10.1080/07055900.1996.9649581>.

- Lafleur, P.M. & Humphreys, E.R. (2008). Spring warming and carbon dioxide exchange over low Arctic tundra in central Canada. *Global Change Biology*, 14(4), 740–756. doi: <https://doi.org/10.1111/j.1365-2486.2007.01529.x>.
- Lei, R., Tian-Kunze, X., Leppäranta, M., Wang, J., Kaleschke, L. & Zhang, Z. (2016). Changes in summer sea ice, albedo, and partitioning of surface solar radiation in the Pacific sector of Arctic Ocean during 1982–2009. *Journal of Geophysical Research: Oceans*, 121(8), 5470–5486. Doi: <https://doi.org/10.1002/2016JC011831>.
- Matsumura, S., Zhang, X. & Yamazaki, K. (2014). Summer Arctic atmospheric circulation response to spring Eurasian snow cover and its possible linkage to accelerated sea ice decrease. *Journal of Climate*, 27(17), 6551–6558. doi: <https://doi.org/10.1175/JCLI-D-13-00549.1>.
- McCabe, G.J. & Dettinger, M.D. (1999). Decadal variations in the strength of ENSO teleconnections with precipitation in the western United States. *International Journal of Climatology*, 19(13), 1399–1410. doi: [https://doi.org/10.1002/\(SICI\)1097-0088\(19991115\)19:133.0.CO;2-A](https://doi.org/10.1002/(SICI)1097-0088(19991115)19:133.0.CO;2-A).
- McKenney, D.W., Hutchinson, M.F., Papadopol, P., Lawrence, K., Pedlar, J., Campbell, K. & Owen, T. (2011). Customized spatial climate models for North America. *Bulletin of the American Meteorological Society*, 92(12), 1611–1622. doi: <https://doi.org/10.1175/2011BAMS3132.1>.

- Mekonnen, Z.A., Riley, W.J., Berner, L.T., Bouskill, N.J., Torn, M.S., Iwahana, G., Breen, A.L., Myers-Smith, I.H., Criado, M.G., Liu, Y. & Euskirchen, E.S. (2021). Arctic tundra shrubification: a review of mechanisms and impacts on ecosystem carbon balance. *Environmental Research Letters*, 16(5), 053001. doi: <https://doi.org/10.1088/1748-9326/abf28b>.
- Newton, B.W., Prowse, T.D. & Bonsal, B.R. (2014). Evaluating the distribution of water resources in western Canada using synoptic climatology and selected teleconnections. Part 2: summer season. *Hydrological Processes*, 28(14), 4235–4249. doi: <https://doi.org/10.1002/hyp.10235>.
- NOAA. (2020). NOAA Climate Analysis and Plotting tool. Boulder, CO: NOAA PSL. Available at: <https://psl.noaa.gov/cgi-bin/data/getpage.p> [Accessed on 15th December 2020].
- NOAA. (2021). Bering climate. Boulder, CO: NOAA. Accessed on 15th August 2021 at: <https://www.beringclimate.noaa.gov/data/index.php>.
- NRCAN. (2019). Natural resources Canada ANUSPLIN data. Available at: ftp://ftp.nrcan.gc.ca/pub/outgoing/canada_daily_grids.
- Overland, J.E., Francis, J.A., Hanna, E. & Wang, M. (2012). The recent shift in early summer Arctic atmospheric circulation. *Geophysical Research Letters*, 39(19), L19804. doi: <https://doi.org/10.1029/2012GL053268>.

- Overland, J.E. & Wang, M. (2010). Large-scale atmospheric circulation changes are associated with the recent loss of Arctic Sea ice. *Tellus, Series A: Dynamic Meteorology and Oceanography*, 62(1), 1–9. doi: <https://doi.org/10.1111/j.1600-0870.2009.00421.x>.
- Persaud, B.D., Whitfield, P.H., Quinton, W.L. & Stone, L.E. (2020). Evaluating the suitability of three gridded-datasets and their impacts on hydrological simulation at Scotty Creek in the southern Northwest Territories, Canada. *Hydrological Processes*, 34(4), 898–913. doi: <https://doi.org/10.1002/hyp.13663>.
- Phillips, D. (1990). The climates of Canada. Ottawa, ON: Ministry of Supply and Services Canada. Catalogue no. En56-1/1990E, 176 pp.
- Quinton, W.L., Hayashi, M. & Chasmer, L.E. (2011). Permafrost- thaw-induced land-cover change in the Canadian subarctic: implications for water resources. *Hydrological Processes*, 25(1), 152–158. doi: <https://doi.org/10.1002/hyp.7894>.
- R Development Core Team. (2016). R: a language and environment for statistical computing. Vienna: R Foundation for Statistical Computing. Available at: <https://www.R-project.org/>.
- Rouse, W.R., Douglas, M.S., Hecky, R.E., Hershey, A.E., Kling, G.W., Lesack, L., Marsh, P., McDonald, M., Nicholson, B.J., Roulet, N.T. & Smol, J.P. (1997). Effects of climate change on the freshwaters of Arctic and Subarctic North America. *Hydrological Processes*, 11(8), 873–902. doi: [https://doi.org/10.1002/\(SICI\)1099-1085\(19970630\)11:8<873::AID-HYP510>3.0.CO;2-6](https://doi.org/10.1002/(SICI)1099-1085(19970630)11:8<873::AID-HYP510>3.0.CO;2-6).

Serreze, M.C. & Barry, R.G. (2014). *The Arctic Climate System*. New York, NY: Cambridge University Press.

Serreze, M.C., Stroeve, J., Barrett, A.P. & Boisvert, L.N. (2016). Summer atmospheric circulation anomalies over the Arctic Ocean and their influences on September Sea ice extent: a cautionary tale. *Journal of Geophysical Research: Atmospheres*, 121(19), 11463–11485. doi: <https://doi.org/10.1002/2016JD025161>.

Shabbar, A., Bonsal, B. & Khandekar, M. (1997). Canadian precipitation patterns associated with the Southern Oscillation. *Journal of Climate*, 10(12), 3016–3027. doi: [https://doi.org/10.1175/1520-0442\(1997\)0102.0.CO;2](https://doi.org/10.1175/1520-0442(1997)0102.0.CO;2).

Shi, X., Marsh, P. & Yang, D. (2015). Warming spring air temperatures, but delayed spring streamflow in an Arctic headwater basin. *Environmental Research Letters*, 10(6), 64003. doi: <https://doi.org/10.1088/1748-9326/10/6/064003>.

Skinner, W.R., Flannigan, M.D., Stocks, B.J., Martell, D.L., Wotton, B. M., Todd, J.B., Mason, J.A., Logan, K.A. & Bosch, E.M. (2002). A 500 hPa synoptic wildland fire climatology for large Canadian forest fires, 1959–1996. *Theoretical and Applied Climatology*, 71(3), 157–169. doi: <https://doi.org/10.1007/s007040200002>.

Skinner, W.R., Stocks, B.J., Martell, D.L., Bonsal, B. & Shabbar, A. (1999). The association between circulation anomalies in the mid-troposphere and area burned by wildland fire in Canada. *Theoretical and Applied Climatology*, 63(1), 89–105. doi: <https://doi.org/10.1007/s007040050095>.

- Sniderhan, A.E. & Baltzer, J.L. (2016). Growth dynamics of black spruce (*Picea mariana*) in a rapidly thawing discontinuous permafrost peatland. *Journal of Geophysical Research: Biogeosciences*, 121(12), 2988–3000. doi: <https://doi.org/10.1002/2016JG003528>.
- Tan, X., Gan, T.Y., Chen, S. & Liu, B. (2019). Modeling distributional changes in winter precipitation of Canada using Bayesian spatiotemporal quantile regression subjected to different teleconnections. *Climate Dynamics*, 52(3), 2105–2124. doi: <https://doi.org/10.1007/s00382-018-4241-0>.
- Tang, Q., Zhang, X. & Francis, J.A. (2014). Extreme summer weather in northern mid-latitudes linked to a vanishing cryosphere. *Nature Climate Change*, 4(1), 45–50. doi: <https://doi.org/10.1038/nclimate2065>.
- Thompson, D.W. & Wallace, J.M. (1998). The Arctic Oscillation signature in the wintertime geopotential height and temperature fields. *Geophysical Research Letters*, 25(9), 1297–1300.
- Trenberth, K.E. (1997). The definition of El Niño. *Bulletin of the American Meteorological Society*, 78(12), 2771–2778. doi: [https://doi.org/10.1175/1520-0477\(1997\)0782.0.CO;2](https://doi.org/10.1175/1520-0477(1997)0782.0.CO;2).
- Tukey, J.W. (1949). Comparing individual means in the analysis of variance. *Biometrics*, 5, 99–114.
- Turetsky, M.R., Wieder, R.K., Vitt, D.H., Evans, R.J. & Scott, K.D. (2007) The disappearance of relict permafrost in boreal North America: effects on peatland carbon storage and fluxes.

Global Change Biology, 13(9), 1922–1934. doi: <https://doi.org/10.1111/j.1365-2486.2007.01381.x>.

Vincent, L.A., Zhang, X., Brown, R.D., Feng, Y., Mekis, E., Milewska, E.J., Wan, H. & Wang, X.L. (2015). Observed trends in Canada's climate and influence of low-frequency variability modes. *Journal of Climate*, 28(11), 4545–4560. doi: <https://doi.org/10.1175/JCLI-D-14-00697.1>.

Wallace, J.M. & Gutzler, D.S. (1981). Teleconnections in the geopotential height field during the northern hemisphere winter. *Monthly Weather Review*, 109(4), 784–812. doi: [https://doi.org/10.1175/1520-0493\(1981\)109<0784:TITGHF>2.0.CO;2](https://doi.org/10.1175/1520-0493(1981)109<0784:TITGHF>2.0.CO;2).

Wang, J., Zhang, J., Watanabe, E., Ikeda, M., Mizobata, K., Walsh, J.E., Bai, X. & Wu, B. (2009). Is the dipole anomaly a major driver to record lows in Arctic summer sea ice extent? *Geophysical Research Letters*, 36(5), L05706. doi: <https://doi.org/10.1029/2008GL036706>.

Watanabe, E., Wang, J., Sumi, A. & Hasumi, H. (2006). Arctic Dipole anomaly and its contribution to sea ice export from the Arctic Ocean in the 20th century. *Geophysical Research Letters*, 33(23), L23703. doi: <https://doi.org/10.1029/2006GL028112>.

Westerling, A.L. (2016). Increasing western US forest wildfire activity: sensitivity to changes in the timing of spring. *Philosophical Transactions of the Royal Society of London. Series B, Biological Sciences*, 371(1696), 20150178. doi: <https://doi.org/10.1098/rstb.2015.0178>.

Wilcox, E.J., Keim, D., de Jong, T., Walker, B., Sonnentag, O., Sniderhan, A.E., Mann, P. & Marsh, P. (2019). Tundra shrub expansion may amplify permafrost thaw by advancing

snow- melt timing. *Arctic Science*, 5(4), 202–217. doi: <https://doi.org/10.1139/as-2018-0028>.

Wong, J.S., Razavi, S., Bonsal, B.R., Wheeler, H.S. & Asong, Z.E. (2017). Inter-comparison of daily precipitation products for large-scale hydro-climatic applications over Canada. *Hydrology and Earth System Sciences*, 21(4), 2163–2185. doi: <https://doi.org/10.5194/hess-21-2163-2017>.

Woo, M., Rouse, W.R., Stewart, R.E. & Stone, J.M.R. (2008). The Mackenzie GEWEX Study: A Contribution to Cold Region Atmospheric and Hydrologic Sciences. Berlin-Heidelberg: Springer. https://doi.org/10.1007/978-3-540-73936-4_1.

Wright, N., Hayashi, M. & Quinton, W.L. (2009). Spatial and temporal variations in active layer thawing and their implication on run- off generation in peat-covered permafrost terrain. *Water Resources Research*, 45(5), W05414. doi: <https://doi.org/10.1029/2008WR006880>.

Wu, B., Zhang, R., Wang, B. & D'Arrigo, R. (2009). On the association between spring Arctic Sea ice concentration and Chinese summer rainfall. *Geophysical Research Letters*, 36(9), L09501. doi: <https://doi.org/10.1029/2009GL037299>.

Wu, B., Zhang, R. & Wang, J. (2005). Dipole anomaly in the Arctic atmosphere and winter Arctic Sea ice motion. *Science in China Series D, Earth Sciences*, 48(9), 1529–1536. doi: <https://doi.org/10.1360/04yd0174>.

Xiao, K., Chen, M., Wang, Q., Wang, X. & Zhang, W. (2020). Low frequency sea level variability and impact of recent sea ice decline on the sea level trend in the Arctic Ocean

from a high- resolution simulation. *Ocean Dynamics*, 70(6), 787–802. doi: <https://doi.org/10.1007/s10236-020-01373-5>.

Zhang, J., Lindsay, R., Steele, M. & Schweiger, A. (2008). What drove the dramatic retreat of Arctic Sea ice during summer 2007? *Geophysical Research Letters*, 35(11), L11505. doi: <https://doi.org/10.1029/2008GL034005>.

4 Trend analysis of surface shortwave radiation across continental Northwest Territories, Canada (1980-2020)

4.1 Abstract

Incoming incident surface shortwave radiation (SSR) is a critical driver of energy balance in lakes, yet long-term patterns of this climate variable are not well understood over northern high latitude regions. To understand the feedbacks of SSR influences on northern lake energy balance, there is a need to quantify spatiotemporal trends in SSR that reaches Earth's surface. This is important in northern regions, such as Northwest Territories (NWT), Canada, where lakes are undergoing environmental shifts in response to climate warming. Using modelled SSR based on air temperatures and remotely sensed thermal skin temperatures from lakes, this study quantifies trends in SSR receipt from 1980 to 2020, examines the association between total cloud cover and SSR, and explores the sensitivity of lake surface water temperature (LSWT) to changing SSR across the continental NWT.

SSR trends in ecozones of the continental NWT show clear spatial and temporal patterns between 1980 and 2020. There was an general decrease in annual mean SSR across the Taiga Plains and Northern Arctic ecozones by an average of $\sim 0.8 \text{ Wm}^{-2}$ with contrasting increasing and decreasing trends in the Taiga Shield and Southern Arctic ecozones, respectively. In summer, reduction in SSR is evident in all ecozones, where the rate of decline since 1980 ranges between 0.6 and $4.1 \text{ Wm}^{-2}\text{decade}^{-1}$. Generally, a negative correlation was identified between cloud cover and SSR, with the Taiga Plains ecozone showing the strongest negative relationship. LSWT in small lakes was positively correlated with SSR, while a mixture of positive and negative correlations in the Taiga Plains and Taiga Shield ecozones is noted for LSWT for medium and large lakes. This study captures spatiotemporally heterogeneity in SSR trends that will be useful to represent in climate

predictions in NWT. Also, understanding changes in SSR and LSWT is important for NWT communities who depend on winter roads, which are constructed across lakes.

4.2 Introduction

Incident surface shortwave radiation (SSR) is energy from the Sun that reaches the Earth's surface, driving both Earth's energy balance and the climate system, as well as important ecological processes (Budyko, 1969; Wild, 2009). Numerous studies have reported a decrease (3–9 Wm^{-2}) in global annual mean SSR from the 1950s to the 1980s, which was followed by an increase (1–4 Wm^{-2}) after this time period (Wild, 2009; Yuan et al., 2021). In North America, SSR trends fluctuate (Yuan et al., 2021), and earlier studies are limited to the United States or specific cities in Canada (Weston et al., 2007; Cutforth & Judiesch, 2007; Chiacchio et al., 2010). Increasing trends of SSR reported in parts of Alaska, during the early 1960s to mid-1970s, were followed by a predominant decrease until the late 1990s (Chiacchio et al., 2010). In contrast, and at higher latitudes, a reduction in SSR by 2.25% and 2.50% per decade was observed at Alert and Resolute Bay in Nunavut, respectively, between 1964 and 2003 (Weston et al., 2007). In the Canadian Prairies, average daily SSR was reduced by approximately 1.7% per decade between 1951 and 2005, while air temperature increased during the same period (Cutforth & Judiesch, 2007). Despite the importance of SSR to Earth's energy balance and that historical SSR trends are well documented in other parts of the world, only a few studies have investigated long-term temporal changes of SSR in Arctic regions including northern Canada (AMAP, 2021).

While external factors such as seasonal changes in Earth's orbit and solar output from the Sun can affect SSR incident on Earth's stratosphere, internal factors within the troposphere such as water vapour, aerosol type and concentration, and cloud cover also have important roles in SSR trends and variability (Wild, 2009). Cloud cover, in particular, has a notable influence on modulating the amount of incoming SSR that reaches the Earth's surface (Twomey, 1976). Variations in SSR are

explained primarily by the differences between maximum and minimum air temperatures (*i.e.*, the diurnal temperature range), which influence cloud formation (Bristow & Campbell 1984). The relationship between cloud cover and incoming SSR is complex. Moreover, cloud types are also known to influence SSR. For example, low clouds have higher albedo and reflect SSR, whereas high altitude clouds may allow SSR into the lower atmosphere (NASA, 1999). However, increases in high altitude clouds may capture longwave radiation and remit it back to the lower troposphere, thereby increasing air temperature (NASA, 1999). Collectively, these processes can contribute to a further amplification of climate warming (NASA, 1999; Abe et al., 2016; Box et al., 2019).

Climate warming has multiple implications to permafrost thaw, which impacts hydrology and ecology in northern regions and it is reported that SSR also plays a primary driving role in both the hydrological cycle (Shook & Pomeroy, 2011; Wild & Liepert, 2010) and lake productivity (Tian et al., 2017; van de Poll, 2021; Adams et al., 2021). For example, during summer, Hinkel et al. (2012) found that SSR had a strong control on lake near-surface temperature causing two lakes in Barrow, Alaska to be warmer by 1.0°C to 4.0°C. Schmid & Köster (2016) reported that approximately 40% of the spring and summer lake surface temperature increases at Lake Zurich, Switzerland, was caused by increasing SSR between 1981 and 2013. In Canada's northern latitude regions, high density of lakes plays a vital role in regional energy balance because of the high heat capacity of water and the ability of lakes to store energy (Rouse et al. 2005). . In the Mackenzie River Basin, lakes facilitate the exchange of heat, energy, and water by regulating evaporation, runoff, and basin water storage (Oswald & Rouse, 2004). SSR, longwave radiation, and latent heat fluxes tend to dominate the energy budget of most lakes (Fink et al., 2014; Schmid & Read, 2022). Although lakes are ecologically important and their characteristics are considered indicators

of climate warming (Adrian et al., 2009; O'Reilly et al., 2015; Fabris et al., 2020), understanding how lake temperatures vary in response to changes in SSR is limited. In addition, long-term trends in SSR receipt are not well documented across high latitude regions.

Canada's Changing Climate Report (Bush & Lemmen, 2019) states SSR is an important climate variable, but focuses its review specifically on how air temperature, precipitation and other lake ecosystem indicators in Canada have changed during the past five decades without incorporating SSR trends. This is due to a scarcity of *in situ* SSR data a result of the paucity of actinometric stations, and relatively few long-term SSR measurements in high latitude regions (Przybylak et al., 2021). Consequently, the primary indicator for determining long-term trends in global and regional climate change tend to be based largely on surface air temperature, for which long-term records are only available near areas of higher population density (Arias et al., 2021). While measurements of *in situ* SSR are disparate, estimates of SSR may be found in model reanalysis, remote sensing observations, as well as spatially interpolated diurnal temperature-range-based modelled data (Bristow & Campbell 1984; Hungerford et al., 1989; Thornton & Running 1999). Temperature-based SSR models assume maximum air temperature decreases with lower atmospheric transmissivity and minimum air temperature increases with increased cloud cover (Bristow & Campbell 1984; Hungerford et al., 1989). Clear sky, on the other hand, will result in greater maximum air temperatures due to more SSR, and minimum air temperatures will decrease due to reduced atmospheric emissivity (Bristow & Campbell 1984; Hungerford et al., 1989). That is, Bristow & Campbell (1984) and Hungerford et al., (1989) assumed cloudier conditions when diurnal temperature ranges are small, and clear conditions when diurnal temperature ranges are large in their model. Temperature-based SSR estimates have been found to align closely with

available *in situ* SSR data in North America and in other continents (Bristow & Campbell 1984; Hungerford et al., 1989; Hasenauer et al. 2003; Stettz et al., 2019; Thornton, et al., 2021; Yuan et al., 2021) and have been used to characterize the variability and trends of SSR, as they offer wide spatial and temporal coverage (e.g., Wild et al., 2009; Yuan et al., 2021). Notwithstanding, limited attention has been paid in quantifying SSR long-term patterns and implications of these changing SSR patterns on northern lakes. These types of temperature-based SSR data can provide extensive spatiotemporal coverage and help improve our understanding of SSR variability in northern Canada.

As outlined in preceding paragraphs, prior studies focused on trends in SSR and LSWT at a global and continental scale, however the high degree of spatial and temporal variability of these trends reported (Wild, 2009; Yuan et al., 2021; O'Reilly et al., 2015) warrants further investigation in these trend patterns at the regional and local level across northern regions. Hence, the objectives of this research are: (1) to quantify spatial and temporal trends of SSR in continental NWT, Canada, during the 1980 to 2020 period, (2) to explore whether observed changes in SSR can be attributed to cloud cover, and (3) to evaluate the responses of lake surface water temperature (LSWT) to SSR trends by focusing on lakes in the North Slave Region, as a case study to advance understanding of SSR spatiotemporal patterns and potential implications to lake energy balance during the warm season. It is important to detect and understand changes in SSR especially since it a significant driver of the Earth's energy budget which may influence the rate at which the atmosphere and lakes warm. Warming have impacted the rate of permafrost thaw and productivity of lakes, both of which have been documented since the 1980s in the NWT (Kwong & Gan, 1994; Rouse et al., 1997; Kuhn & Butman 2021, DeBeer et al., 2021).

4.3 Study Area

The study area, continental NWT, spans seven ecozones from the southern boreal at 60° N to the Arctic Ocean at 70° N, from Boreal and Taiga Cordillera in the west to the Taiga Shield and Southern Arctic in the east covering an area of 1.0 million km² (Figure 4.1). The region is dominated by arctic and subarctic continental climate, typified by short cool summers and long cold winters (Phillips, 1990). Although much surface freshwater is present, this region is considered relatively dry (Phillips, 1990). This is due to low total annual precipitation which averages between 200 and 400 mm per year, with at least 50% falling as snow between November and March (Phillips, 1990; Bailey et al., 1997). Summer air temperatures are highest in July (daily mean air temperature ranging from 7°C to 17°C) and lowest in January (daily mean air temperature varies from -17°C to -29 °C) (ECCC, 2022). SSR is at a minimum in winter months when daylight hours are reduced and at these latitudes the declination of the sun is at its lowest (Bailey, Oke & Rouse, 1997). During this period, the persistence of snow and ice in this region reflects a large proportion of incoming SSR (Bailey et al., 1997; Serreze & Barry, 2014). In contrast during the summer months, when the Earth's northern hemisphere is tilted towards the sun, SSR is at its highest and maximum in June (Bailey et al., 1997). Objective three of this study focuses on the SSR – LSWT relationship with an emphasis on the North Slave Region due to a very high density of lakes (approximately 38% of NWT lakes are located in the North Slave Region; Messenger et al., 2016). The North Slave Region comprises a mosaic of forest, grassland and shrubs, wetlands, rivers and lakes, with approximately 24% of the surface area covered with wetlands, rivers and lakes (Ecosystem Classification Group, 2009).

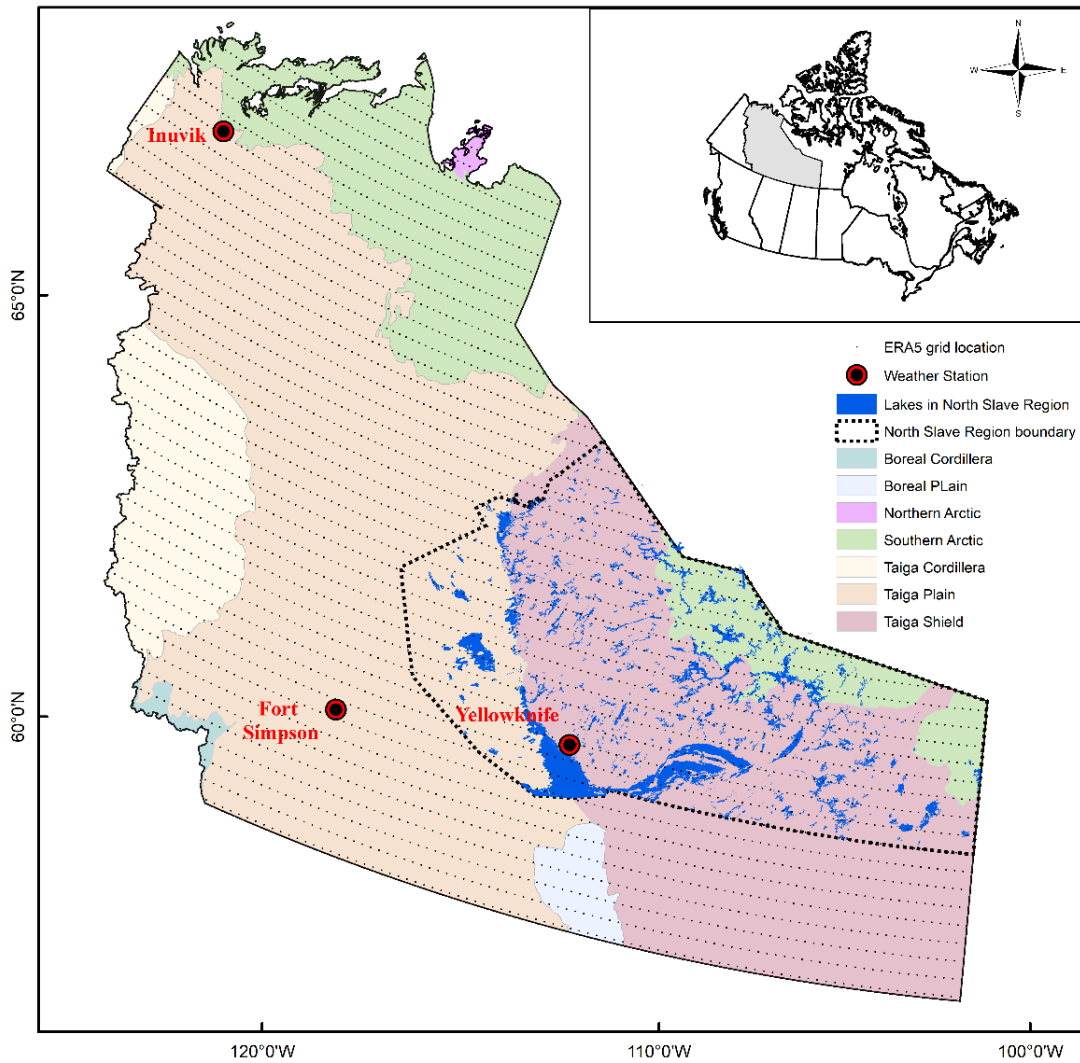


Figure 4.1 Map shows the study area with the SSR, and cloud cover data grid points (black dots) extracted from Daymet and ERA5 databases, respectively. Different colours in the map indicate ecozones of the Northwest Territories. Three independent weather stations are shown in red & black circles and the location of selected lakes within the North Slave region are shown with the blue shapefiles.

4.4 Data and Methods

4.4.1 Databases

Continuous and long-term *in situ* climate data are spatially and temporally limited in NWT due to the remote and vast area of this northern region (Mekis et al., 2018). To address this issue, Daymet (Daily surface weather and climatological summaries) SSR interpolated data (1-km grid

resolution) from Oak Ridge National Laboratory Distributed Active Archive (ORNL DDAA) were used to understand how SSR receipt varied over the study area. Fifth generation reanalysis (ERA5) cloud cover data (31-km grid resolution) from the European Centre for Medium-Range Weather Forecast (ECMWF) were used to determine the correspondence between cloud cover and SSR. Landsat-derived LSWT data (30-m resolution) were used to quantify changes in LSWT response to SSR. These datasets were used to understand changing trends in SSR for the following reasons: (1) they cover the significant gap of *in situ* observations for the study area by providing continuous and long-term spatial and temporal data (daily estimates of SSR and ERA5 since 1980 and 16-day overpass of LSWT data since 1984); and (2) databases are freely distributed and easy to access. Additional details on these datasets are provided in the following paragraphs.

4.4.1.1 Shortwave radiation data

Daymet SSR (sum of diffuse and direct radiation) data for 1980-2020, version 4, were used in this study (Thornton et al., 1997; Thornton & Running, 1999; Thornton et al., 2021). Thornton et al. (2021) computed incoming SSR using the Mountain Microclimate Simulation Model version 4.3 (Bristow & Campbell 1984; Hungerford et al., 1989; Thornton & Running 1999). The model utilizes *in situ* daily minimum and maximum air temperature and daily precipitation from Environment and Climate Change Canada (ECCC) weather stations, along with other geographic attributes such as elevation, geographic coordinates, and azimuth angle to generate SSR over Canada (Thornton & Running, 1999; Thornton et al., 2021). In any given year, at least 1000 to 1500 *in situ* Canadian stations were used in Daymet to develop interpolated gridded products at 1-km resolution over Canada, but the quantity of *in situ* locations in northern Canada were much less when compared with southern Canada. Daymet SSR has relatively low mean error (0.02 MJ m⁻²; max error of 2.5 MJ m⁻²) compared with SSR in areas with dense networks of weather stations,

however, mean bias increases in areas with sparse monitoring networks, as expected (Thornton et al., 2000; Hasenauer et al., 2003; Thornton et al., 2021). Additional details on Daymet modelled SSR data generation and validation can be found in Thornton & Running (1997), Thornton et al. (2000) and Thornton et al. (2021). For this study, daily Daymet SSR were obtained nearest to the centroid of ERA5 (described in next paragraph) grids (Figure 4.1) across the continental NWT using Package Daymetr R (Hufkens et al., 2018). Daily data were aggregated to compute annual and seasonal average SSR for each year (1980-2020). Meteorological seasons analysed were defined as spring (March-April-May), summer (June-July-August), and autumn (September-October-November), temporally consistent with prior SSR trend studies (Chiacchio et al., 2010; Yuan et al., 2021).

4.4.1.2 Total cloud cover data

To explore how cloud cover influences incoming modelled SSR, ERA5 total cloud cover data were used as it provides spatial coverage across NWT, coincident with Daymet modelled radiation. ERA5 is the fifth-generation global atmospheric reanalysis of the ECMWF, developed as an improvement from its predecessor ERA-Interim (Hersbach et al., 2020), which assimilates several moisture-sensitive satellite channels, thereby improving estimates of cloud cover areas (Hersbach et al., 2020). The spatial and temporal resolution of ERA5 is approximately 31 km grid spacing and available from 1979 to the present at hourly scale. To address objective 2, ERA5 total cloud data were extracted from 1980 to 2020 for continental NWT. Finally, to determine how well ECMWF ERA-5 data corresponded with measured cloud cover, as an independent assessment of SSR-cloud cover relationship, *in situ* total cloud cover data archived by ECCC for 1980-2020 were examined at three locations: Fort Simpson, Yellowknife, and Inuvik (Figure 4.1). Total cloud cover is estimated every one to three hours by human observers at meteorological stations operated by

Nav Canada and represent line of sight of total cloud cover (Milewska, 2004). Data were aggregated to seasonal averages to coincide with grouping of Daymet SSR and the difference from the long-term 1980-2020 averages (anomalies) were computed and normalised (divided by standard deviation).

4.4.1.3 Lake surface water temperature data

Remote sensed lake surface water temperature (LSWT) data were used to explore how LSWT varies with SSR as *in situ* LSWT observations are sparse for lakes in the NWT (Attiah et al., 2022). Remote sensed observation is one method that may be used for estimating lake surface water temperature as has been previously demonstrated (e.g., Wloczyk et al., 2006; Dörnhöfer & Oppelt, 2016; Pareeth et al., 2016; Schaeffer et al., 2018; Sharaf et al., 2019; Vanhellemont, 2020). For example, Pareeth et al. (2016) reported that differences between satellite thermal and measured lake surface temperature ranged from 0.38°C to 1.28°C (root mean squared error, RMSE) in a sub-alpine lake. A comparison of Landsat-derived and *in situ* lake surface temperature for five lakes in Alaska RSME was 0.41°C (Huang et al., 2017).

Here, 500 lakes were selected in the North Slave Region (Figure 4.1) and classified based on their surface area: small lakes less than 1 km², medium lakes between 1 km² and 100 km² and large lakes greater than 100 km² by adapting Rouse et al. (2005) classification of lakes. Lake boundaries were obtained from the HydroLakes database (Messenger et al., 2016). Surface temperature for the 500 lakes were derived from the thermal infrared (TIR) band of Landsat-5 TM (Thematic Mapper), Landsat-7 ETM+ (Enhanced Thematic Mapper Plus), and Landsat-8 OLI/TIRS (Operational Land Imager and the Thermal Infrared Sensor) between 1984 and 2020 (North Slave Region LSWT). A comprehensive data generation and description is available in Attiah et al. (2022). North Slave

Region Landsat derived LSWT has shown a mean bias of 0.12°C and an RMSE of 1.7°C compared with *in situ* surface water temperature measurements from 2014 to 2019 (Attiah et al., 2022). To compare LSWT with SSR, the corresponding SSR estimates were extracted from the nearest LSWT pixels at each lake centroid.

4.4.2 Statistical Analysis

The non-parametric Mann–Kendall test and the Theil-Sen slope were used to determine trend significance and rate of change in SSR and LSWT (Mann 1945; Kendall 1975; Yue *et al.*, 2002). To understand if SSR is changing, we followed the null hypothesis that contends there is no trend in SSR time series data. The SSR trend analyses were conducted for the periods 1980-2020, 1980-2000 and 2001-2020 for each grid. The additional defined time periods (1980-2000 and 2001-2020) were added to the analysis to account for exacerbated thaw of permafrost from 2000 onwards, resulting in expansion of wetlands (Chasmer & Hopkinson 2016) and the potential for greater evaporative losses and higher atmospheric moisture content as shown previously (Helbig et al., 2016). Nonparametric Spearman correlation analysis (Wilks, 2006) was conducted to investigate whether SSR was negatively correlated with increasing cloud cover across NWT.

To better understand the potential correspondence between SSR and LSWT in the North Slave Region, Spearman correlation analysis was also carried out from 1984 to 2020 between these two variables. We applied the Kruskal-Wallis test to detect if correlation values were different among lake sizes. All statistical analyses were performed using R 4.1.0 Project software (R Development Core Team, 2021). Trend significance was assessed at $p \leq 0.05$, unless otherwise stated.

4.5 Results

4.5.1 Characterizing trends in annual and seasonal mean SSR in the NWT

4.5.1.1 Annual mean SSR trends

Trends in mean annual SSR varied spatially and temporally across NWT from 1980 to 2020 (Figure 4.2). SSR generally decreased from 1980 (negative trend) in western NWT and increased from 1980 in eastern NWT (positive trend) (Figure 4.2a). The largest reduction in mean annual SSR was detected in the Boreal Cordillera ($-1.2 \text{ Wm}^{-2} \text{ decade}^{-1}$), Taiga Cordillera ($-1.2 \text{ Wm}^{-2} \text{ decade}^{-1}$), Taiga Plains, and Northern Arctic ($-0.8 \text{ Wm}^{-2} \text{ decade}^{-1}$) ecozones (Figure 4.2a.). The Southern Arctic ecozone had a mixture of positive and negative SSR with rate of change ranging from -1.8 to $+2.3 \text{ Wm}^{-2} \text{ decade}^{-1}$, with a mean of $-0.9 \text{ Wm}^{-2} \text{ decade}^{-1}$. In contrast, SSR trends in the majority of the Taiga Shield ecozone were generally increasing during the past 40 years with trend magnitude varying from $+0.4$ to $+3.0 \text{ Wm}^{-2} \text{ decade}^{-1}$ (Figure 4.2b).

During the 1980-2000 period, apart from the Taiga Cordillera ecozone, mean annual trends in SSR generally decreased across NWT (Figure 4.2b). The Taiga Cordillera had a mixture of increasing and decreasing SSR trends while the mean annual SSR decreased by approximately $-2.1 \text{ Wm}^{-2} \text{ decade}^{-1}$ between 1980 and 2000 in the Taiga Plains ecozone with largest decreases ($-12.8 \text{ Wm}^{-2} \text{ decade}^{-1}$) in the southern Taiga Plains and Boreal Cordillera ($-3.7 \text{ Wm}^{-2} \text{ decade}^{-1}$) ecozones (Figure 4.2b). In contrast, during the 2001-2020 interval, with exception of the Cordilleran ecozones (Boreal and Taiga Cordillera), a large proportion of NWT showed an increase in mean annual SSR (Figure 4.2c). Mean annual SSR increased by $+1.0 \text{ Wm}^{-2} \text{ decade}^{-1}$, $+1.7 \text{ Wm}^{-2} \text{ decade}^{-1}$ and $+1.1 \text{ Wm}^{-2} \text{ decade}^{-1}$ in the Northern Arctic, Boreal Plain and Taiga Shield ecozones, respectively. Taiga and Boreal Cordillera ecozones decreased at a mean rate of $-4.1 \text{ Wm}^{-2} \text{ decade}^{-1}$ and $-4.9 \text{ Wm}^{-2} \text{ decade}^{-1}$, respectively, between 2001 and 2020. For both periods, mean annual

SSR values fluctuated from year to year, with prominent peaks between 2000 and 2010 for the majority of the ecozones (Figure S4.1).

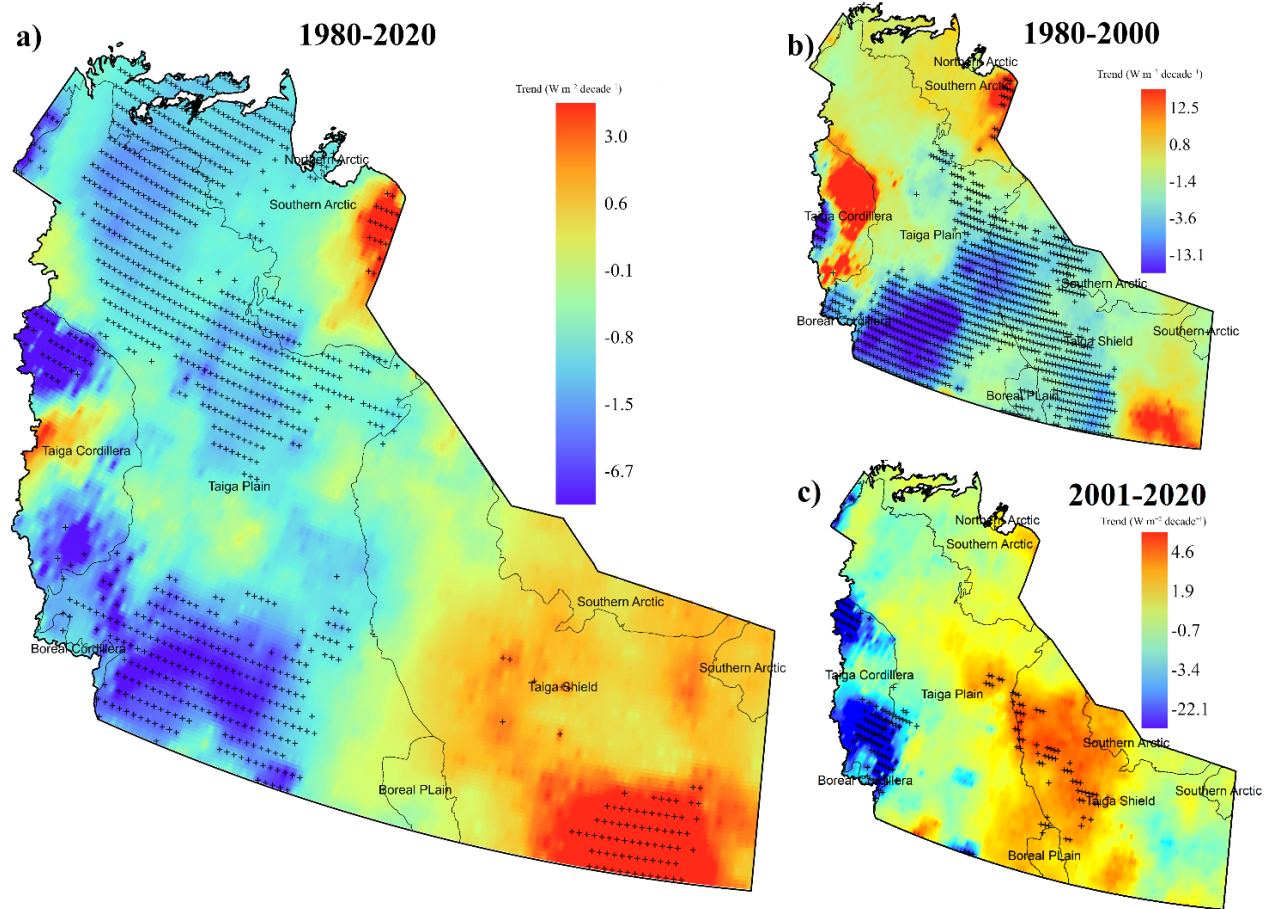


Figure 4.2 Spatial distribution of mean annual SSR trends magnitudes across the NWT for the following periods: a) 1980 to 2020, b) 1980-2000, and c) 2001-2020. Cross denotes the long-term trends at grids are significant at $p \leq 0.05$. The values are estimated for each grid and rate of change in colour bar is expressed as $W m^{-2} decade^{-1}$.

4.5.1.2 Seasonal mean SSR trends

The analysis showed varying but distinctive seasonal patterns in SSR trends that aligned with the seasons and ecozones across NWT between 1980 and 2020 (Figure 4.3). During spring, incoming SSR generally increased across most ecozones with the largest rate of change in the Taiga Shield

(+1.5 $\text{Wm}^{-2} \text{decade}^{-1}$) and Southern Arctic (+1.2 $\text{Wm}^{-2} \text{decade}^{-1}$) ecozones (Figure 4.3a). In contrast during summer, the largest decreases in SSR occurred in the Taiga Plain (-3.8 $\text{Wm}^{-2} \text{decade}^{-1}$), Taiga Cordillera (-3.5 $\text{Wm}^{-2} \text{decade}^{-1}$), and Boreal Cordillera (-4.9 $\text{Wm}^{-2} \text{decade}^{-1}$) ecozones, while southern and eastern locations in the Taiga Shield ecozone showed some of the largest increases (+5.7 $\text{Wm}^{-2} \text{decade}^{-1}$) (Figure 4.3b). In autumn, a mixture of positive and negative SSR trends were observed with rate of change varying from -5.6 $\text{Wm}^{-2} \text{decade}^{-1}$ to +3.3 $\text{Wm}^{-2} \text{decade}^{-1}$ (Figure 4.3c). The Taiga Shield ecozone showed both negative and positive trends, with southeastern areas of Taiga Shield showing an increase (+3.3 $\text{Wm}^{-2} \text{decade}^{-1}$) in SSR.

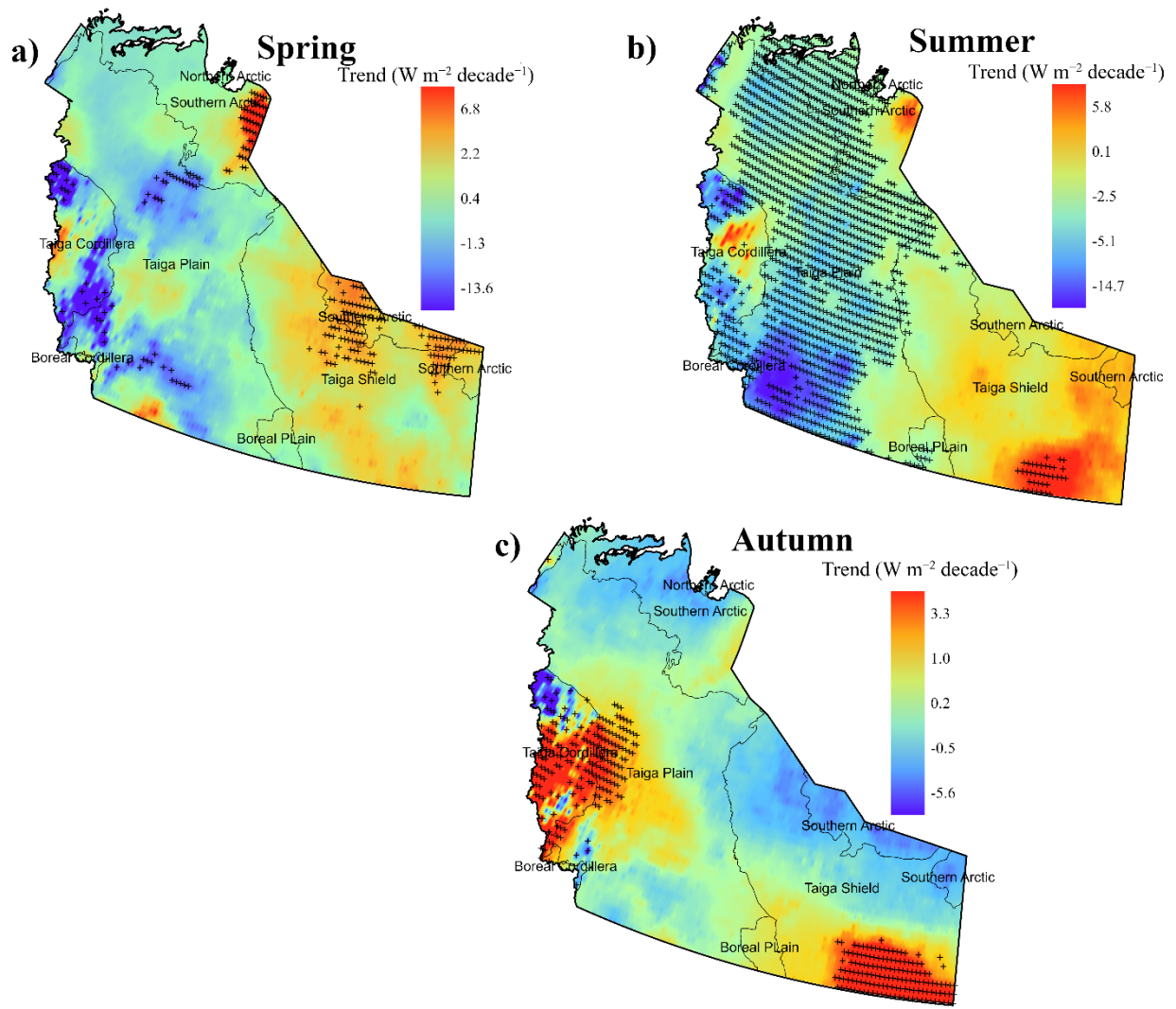


Figure 4.3 Distribution of mean shortwave radiation trend for a) Spring, b) Summer and c) Autumn from 1980 to 2020 across continental NWT. Cross denotes the long-term trends at grids are significant at $p \leq 0.05$. The values are estimated for each grid and rate of change on colour bar is expressed as $\text{W m}^{-2} \text{ decade}^{-1}$.

4.5.2 Correlation between total cloud cover and SSR

Focus was placed on examining the relationship between total cloud cover and SSR to determine the extent at which total cloud cover may impact the SSR trends detected over NWT (Figures 4.2 and Figure 4.3). This relationship was first examined for three locations (Inuvik, Yellowknife, and Fort Simpson) with existing independent measures of *in situ* total cloud cover data. The correlation coefficients were negative at Inuvik ($R = -0.33$, $p < 0.05$), Yellowknife (-0.5 , $p < 0.05$) and Fort Simpson (-0.51 , $p < 0.05$) (Figures 4.4 & 4.5), indicating that cloud cover increases as SSR decreases. Figure 4.4 also showed that in most years when total cloud cover was above its long-term average, SSR was typically below its long-term average and vice versa. Higher total cloud cover and SSR variability were observed from 2001 through 2020 (varying from ± 1 standard deviation) for Inuvik and Yellowknife when compared with the rest of the time series (Figure 4.4).

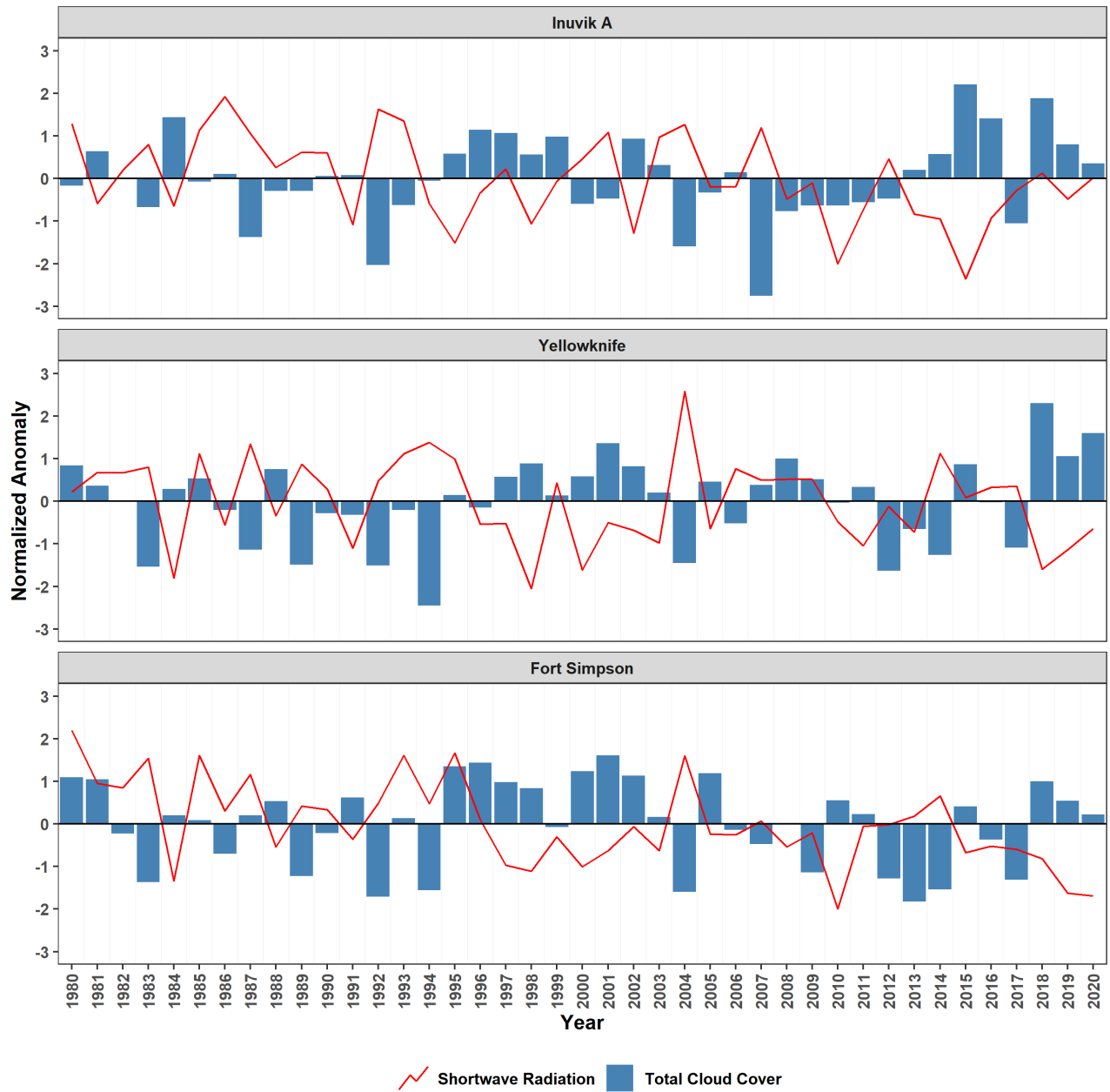


Figure 4.4 Annual normalized total cloud cover (blue) and Daymet shortwave radiation estimates (red) for Inuvik, Yellowknife and Fort Simpson during summer seasons. The zero line is the 1980-2020 long term average.

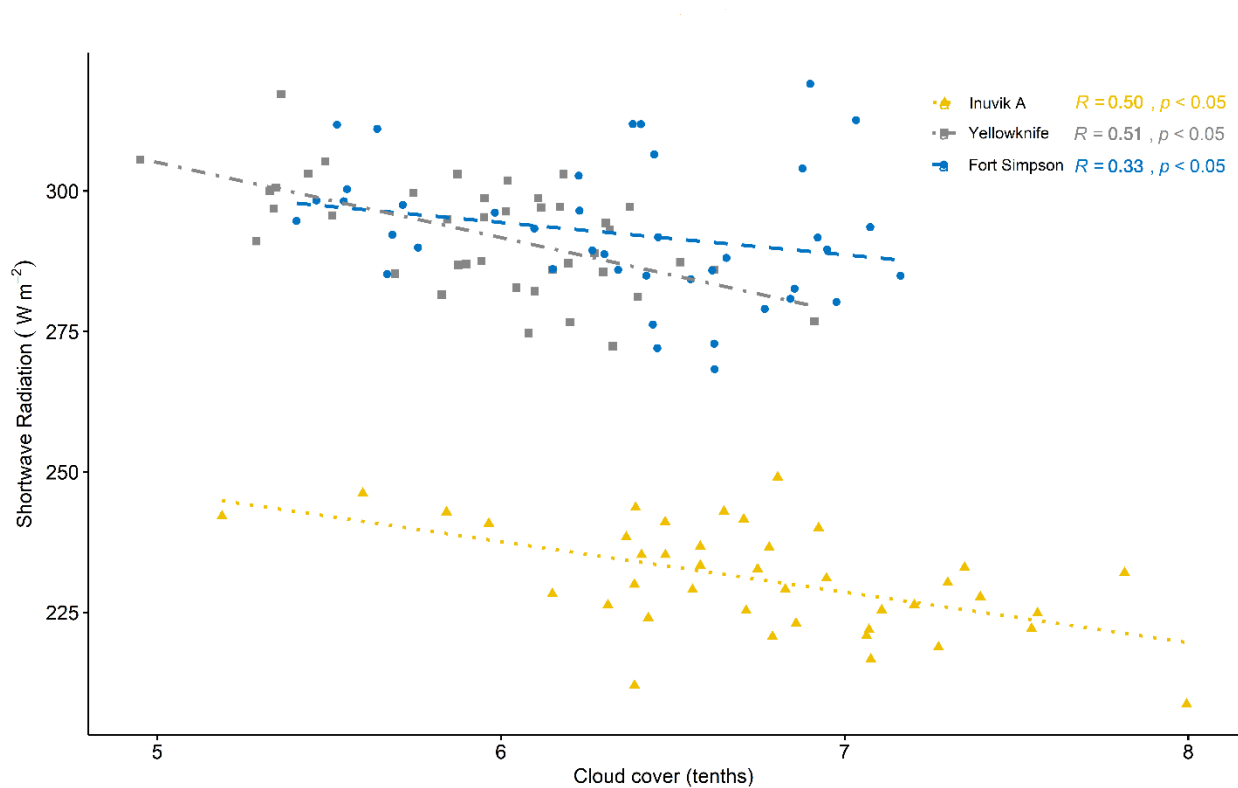


Figure 4.5 Scatter plot showing relationship between mean total cloud cover and shortwave radiation in summer for three locations in the NWT.

The correlation coefficient between ERA5 total cloud cover and Daymet SSR estimates are between -0.8 and 0.4 (Figure 4.6). SSR correlated negatively with increasing cloud cover, notably during the summer months, but less so in the spring and autumn. Most of the strong negative correlations were clustered over the Taiga Plains ecozone in summer where values were greater than -0.5 (Figure 4.6). Except for some areas in the Taiga Shield ecozone, where weak but positive correlations were evident, all other ecozones exhibited negative correlations.

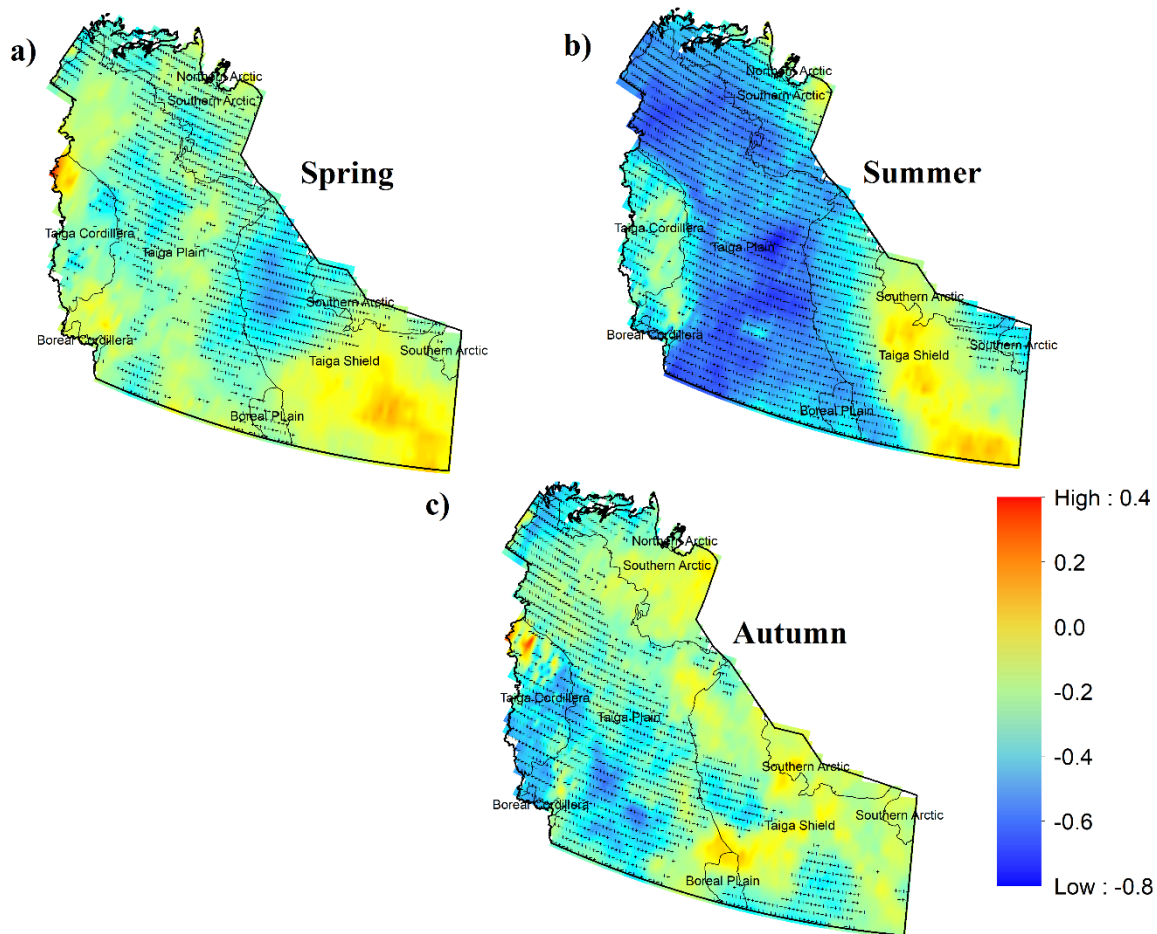


Figure 4.6 Correlation Coefficient R between total cloud cover and shortwave radiation over NWT from 1980 to 2020 during a) Spring b) Summer and c) Autumn. Cross denotes the correlation coefficient at grids are significant at $p \leq 0.05$.

4.5.3 Correlation between SSR and lake surface water temperature in North Slave Region

In the high lake density North Slave Region, where both increasing and decreasing SSR trends occur, the linkage between SSR and LSWT was explored. Increasing magnitude of SSR trends (rate varied from: $+0.5$ to $+3.6 \text{ W m}^{-2} \text{ decade}^{-1}$) were observed for approximately 14% of lakes, while decreasing SSR trends (rate varied from: -0.1 to $-11.0 \text{ W m}^{-2} \text{ decade}^{-1}$) were observed for the remaining 86% of lakes from 1984 to 2020 (Figure 4.7a). During the same period, 35% of

lakes showed significant increasing trend of LSWT (Figure 4.7b). The rate of change varied between +1.2 and +4.6°C ($p \leq 0.05$).

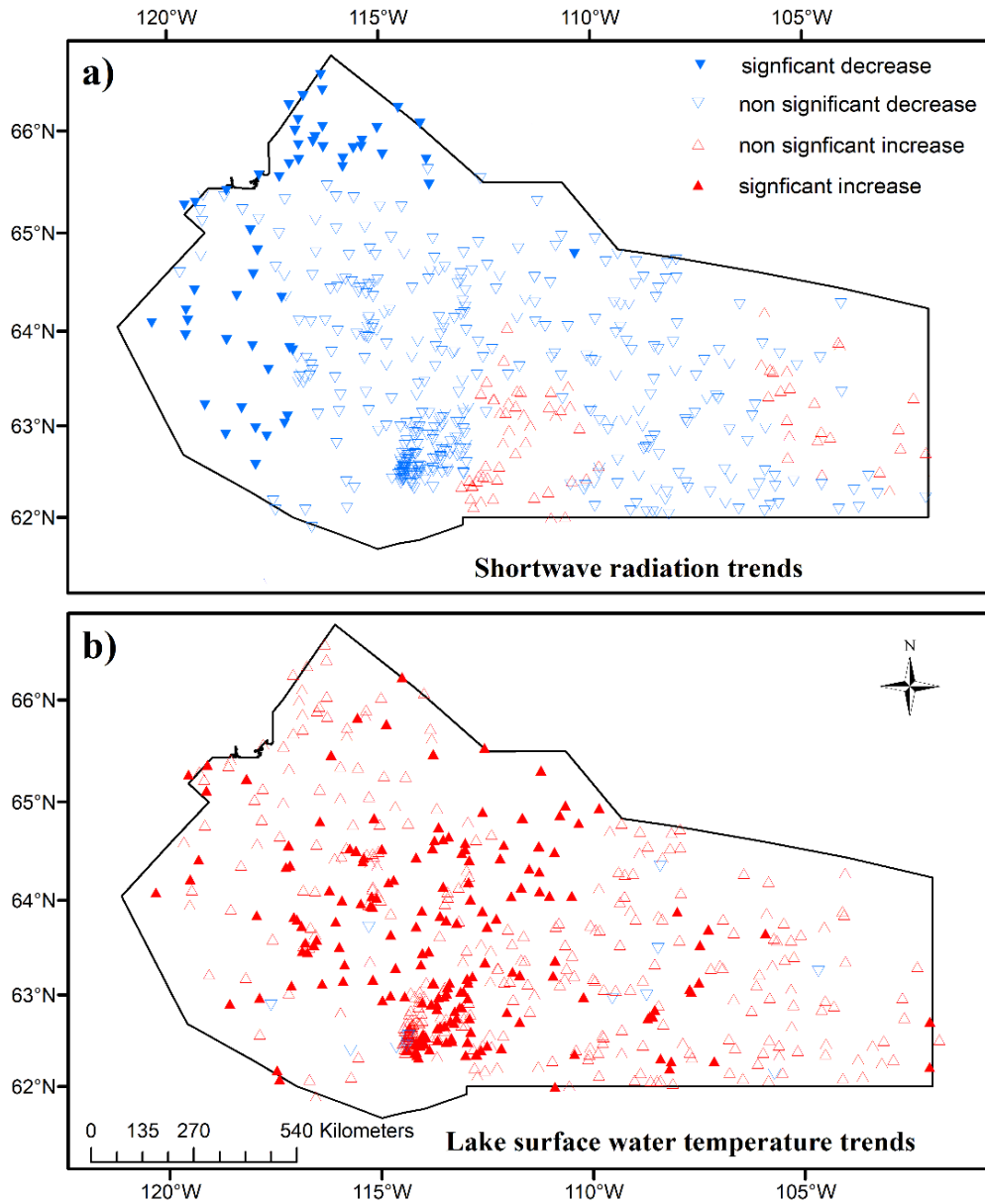


Figure 4.7 Trend analysis in a) shortwave radiation, b) lake surface water temperature estimates annual summer from 1984 to 2020 for North Slave Region. Solid red or blue triangle indicate trends are significant at $p \leq 0.05$.

The distribution of correlation coefficients suggests that there are also some spatial heterogeneities between SSR and LSWT that appear to be coincident with the northern treeline boundary in the North Slave Region (Figure 4.8a). Majority of the positive correlations were found for lakes in the western part of North Slave Region near Great Slave Lake (south of treeline), but negative correlations occur for the majority of lakes in the southern, northern, and eastern most parts of the North Slave Region (north of treeline). Furthermore, small lakes have a stronger positive SSR-LSWT correlation value than medium and large lakes (Figure 4.8b). It was noted that 84% (n=64) of small lakes had positive correlation between SSR and LSWT while in contrast, 57% (n=464) and 58% (n=12) of medium and large lakes, respectively, had mostly negative correlation between SSR and LSWT (Figure 4.8b) in the North Slave Region.

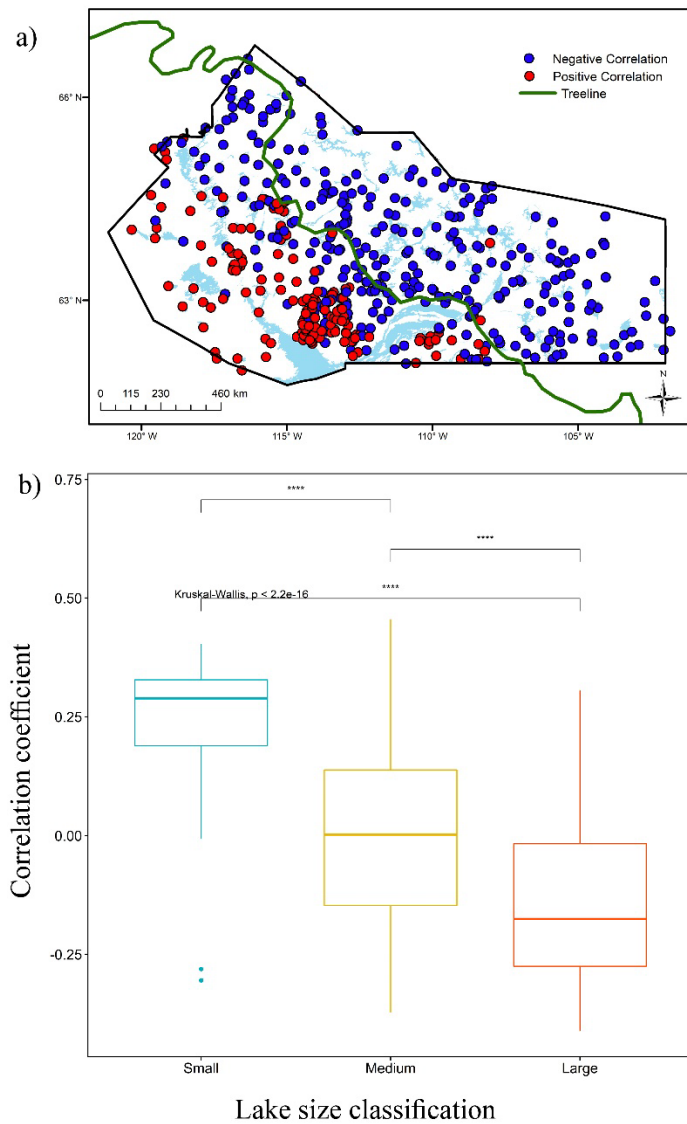


Figure 4.8 a) Spatial distribution of the correlation coefficient across the North Slave Region during summer (June, July, August) for 1984-2020. **Blue circles** represent a negative correlation between LSWT compared with SSR, while **red circles** represent a positive correlation. b) Correlation coefficient between SSR and LSWT during summer months for lakes in the North Slave Region for the period of 1984-2020. Lakes $<1 \text{ km}^2$ area are considered small ($n=64$), while lakes between 1 km^2 and 100 km^2 are medium ($n=464$) and lakes greater than $>100 \text{ km}^2$ are large ($n=12$). Asterisks indicate that differences in correlations value among lake sizes are significant at $p \leq 0.05$.

4.6 Discussion

This study analysed trends in SSR over four decades (1980-2020) across the continental NWT using several data products including Daymet interpolated SSR data, ERA5 reanalysis cloud cover data, and Landsat-derived LSWT observations. The results indicate that there was an overall decrease in mean SSR between 1980 and 2000 followed by an increase in most ecozones between 2000 and 2020 (Figure 4.2). The directions and magnitudes of the SSR trends are consistent and comparable with previous studies that used other datasets (including *in situ* data), and which focused on other geographical areas in northern high latitudes in earlier periods (Weston et al., 2007; Wild, 2009; Sanchez-Lorenzo, 2015; Yuan, et al., 2021). The following paragraphs discuss some potential causes of the observed spatial and temporal patterns in SSR trends and discusses implications of warming LSWT on northern communities and lake ecosystem health.

4.6.1 Causes of observed changes in SSR trends

Long-term SSR trends have been attributed to multiple drivers of change within the Earth's climate system (Wild, 2009; Chiacchio et al., 2010; Huang et al., 2019). These include changes in radiatively active gases in the atmosphere (e.g., water vapour), changes in aerosols, sea ice reduction in the Arctic Ocean, intensity and frequency of atmospheric-oceanic circulation changes (e.g., North Atlantic Oscillation, Pacific Decadal Oscillation) and changes in cloud characteristics (Wild, 2009; Chiacchio et al., 2010; Huang et al., 2019). Yuan et al. (2021) found that the cloud cover and the differences between daily maximum and minimum air temperatures (*i.e.*, the diurnal temperature range) are the two most important variables that predict long-term SSR reductions and increases globally. The relationship and positive correlation between diurnal temperature range and SSR is expected – as daytime SSR increases, the increase in thermal energy increases the

difference between daytime maximum and nighttime minimum temperatures (Bristow & Campbell 1984). Thus, trends in the diurnal temperature range can be used as a proxy for trends in SSR (Bristow & Campbell 1984). There has been a long-term decrease in the diurnal temperature range observed in Canada since 1950, which has been attributed to increases in cloud cover (Vincent et al., 2006). Milewska (2004) showed that total cloud cover in NWT increased from 3% to 9% between 1953 and 2002. Here, the study results support earlier findings that there is negative relationship between cloud cover and SSR from 1980 to 2020 (Figure 4.5, 4.6 & 4.7). This phenomenon is consistent with known relationships between cloud cover and SSR (Twomey, 1976; Zhang, 1996; Kejna et al., 2021). This is particularly true in the summer (Figures 4.5 & 4.6) when SSR is at its maximum (Box et al., 2019). In the central Canadian Arctic region, during the summer, typically the total cloud cover is greatest when compared with the other seasons and low and middle cloud types are most prevalent (Box et al., 2019). Additionally, a recent modelling study by Dong et al. (2022) concluded that changes to anthropogenic aerosol emissions, greenhouse gas concentrations, sea surface temperature and sea ice extent contributed to SSR decadal trends patterns observed over North America. These authors considered decadal changes in sea surface temperature and sea ice extent to be the primary drivers responsible for the SSR and cloud cover trends reported (Dong et al., 2022). Consequently, it is hypothesized that observed sea ice reduction and longer periods of open water in the Beaufort Sea and in the Mackenzie River Basin (Duguay et al., 2006; Box et al., 2019; Heo et al., 2021) may have led to increases in the local total cloud cover, thus reducing SSR receipt along the northern Taiga Plains and Northern Arctic ecozone (Figures 4.2 & 4.3) but this requires further investigation.

4.6.2 Response of LSWT to SSR changes

This study indicates that the incident summer SSR in the North Slave Region has generally decreased between 1984 and 2020 (Figure 4.7a). Despite this, summer LSWT generally increased by +1.2 to +4.6°C during the same period (Figure 4.7b). Warmer lake surfaces have been shown to increase evaporation (Rouse et al., 2005). Thus, it is possible that increased evaporation may have led to elevated amounts of local total cloud cover and a decrease in SSR (Figures 4.5 & 4.6). The difference in the direction of the correlation between LSWT and SSR in summer in medium and large lakes (negative correlation) versus in small lakes (positive correlation) is likely driven by the higher heat capacity of medium and large lakes which makes them less sensitive to changes in SSR, and consequently, in thermal energy (Bailey et al., 1997). Rouse et al. (2005) reported that medium and large lakes are subject to mechanical mixing by wind and at times this will serve to mix cooler subsurface water with warmer upper lake water. Consequently, large lakes take a longer time to heat up when compared with small lakes, resulting in the delay of the spring release of latent and sensible heat fluxes. For example, large lakes near the Central Mackenzie River Basin in the NWT tend to lose heat and water vapour almost as quickly at night as during the day, and more so in late summer and autumn than in spring and early summer (Rouse et al., 2005). These large lakes are particularly sensitive to the surrounding air; a warm, calm, and sunny period may be followed by a cold, dry air mass with more cloudiness, windy conditions that can increase convection and latent heat energy, even without direct solar input (Rouse et al., 2005). Increased cloudiness can also enhance SSR reflection at the top of the atmosphere, which may reduce the amount of SSR absorbed by the Earth's surface leading to an increase in the downward longwave radiation (Twomey, 1976; Zhang et al., 1996). As longwave radiation input increases, heat loss

from lakes during the night-time decreases (Livingstone, 2003; Fink et al., 2014) which may lead to the increased warming observed for some of the lakes in the North Slave Region.

The correlation between SSR and LWST also have a spatial pattern that appears to be consistent with the northern treeline boundaries (Figure 4.8a). These boundaries are characterized by the transition of the boreal forest northward into tundra, approximating the summer position of the Arctic Front (Pienitz et al., 1997). The heating differences between boreal forest and tundra can drive local scale circulations and have ecological impacts (Beringer et al., 2001). Green et al. (2017) reported that the interactions between the atmosphere and vegetation can account for up to at least 30% of variability in surface radiation and precipitation patterns due to the release of water vapour during photosynthesis. The lakes in the tundra are governed by an open canopy that may allow SSR to penetrate lakes (Bailey, Oke & Rouse, 1997) hence more evaporation and more clouds at the local level. Therefore, all these factors may also affect SSR receipt, leading to a rapid change in surface characteristics and microclimates at the local scale, but confirming that the northern treeline is the primary control on the change in SSR trends and SSR-LWST correlation will require more research.

4.6.3 Implications of warming lakes for northern communities and ecosystems

In this study, it was found that during summer, LSWT increased between 1984 and 2020 ranging from +1.2°C to +4.6°C in 45% of lakes in the North Slave Region (Figure 4.8) as also reported by Attiah et al. (2022). This observed increase is consistent with LSWT trend magnitudes reported globally (O'Reilly et al., 2015). Sharma et al., (2007) projected that by July 2100, many lakes in Canada may experience lake water temperatures rising to a maximum of 30°C. In a recent modelling scenario, Råman Vinnå et al. (2021) reported that for 29 high latitude lakes, a 1.0°C

change in air temperature or 10 W m^{-2} change in SSR can lead to LSWT increases of $\sim 0.8^\circ\text{C}$ and $\sim 0.4^\circ\text{C}$, respectively, by 2099. These consistent long-term variations in lake temperatures and SSR may have implications for ice road constructions for transportation networks in northern communities especially during autumn to early winter by delaying ice formation since there is an abundance of lakes in northern Canada. For example, there are over one million lakes in the Canadian Arctic representing 42% of all lakes over this region, many of which are considered small (Paltan et al., 2015). Some of these lakes form part of the northern transportation network and depend on the weather and climate to commence construction which typically begins in November and is maintained until April of the following year (Knowland et al., 2010). Hence, if there are sustained periods of open water of northern lakes caused by warming as found by Duguay et al. (2006), then construction of these winter roads will continue to be challenging as described by Levin (2017). The lack of strong and safe ice roads has been reported to limit NWT communities from accessing food and other key resources necessary for their sustenance (Levin 2017).

In addition, changes to SSR are anticipated also have implications for lake conditions. As previously discussed, there is a typically negative correlation between total cloud cover and SSR during the summer (Figures 4.6 and 4.7). Increasing cloud cover during spring and summer may lead to reduced SSR (Twomey, 1976; Zhang et al., 1996; Kejna et al., 2021). When there is limited SSR, photosynthesis in lakes decrease, resulting in a reduction in the concentration of dissolved oxygen available to support aquatic plant and animal life (Woolway et al., 2022). On the other hand, water quality/turbidity of lakes can also influence SSR absorption by water (Adams et al., 2021). For example, dissolved organic carbon (DOC) in lakes is important for controlling SSR

absorption. Lakes with high DOC would lead to more SSR attenuation and which would only warm the lake's epilimnion; because of this stratification becomes very pronounced, dampening mixing with the hypolimnion which is normally much cooler (Pienitz et al., 1997; Molot et al., 2005; Pilla & Couture, 2021). Consequently, as reiterated by Sharma et al. (2007) increasing temperatures may lead to deterioration of lake water quality because of shifts in the lake thermal structure, endangering communities that rely on fisheries as a source of income and food (Moslemi-Aqdam et al., 2022).

4.6.4 Use of gridded and remote sensing data, potential limitations, and opportunities

This research used Daymet interpolated SSR data, ERA5 reanalysis data for cloud cover, and Landsat-derived LSWT data to understand historical changes in climate across the continental NWT. Therefore, it is acknowledged that there are likely uncertainties associated with gridded interpolated and remote sensing data which may lead to a conservative or amplified trend magnitude. For example, Daymet SSR estimates used in this study are based on the difference between maximum and minimum air temperature. Consequently, SSR estimates may be sensitive to these *in situ* input data which is limited in northern regions (Thornton et al., 2021). However, the *in situ* SSR and LSWT data needed to cover extensive spatial remote areas does not exist or may not be easily accessible (GNWT, 2018). Moreover, frequent and uninterrupted data collection in northern Canada can also be labour intensive, expensive, and logistically challenging for the research community (Prowse & Ommanney, 1990; Mekis et al., 2018; GNWT, 2018). Consequently, using gridded and remote sensing data allows climate researchers to detect and attribute change over a large spatial area in Canada and elsewhere (Zhang et al., 2000; Derksen, et al., 2008; Murfitt & Brown 2017). The dataset used here provides a reasonable quantification and insights on spatiotemporal evolution of SSR and LSWT in many unmonitored locations, in

response to the documented warming in the NWT (Kwong & Gan, 1994; Rouse et al., 1997; Kuhn & Butman 2021; DeBeer et al., 2021). Notwithstanding, in this research we used independent cloud datasets (ERA5 and *in situ* data) to explore association between total cloud cover and SSR (Figures 4.4 to 4.6) and suggested some plausible explanations of SSR trends reported here.

Nevertheless, there are still opportunities for future research as it is acknowledged that historical SSR patterns over continental NWT can be triggered by many complex processes in the atmosphere and a thorough investigation into the cloud characteristics and other drivers of the observed SSR trends is required. It is recognized that the relationship between SSR and LSWT is more complex than what a correlation analysis and this discussion can address. A lake's energy balance also depends on a number of factors in addition to SSR, including catchment geology and soil type, geographic region, topography, aspect and vegetation (Bigras, 1990; O'Reilly et al., 2015). Furthermore, the process by which SSR may influence lake surface temperatures does not rely solely on changes in the receipt of SSR at lakes but may also be a combination of lake physical and chemical characteristics (e.g., mean depth, trophic status, DOC, vegetation) and other local climate conditions (e.g., air temperature, wind direction and speed) (Bigras, 1990; O'Reilly et al., 2015; Thompson et al., 2020). However, exploring these controls on LSWT sensitivity to SSR across a longer temporal scale with respect to all these processes will require investigations and data. Nevertheless, in contrast to previous studies (e.g., Oswald & Rouse 2004; Rouse et al., 2005) which focused on a single lake or a limited number of lakes in the North Slave Region over short temporal periods, this research explores the SSR-LSWT relationship for a greater proportion of lakes and over a longer period--for almost four decades (1984-2020). The important contribution

of lake size to determining lake surface temperature sensitivity to SSR was also identified during the same period.

Conclusion

This study improves our understanding of long-term historical trends and patterns of SSR receipt across continental NWT as derived from Daymet SSR interpolated estimates. Additionally, we evaluated the association of Daymet SSR estimates with ERA5 total cloud cover from ECMWF and explored linkages between SSR and lake surface water temperature in the North Slave Region using Landsat remote sensing data. Key findings are highlighted below:

- i) During the entire period of 1980-2020, the SSR trend at the annual scale showed significant decrease in most northern and southern areas of the Taiga Plains ecozone, while a generally positive trend was observed in lakes in the southern Taiga Shield ecozone. The greatest rate of change was over the Taiga Plains ecozone. The trends in SSR across Taiga Shield and Boreal Plain ecozones typically decreased from 1980 to 2000 and increased from 2000 to 2020.
- ii) Seasonally, the SSR trend distribution showed varying but distinctive patterns across ecozones from 1980 to 2020. In spring, the increasing trend magnitudes in SSR were observed in the Taiga Shield (average rate of change $+1.50 \text{ Wm}^{-2} \text{ decade}^{-1}$) and the Southern Arctic ($+1.2$ average rate of change $\text{Wm}^{-2} \text{ decade}^{-1}$) ecozones. In contrast, summer SSR showed a reduction and trend magnitudes varied from -0.4 to $-4.1 \text{ Wm}^{-2} \text{ decade}^{-1}$ throughout most ecozones with the largest declining rates in the Taiga Plain, Taiga Cordillera and Boreal Cordillera ecozones.

- iii) SSR receipt negatively corresponded with increasing cloud cover, especially during summer months, but corresponded to a lesser degree in spring and autumn. Apart from some exceptions, increases in cloud cover is generally coincident with decreases in SSR and vice versa. The correspondence observed between clouds and SSR are consistent with the local and regional cloud-climate relationship that were observed over the Arctic in prior research.
- iv) LSWT for small lakes have a positive correlation with incoming SSR when compared with medium and large lakes in the North Slave Region. The adverse implication of persistent lake warming and changing SSR on northern communities and lake ecosystems were discussed.
- v) Results support the value of using gridded and remote sensing data to help advance understanding of the responses of northern lakes to changing climate.

Together, these findings provide new insights into how SSRs trends have changed during the past 40 years, during which time the NWT climate has warmed significantly, and highlights some of the implications of these changes for lake-rich regions in NWT. These high-latitude lakes are and will continue to be critical for the functioning of the Earth system because they cover a large area in the Arctic. Nonetheless, the heterogeneity in long term trends in SSR receipt across NWT underscores the importance of considering interactions among climate and other variables across spatial and temporal scales, as one cannot assume that any individual lake will concomitantly warm with increasing SSR or that all lakes in NWT will be warming at the same rate. Thus, monitoring mechanisms responsible for changing lake behaviour will continue to be important for researchers and decision makers because lake data are needed to support weather, climate and hydrological

predictions. To best of our knowledge, this work also represents one of the first attempts using Daymet and ERA5 data to quantitatively examine long-term SSR trends while relating the changes to cloud cover for four decades (1980 to 2020) in the continental NWT. Thus, it can serve as a benchmark for policy makers when synthesising future climate reports for Northern regions.

4.7 Acknowledgements

We are grateful to Global Water Futures Programme for providing access to their research facilities that is supported by the Canada First Research Excellence Fund, which helped with this study completion. Thanks to Ariel Lisogorsky and Ali Reza Shahvaran for their assistance and guidance with R programming and ArcMap respectively. Thank you also to Julie Grant for some of the figure's aesthetics and Stephanie Slowinski for providing feedback on an earlier version of the Discussion.

4.8 Data availability statement

Daymet data were downloaded from <https://daymet.ornl.gov/>, while Landsat data are available from <https://earthexplorer.usgs.gov/>. *In situ* cloud cover data for Inuvik, Fort Simpson, and Yellowknife can be access via Environment Canada and Climate Change Canada (see additional details [here](#)). Total cloud cover data were downloaded from European Centre for Medium-Range Weather Forecast Climate Data Store (<https://cds.climate.copernicus.eu/cdsapp#!/home>).

4.9 References

- Abe, M., Nozawa, T., Ogura, T., & Takata, K. (2016). Effect of retreating sea ice on arctic cloud cover in simulated recent global warming. *Atmospheric Chemistry and Physics*, *16*(22), 14343-14356. doi:10.5194/acp-16-14343-2016.
- Adams, H., Ye, J., Persaud, B. D., Slowinski, S., Kheyrollah Pour, H., & Van Cappellen, P. (2022). Rates and timing of chlorophyll-a increases and related environmental variables in global temperate and cold-temperate lakes. *Earth System Science Data*, *14*(11), 5139-5156. doi: <https://doi.org/10.5194/essd-14-5139-2022>.
- Adrian, R., O'Reilly, C. M., Zagarese, H., Baines, S. B., Hessen, D. O., Keller, W., . . . Winder, M. (2009). Lakes as sentinels of climate change. *Limnology and Oceanography*, *54*(6), 2283-2297. doi: https://doi.org/10.4319/lo.2009.54.6_part_2.2283.
- AMAP. (2021). Arctic Monitoring and Assessment Programme (AMAP) Arctic Climate Change Update 2021: Key Trends and Impacts. Arctic Monitoring and Assessment Programme (AMAP), Tromsø, Norway. viii+148pp
<https://www.amap.no/documents/download/6890/inline>
- Arias, P.A., N. Bellouin, E. Coppola, R.G. Jones, G. Krinner, J. Marotzke, . . . , & K. Zickfeld, 2021: Technical Summary. In *Climate Change 2021: The Physical Science Basis. Contribution of Working Group I to the Sixth Assessment Report of the Intergovernmental Panel on Climate Change* [Masson-Delmotte, V., P. Zhai, A. Pirani, S.L. Connors, C. Péan, S. Berger, N. Caud, Y. Chen, L. Goldfarb, M.I. Gomis, M. Huang, K. Leitzell, E. Lonnoy, J.B.R. Matthews, T.K. Maycock, T. Waterfield, O. Yelekçi, R. Yu, and B. Zhou (eds.)].

Cambridge University Press, Cambridge, United Kingdom and New York, NY, USA, pp. 33–144. doi:10.1017/9781009157896.002.

Attiah, G., Kheyrollah Pour, H., Scott, A.K. Lake Surface Temperature Dataset in the North Slave Region Retrieved from Landsat Satellite Series - 1984 to 2021. (2022) *Earth System Science Data Discussions*. <https://doi.org/10.5194/essd-2022-289>.

Bailey, W. G., Bailey, W. G., Oke, T. R., & Rouse, W. R. (1997). *Surface climates of Canada* McGill-Queen's Press-MQUP.

Beringer, J., Tapper, N. J., McHugh, I., Chapin III, F. S., Lynch, A. H., Serreze, M. C., & Slater, A. (2001). Impact of Arctic treeline on synoptic climate. *Geophysical Research Letters*, 28(22), 4247-4250. doi: <https://doi.org/10.1029/2001GL012914>

Bigras, S. C. (1990). Hydrological regime of lakes in the Mackenzie delta, Northwest Territories, Canada. *Arctic and Alpine Research*, 22(2), 163-174.
doi:10.1080/00040851.1990.12002778.

Box, J. E., Colgan, W. T., Christensen, T. R., Schmidt, N. M., Lund, M., Parmentier, F. W., . . . Olsen, M. S. (2019). Key indicators of arctic climate change: 1971–2017. *Environmental Research Letters*, 14(4), 045010. doi:10.1088/1748-9326/aafc1b.

Bristow, K. L., & Campbell, G. S. (1984). On the relationship between incoming solar radiation and daily maximum and minimum temperature. *Agricultural and Forest Meteorology*, 31(2), 159-166. doi: [https://doi.org/10.1016/0168-1923\(84\)90017-0](https://doi.org/10.1016/0168-1923(84)90017-0).

- Budyko, M. I. (1969). The effect of solar radiation variations on the climate of the earth. *Tellus*, 21(5), 611-619. doi:10.3402/tellusa.v21i5.10109.
- Bush E., Lemmen D. S. (2019). *Canada's climate change report*. Government of Canada. Retrieved from <https://changingclimate.ca/CCCR2019/>.
- Chasmer, L., & Hopkinson, C. (2017). Threshold loss of discontinuous permafrost and landscape evolution. *Global Change Biology*, 23(7), 2672-2686. doi:10.1111/gcb.13537.
- Chiacchio, M., Ewen, T., Wild, M., & Arabini, E. (2010). Influence of climate shifts on decadal variations of surface solar radiation in Alaska. *Journal of Geophysical Research: Atmospheres*, 115 doi: <https://doi.org/10.1029/2009JD012533>.
- Cutforth, H. W., & Judiesch, D. (2007). Long-term changes to incoming solar energy on the Canadian Prairie. *Agricultural and Forest Meteorology*, 145(3), 167-175. doi: <https://doi.org/10.1016/j.agrformet.2007.04.011>.
- DeBeer, C. M., Wheater, H. S., Pomeroy, J. W., Barr, A. G., Baltzer, J. L., Johnstone, J. F., . . . Pietroniro, A. (2021). Summary and synthesis of changing cold regions network (CCRN) research in the interior of western Canada -- Part 2: Future change in cryosphere, vegetation, and hydrology. *Hydrology and Earth System Sciences*, 25(4), 1849-1882. doi:10.5194/hess-25-1849-2021.
- Derksen, C., Brown, R., & MacKay, M. (2008). Mackenzie Basin Snow Cover: Variability and Trends from Conventional Data, Satellite Remote Sensing, and Canadian Regional Climate Model Simulations. In: Woo, Mk. (eds) Cold Region Atmospheric and Hydrologic Studies.

The Mackenzie GEWEX Experience. Springer, Berlin, Heidelberg.

https://doi.org/10.1007/978-3-540-73936-4_13.

Dong, B., Sutton, R. T., & Wilcox, L. J. (2022). Decadal trends in surface solar radiation and cloud cover over the North Atlantic sector during the last four decades: drivers and physical processes. *Climate Dynamics*, 1-14. doi: <https://doi.org/10.1007/s00382-022-06438-3>

Dörnhöfer, K., & Oppelt, N. (2016). Remote sensing for lake research and monitoring – recent advances. *Ecological Indicators*, 64, 105-122. doi: <https://doi.org/10.1016/j.ecolind.2015.12.009>.

Duguay, C. R., Prowse, T. D., Bonsal, B. R., Brown, R. D., Lacroix, M. P., & Ménard, P. (2006). Recent trends in Canadian lake ice cover. *Hydrological Processes: An International Journal*, 20(4), 781-801. doi: <https://doi.org/10.1002/hyp.6131>.

ECCC (2022), Canadian Climate Normal. Retrieved June 14, 2022, from https://climate.weather.gc.ca/climate_normals/index_e.html.

Ecosystem Classification Group. (2009). Ecological regions of the Northwest Territories, Taiga Plains. Yellowknife, NT: Department of Environment and Natural Resources, Government of the Northwest. Available at: https://www.enr.gov.nt.ca/sites/enr/files/resources/taiga_plains_ecological_land_classification_report.pdf.

Fabris, L., Rolick, R. L., Kurylyk, B. L., & Carey, S. K. (2020). Characterization of contrasting flow and thermal regimes in two adjacent subarctic alpine headwaters in northwest

Canada. *Hydrological Processes*, 34(15), 3252-3270. doi:

<https://doi.org/10.1002/hyp.13786>.

Fink, G., Schmid, M., Wahl, B., Wolf, T., & Wüest, A. (2014). Heat flux modifications related to climate-induced warming of large European lakes. *Water Resources Research*, 50(3), 2072-2085. doi: <https://doi.org/10.1002/2013WR014448>.

Government of the Northwest Territories [GNWT]. (2018). 2030 NWT Climate Change Strategic Framework. https://www.enr.gov.nt.ca/sites/enr/files/resources/128-climate_change_strategic_framework_web.pdf.

Green, J. K., Konings, A. G., Alemohammad, S. H., Berry, J., Entekhabi, D., Kolassa, J., ... & Gentine, P. (2017). Regionally strong feedbacks between the atmosphere and terrestrial biosphere. *Nature geoscience*, 10(6), 410-414. doi: <https://doi.org/10.1038/ngeo2957>

Hasenauer, H., Merganicova, K., Petritsch, R., Pietsch, S. A., & Thornton, P. E. (2003). Validating daily climate interpolations over complex terrain in Austria. *Agricultural and Forest Meteorology*, 119(1), 87-107. doi:[https://doi.org/10.1016/S0168-1923\(03\)00114-X](https://doi.org/10.1016/S0168-1923(03)00114-X).

Helbig, M., Wischnewski, K., Kljun, N., Chasmer, L. E., Quinton, W. L., Detto, M., & Sonnentag, O. (2016). Regional atmospheric cooling and wetting effect of permafrost thaw-induced boreal forest loss. *Global Change Biology*, 22(12), 4048-4066. doi: <https://doi.org/10.1111/gcb.13348>

- Heo, E., Sung, M., An, S. & Yang, Y. (2021). Decadal phase shift of summertime Arctic Dipole pattern and its nonlinear effect on sea ice extent. *International Journal of Climatology*, 41(9), 4732–4742. doi: <https://doi.org/10.1002/joc.7097>.
- Hersbach, H., Bell, B., Berrisford, P., Hirahara, S., Horányi, A., Muñoz-Sabater, J., . . . Thépaut, J. (2020). The ERA5 global reanalysis. *Quarterly Journal of the Royal Meteorological Society*, 146(730), 1999-2049. doi: <https://doi.org/10.1002/qj.3803>.
- Hinkel, K. M., Lenters, J. D., Sheng, Y., Lyons, E. A., Beck, R. A., Eisner, W. R., . . . Potter, B. L. (2012). Thermokarst lakes on the Arctic coastal plain of Alaska: Spatial and temporal variability in summer water temperature. *Permafrost and Periglacial Processes*, 23(3), 207-217. doi: <https://doi.org/10.1002/ppp.1743>.
- Huang, Y., Liu, H., Hinkel, K., Yu, B., Beck, R., & Wu, J. (2017). Analysis of thermal structure of arctic lakes at local and regional scales using in situ and multirate Landsat-8 data. *Water Resources Research*, 53(11), 9642-9658. doi: <https://doi.org/10.1002/2017WR021335>.
- Huang, Y., Dong, X., Bailey, D. A., Holland, M. M., Xi, B., DuVivier, A. K., ... & Deng, Y. (2019). Thicker clouds and accelerated Arctic Sea ice decline: The atmosphere-sea ice interactions in spring. *Geophysical Research Letters*, 46(12), 6980-6989. doi: <https://doi.org/10.1029/2019GL082791>.
- Hungerford, R. D. (1989). *MTCLIM: A mountain microclimate simulation model* US Department of Agriculture, Forest Service, Intermountain Research Station. doi: <https://doi.org/10.2737/INT-RP-414>.

- Hufkens K., Basler J. D., Milliman T. Melaas E., Richardson A.D. (2018). An integrated phenology modelling framework in R: Phenology modelling with phenor. *Methods in Ecology & Evolution*, 9: 1-10. doi: <https://doi.org/10.1111/2041-210X.12970>.
- Kejna, M., Uscka-Kowalkowska, J., & Kejna, P. (2021). The influence of cloudiness and atmospheric circulation on radiation balance and its components. *Theoretical and Applied Climatology*, 144(3), 823-838. doi:10.1007/s00704-021-03570-8.
- Kendall, M. G. (1970). Rank correlation methods. Griffin, London.
- Knowland, K. E., Gyakum, J. R., & Lin, C. A. (2010). A study of the meteorological conditions associated with anomalously early and late openings of a Northwest Territories winter road. *Arctic*, 227-239.
- Kuhn, C., & Butman, D. (2021). Declining greenness in Arctic-boreal lakes. *Proceedings of the National Academy of Sciences*, 118(15), e2021219118. Doi: <https://doi.org/10.1073/pnas.202121911>
- Kwong, Y. T. J., & Gan, T. Y. (1994). Northward migration of permafrost along the Mackenzie highway and climatic warming. *Climatic Change*, 26(4), 399-419. doi:10.1007/BF01094404
- Levin, D. (2017). Ice roads ease isolation in Canada's north, but they're melting too soon. *New York Times*. Access on August 15th, 2022 from <https://www.nytimes.com/2017/04/19/world/canada/ice-roads-ease-isolation-in-canadas-north-but-theyre-melting-too-soon.html>.

- Livingstone, D. M. (2003). Impact of secular climate change on the thermal structure of a large temperate central European lake. *Climatic Change*, 57(1), 205-225. doi:
<https://doi.org/10.1023/A:1022119503144>.
- Mann, H. B. Non-Parametric Test Against Trend. *Econometrical*, 1945 (13): 245-259
- Mekis, E., Donaldson, N., Reid, J., Zucconi, A., Hoover, J., Li, Q., . . . Melo, S. (2018). An overview of surface-based precipitation observations at environment and climate change Canada. *Atmosphere-Ocean*, 56(2), 71-95. doi:10.1080/07055900.2018.1433627.
- Messenger, M. L., Lehner, B., Grill, G., Nedeva, I., & Schmitt, O. (2016). Estimating the volume and age of water stored in global lakes using a geo-statistical approach. *Nature Communications*, 7(1), 13603. doi:10.1038/ncomms13603.
- Milewska, E. J. (2004). Baseline cloudiness trends in Canada 1953–2002. *Atmosphere-Ocean*, 42(4), 267-280. doi:10.3137/ao.420404.
- Molot, L. A., Hudson, J. J., Dillon, P. J., & Miller, S. A. (2005). Effect of pH on photo-oxidation of dissolved organic carbon by hydroxyl radicals in a coloured, softwater stream. *Aquatic Sciences*, 67(2), 189-195. doi:10.1007/s00027-005-0754-9.
- Moslemi-Aqdam, M., Baker, L. F., Baltzer, J. L., Branfireun, B. A., Evans, M. S., Laird, B. D., ... & Swanson, H. K. (2022). Understanding among-lake variability of mercury concentrations in Northern Pike (*Esox lucius*): A whole-ecosystem study in subarctic lakes. *Science of The Total Environment*, 822, 153430. doi:
<https://doi.org/10.1016/j.scitotenv.2022.153430>.

- Murfitt, J., & Brown, L. C. (2017). Lake ice and temperature trends for Ontario and Manitoba: 2001 to 2014. *Hydrological Processes*, 31(21), 3596-3609. doi:
<https://doi.org/10.1002/hyp.11295>.
- NASA. (1999). *Clouds & radiation fact sheet*. NASA Earth Observatory. Retrieved September 2, 2022, from <https://earthobservatory.nasa.gov/features/Clouds>
- O'Reilly, C. M., Sharma, S., Gray, D. K., Hampton, S. E., Read, J. S., Rowley, R. J., . . . Zhang, G. (2015). Rapid and highly variable warming of lake surface waters around the globe. *Geophysical Research Letters*, 42(24), 10,773-10,781. doi:
<https://doi.org/10.1002/2015GL066235>.
- Oswald, C. J., & Rouse, W. R. (2004). Thermal characteristics and energy balance of various-size Canadian shield lakes in the Mackenzie River basin. *Journal of Hydrometeorology*, 5(1), 129-144. doi:10.1175/1525-7541(2004)005<0129:TCAEBO>2.0.CO;2.
- Paltan, H., Dash, J., & Edwards, M. (2015). A refined mapping of Arctic lakes using Landsat imagery. *International Journal of Remote Sensing*, 36(23), 5970-5982. doi:10.1080/01431161.2015.1110263.
- Pareeth, S., Salmaso, N., Adrian, R., & Neteler, M. (2016). Homogenised daily lake surface water temperature data generated from multiple satellite sensors: A long-term case study of a large sub-alpine lake. *Scientific Reports*, 6(1), 31251. doi:10.1038/srep31251.
- Phillips, D. W. (1990). *The climates of Canada*. Ottawa, Ont: Supply and Services Canada.

- Pienitz, R., Smol, J. P., & Lean, D. R. S. (1997). Physical and chemical limnology of 24 lakes located between Yellowknife and Contwoyto lake, Northwest Territories (Canada). *Canadian Journal of Fisheries and Aquatic Sciences*, 54(2), 347-358. doi:10.1139/f96-275.
- Pilla, R. M., & Couture, R. (2021). Attenuation of photosynthetically active radiation and ultraviolet radiation in response to changing dissolved organic carbon in browning lakes: Modeling and parametrization. *Limnology and Oceanography*, 66(6), 2278-2289. doi: <https://doi.org/10.1002/lno.11753>.
- Prowse, T. D., & Ommanney, C. S. (1990). *Northern hydrology: Canadian perspectives*. Saskatoon, Sask., Canada: National Hydrology Research Institute.
- Przybylak, R., Svyashchennikov, P. N., Uscka-Kowalkowska, J., & Wyszyński, P. (2021). Solar radiation in the arctic during the early twentieth-century warming (1921–50): Presenting a compilation of newly available data. *Journal of Climate*, 34(1), 21-37. doi:10.1175/JCLI-D-20-0257.1.
- Råman Vinnå, L., Medhaug, I., Schmid, M., & Bouffard, D. (2021). The vulnerability of lakes to climate change along an altitudinal gradient. *Communications Earth & Environment*, 2(1), 1-10. Doi <https://doi.org/10.1038/s43247-021-00106-w>.
- R Development Core Team. (2021). R: a language and environment for statistical computing. Vienna: R Foundation for Statistical Computing. Available at: <https://www.R-project.org/>.

- Rouse, W. R., Douglas, M. S., Hecky, R. E., Hershey, A. E., Kling, G. W., Lesack, L., ... & Smol, J. P (1997). Effects of climate change on the freshwaters of arctic and subarctic north America. *Hydrological Processes*, 11(8), 873-902. doi: [https://doi.org/10.1002/\(SICI\)1099-1085\(19970630\)11:8<873:AID-HYP510>3.0.CO;2-6](https://doi.org/10.1002/(SICI)1099-1085(19970630)11:8<873:AID-HYP510>3.0.CO;2-6).
- Rouse, W. R., Oswald, C. J., Binyamin, J., Spence, C., Schertzer, W. M., Blanken, P. D., . . . Duguay, C. R. (2005). The role of northern lakes in a regional energy balance. *Journal of Hydrometeorology*, 6(3), 291-305. doi:10.1175/JHM421.1.
- Sanchez-Lorenzo, A., Wild, M., Brunetti, M., Guijarro, J. A., Hakuba, M. Z., Calbó, J., . . . Bartok, B. (2015). Reassessment and update of long-term trends in downward surface shortwave radiation over Europe (1939–2012). *Journal of Geophysical Research: Atmospheres*, 120(18), 9555-9569. doi: <https://doi.org/10.1002/2015JD023321>.
- Schaeffer, B. A., Iames, J., Dwyer, J., Urquhart, E., Salls, W., Rover, J., & Seegers, B. (2018). An initial validation of Landsat 5 and 7 derived surface water temperature for U.S. lakes, reservoirs, and estuaries. *International Journal of Remote Sensing*, 39(22), 7789-7805. doi:10.1080/01431161.2018.1471545.
- Schmid, M., & Köster, O. (2016). Excess warming of a central European lake driven by solar brightening. *Water Resources Research*, 52(10), 8103-8116. doi: <https://doi.org/10.1002/2016WR018651>.
- Schmid, M., & Read, J. (2022). Heat budget of lakes. In T. Mehner, & K. Tockner (Eds.), *Encyclopedia of inland waters (second edition)* (pp. 467-473). Oxford: Elsevier. doi: <https://doi.org/10.1016/B978-0-12-819166-8.00011-6>.

- Serreze, M. C., & Barry, Roger G. (Roger Graham). (2014). *The Arctic climate system* (Second edition. ed.). New York, NY: Cambridge University Press.
- Sharaf, N., Fadel, A., Bresciani, M., Giardino, C., Lemaire, B. J., Slim, K., . . . Brigitte Vinçon-Leite. (2019). Lake surface temperature retrieval from landsat-8 and retrospective analysis in Karaoun reservoir, Lebanon. *Journal of Applied Remote Sensing*, *13*(4), 1-14. doi:10.1117/1.JRS.13.044505.
- Sharma, S., Jackson, D. A., Minns, C. K., & Shuter, B. J. (2007). Will northern fish populations be in hot water because of climate change? *Global Change Biology*, *13*(10), 2052-2064. doi: <https://doi.org/10.1111/j.1365-2486.2007.01426.x>.
- Shook, K., & Pomeroy, J. (2011). Synthesis of incoming shortwave radiation for hydrological simulation. *Hydrology Research*, *42*(6), 433-446. doi:10.2166/nh.2011.074.
- Stettz, S., Zaitchik, B. F., Ademe, D., Musie, S., & Simane, B. (2019). Estimating variability in downwelling surface shortwave radiation in a tropical highland environment. *Plos one*, *14*(2), e0211220. doi: <https://doi.org/10.1371/journal.pone.0211220>.
- Thompson, H. D., Déry, S. J., Jackson, P. L., & Laval, B. E. (2020). A synoptic climatology of potential seiche-inducing winds in a large intermontane lake: Quesnel Lake, British Columbia, Canada. *International Journal of Climatology*, *40*(14), 5973-5986. doi: <https://doi.org/10.1002/joc.6560>.

- Thornton, P. E., Running, S. W., & White, M. A. (1997). Generating surfaces of daily meteorological variables over large regions of complex terrain. *Journal of hydrology*, *190*(3-4), 214-251. doi: [https://doi.org/10.1016/S0022-1694\(96\)03128-9](https://doi.org/10.1016/S0022-1694(96)03128-9).
- Thornton, P. E., Hasenauer, H., & White, M. A. (2000). Simultaneous estimation of daily solar radiation and humidity from observed temperature and precipitation: An application over complex terrain in Austria. *Agricultural and Forest Meteorology*, *104*(4), 255-271. doi: [https://doi.org/10.1016/S0168-1923\(00\)00170-2](https://doi.org/10.1016/S0168-1923(00)00170-2).
- Thornton, P. E., & Running, S. W. (1999). An improved algorithm for estimating incident daily solar radiation from measurements of temperature, humidity, and precipitation. *Agricultural and Forest Meteorology*, *93*(4), 211-228. doi: [https://doi.org/10.1016/S0168-1923\(98\)00126-9](https://doi.org/10.1016/S0168-1923(98)00126-9).
- Thornton, P. E., Shrestha, R., Thornton, M., Kao, S., Wei, Y., & Wilson, B. E. (2021). Gridded daily weather data for north America with comprehensive uncertainty quantification. *Scientific Data*, *8*(1), 190. doi:10.1038/s41597-021-00973-0.
- Tian, D., Xie, G., Tian, J., Tseng, K., Shum, C. K., Lee, J., & Liang, S. (2017). Spatiotemporal variability and environmental factors of harmful algal blooms (HABs) over western lake Erie. *Plos One* *12*(6), e0179622. doi: <https://doi.org/10.1371/journal.pone.0179622>.
- Twomey, S. (1976). Computations of the absorption of solar radiation by clouds. *Journal of Atmospheric Sciences*, *33*(6), 1087-1091. doi:10.1175/1520-0469(1976)033<1087:COTAOS>2.0.CO;2.

- van de Poll, Willem H., Maat, D. S., Fischer, P., Visser, R. J. W., Brussaard, C. P. D., & Buma, A. G. J. (2021). Solar radiation and solar radiation driven cycles in warming and freshwater discharge control seasonal and inter-annual phytoplankton chlorophyll a and taxonomic composition in a high arctic fjord (Kongsfjorden, Spitsbergen). *Limnology and Oceanography*, 66(4), 1221-1236. doi: <https://doi.org/10.1002/lno.11677>.
- Vanhellemont, Q. (2020). Automated water surface temperature retrieval from Landsat 8/TIRS. *Remote Sensing of Environment*, 237, 111518. doi: <https://doi.org/10.1016/j.rse.2019.111518>.
- Vincent, L. A., & Mekis, É. (2006). Changes in daily and extreme temperature and precipitation indices for Canada over the twentieth century. *Atmosphere-Oceans*, 44(2), 177-193. doi:10.3137/ao.440205.
- Weston, S. T., Bailey, W. G., McArthur, L. J. B., & Hertzman, O. (2007). Interannual solar and net radiation trends in the Canadian arctic. *Journal of Geophysical Research: Atmospheres*, 112 doi: <https://doi.org/10.1029/2006JD008000>.
- Wild, M. (2009). Global dimming and brightening: A review. *Journal of Geophysical Research: Atmospheres*, 114 doi: <https://doi.org/10.1029/2008JD011470>.
- Wild, M., & Liepert, B. (2010). The earth radiation balance as driver of the global hydrological cycle. *Environmental Research Letters*, 5(2), 025203. doi:10.1088/1748-9326/5/2/025203.
- Wilks, D.S. (2006). *Statistical Methods in the Atmospheric Sciences*, 2nd edition. Academic Press: San Diego US.

- Wloczyk, C., Richter, R., Borg, E., & Neubert, W. (2006). Sea and lake surface temperature retrieval from Landsat thermal data in northern Germany. *International Journal of Remote Sensing*, 27(12), 2489-2502. doi:10.1080/01431160500300206.
- Woolway, R. I., Sharma, S., & Smol, J. P. (2022). Lakes in Hot Water: The Impacts of a Changing Climate on Aquatic Ecosystems. *BioScience*. doi:
<https://doi.org/10.1093/biosci/biac052>.
- Yuan, M., Leirvik, T., & Wild, M. (2021). Global trends in downward surface solar radiation from spatial interpolated ground observations during 1961–2019. *Journal of Climate*, 34(23), 9501-9521. doi:10.1175/JCLI-D-21-0165.1.
- Yue, S., Pilon, P., Phinney, B., & Cavadias, G. (2002). The influence of autocorrelation on the ability to detect trend in hydrological series. *Hydrological Processes*, 16(9), 1807-1829. doi:
<https://doi.org/10.1002/hyp.1095>.
- Zhang, T., Stamnes, K., & Bowling, S. A. (1996). Impact of clouds on surface radiative fluxes and snowmelt in the arctic and subarctic. *Journal of Climate*, 9(9), 2110-2123.
doi:10.1175/1520-0442(1996)009<2110:IOCOSR>2.0.CO;2.
- Zhang, X., Vincent, L. A., Hogg, W. D., & Niitsoo, A. (2000). Temperature and precipitation trends in Canada during the 20th century. *Atmosphere-Ocean*, 38(3), 395-429.
doi:10.1080/07055900.2000.9649654.

5 General conclusion and recommendations

The Northwest Territories (NWT) is responding to climate warming at disproportionately higher rates than other regions in Canada (Bush & Lemmen, 2019; Arias et al., 2021). This warming is of concern from an NWT perspective because this territory has a diversity of landscape features with many unique regional features, which may act in distinct and cumulative ways to influence climate, hydrology, ecosystems and people at local and regional scales (Bailey et al., 1997). Understanding the progression of historical climate changes is vital for establishing adequate climate services that supports proper adaptation and mitigation strategies to ensure the sustainability of natural resources, reduce vulnerability and safeguard livelihoods in northern communities (GNWT, 2018). However, there are insufficient continuous long-term *in situ* climate data in the NWT, thus requiring the consideration of other data sources, such as interpolated, reanalysis and remote sensing data. Hence, the goal of this dissertation was to provide an improved understanding of historical surface climate variables trends and patterns and its implications at local and regional scales across the continental NWT by addressing the following research questions:

1. Can gridded datasets (interpolated and reanalyzed) be used as reliable alternative sources for *in situ* observations in climate and hydrological applications in the NWT subarctic?
2. Are continental NWT seasonal surface climate variables (air temperature, precipitation & snowmelt onset) sensitive to concurrent strong Arctic Dipole (AD) atmospheric circulation modes?
3. Are there systematic trends of incoming surface shortwave radiation (SSR) during the past 40 years (1980-2020) across the continental NWT, and are they consistent over spatial and

temporal scales? and ii) Do SSR changes drive changes in lake surface water temperature (LSWT) during the warm season?

Results demonstrated that 1) interpolated and reanalysis climate data can be considered a reliable alternative for *in situ* meteorological data, 2) the AD anomaly influences surface climate, especially air temperature and snowmelt across southern lakes and foothills regions in summer, and 3) historical trends in SSR are heterogeneous across ecozones and LSWT is sensitive to incoming SSR receipt. Additional details are outlined in Chapter 2, 3 and 4, while key contributions of this dissertation are reiterated in the subsequent paragraphs.

5.1 Summary of major findings

5.1.1 Chapter 2

The first study of this dissertation demonstrates the application and utility of one interpolated (ANUSPLIN) and two reanalysis (ERA-Interim and MERRA-2) datasets in hydrological modelling, which has not been previously assessed in the data sparse NWT. In this chapter, comparisons show daily minimum and maximum air temperatures are more closely related to *in situ* observations in gridded datasets than precipitation. The ANUSPLIN temperature time series reproduces the seasonal and interannual variations in *in situ* temperature more accurately than either ERA-Interim or MERRA-2, based on population statistics and temporal structure. Although the gridded datasets reflect monthly and annual seasonal variations in precipitation, they do so with some bias. Precipitation from ANUSPLIN is more consistent with observations than either ERA-Interim or MERRA-2. Also, the higher the spatial resolution of the interpolated/reanalysis dataset, the better its accuracy in representing *in situ* meteorological observations in the NWT.

Moreover, these interpolated/reanalysis temperature and precipitation data were used as substitutes for *in situ* observations in the Cold Regions Hydrological Model (CRHM) to simulate runoff; ANUSPLIN and ERA-Interim inputs are generally promising; their simulated runoff matches the freshet timing and magnitude quite well at Scotty Creek. The knowledge gained from this chapter enhances the comprehension of interpolated/reanalysis data performance and assesses their usefulness as an additional source of data for researchers, communities, and decision makers in the NWT.

5.1.2 Chapter 3

Chapter 3 used the ANUSPLIN interpolated dataset to explore the teleconnection between strong AD modes on local surface climate (air temperature, precipitation and snowmelt onset) in the NWT. The findings indicate considerable year-to-year fluctuation in the AD pattern, with stronger negative modes occurring more frequently during the 2000s. Between 1950 and 2015, there were 64 and 56 occurrences of strong positive and negative AD modes, respectively, throughout all seasons. During strong positive AD modes, local air temperature anomalies rose in summer when compared with their long-term mean. Positive AD modes also resulted in earlier snowmelt onset, by an average of three to five days. In contrast to the strong linkage between AD and local air temperature, the association between AD and seasonal precipitation was not robust. These findings contribute to our understanding of the AD's impact on local weather and climate, as well as implications for future ecosystem change, such as shrubification and wildland fire. From these findings, it is hypothesised that early prediction of strong AD modes could enable a swifter and more effective response to hazards such as heatwaves and wildfires within the NWT, thus increasing its resilience to the effects of climate change.

5.1.3 Chapter 4

Incoming SSR that reaches the Earth's surface is a significant component of the energy balance and climate system. However, trends in SSR that reaches the Earth's surface in northern high latitude regions are not as well characterised as air temperature and precipitation. The third study in this dissertation identified recent spatiotemporal regional trends of the SSR trends, and to my knowledge, that used Daymet SSR data and focused on the continental NWT. During 1980-2020, the annual SSR trend showed a considerable reduction in the northern Arctic and in northern and southern portions of the Taiga Plains ecozones. In contrast, the Taiga Shield ecozone is characterised by fluctuating trend patterns; that is, the southern Taiga Shield ecozone showed typically increasing trends, while other areas showed decreasing SSR trends. SSR receipt correlated negatively with increasing cloud cover, most notably during the summer months, and to a smaller extent in the spring and autumn. With a few exceptions, increases in cloud cover are associated with decreases in SSR and vice versa. This trend is evident across the majority of the NWT ecozones, with the highest correlation values found in the Taiga Plains ecozone. The observed link between clouds and SSR is consistent with previous studies that found local and regional cloud-climate interactions in other regions (Bristow & Campbell 1984). The LSWT for small lakes had a stronger positive correlation with the incoming SSR when compared with medium and large lakes in the North Slave Region that had weak or negative correlation. The implications of persistent lake warming and changing SSR on northern communities and lake ecosystems were discussed, with special attention to the adverse impacts on northern transportation routes, lake productivity and food security.

5.2 Future research recommendations

The findings in this dissertation contribute to an improved understanding of using interpolated, reanalysis, remote sensing data in the NWT and the potential application of these datasets to understand changes and processes can underpin future prediction in operational meteorology and hydrology across local and regional scales in data sparse regions such as the NWT. Notwithstanding, there are areas in which further research could be done to advance this dissertation, which are discussed below.

5.2.1 Applications of interpolated, reanalysis and remote sensing data

The value of using interpolated, reanalysis, and remote sensing data datasets to collectively advance climate knowledge and use as inputs to hydrological modelling is underscored in this dissertation. However, for this dissertation, validation of these interpolated and reanalysis data were constrained to the availability of *in situ* data, which were limited to a specific period and select locations in the NWT. Therefore, whenever *in situ* data are available, evaluation of interpolated, reanalysis, and remote sensing datasets against *in situ* data should be done iteratively. Institutions responsible for generating/collecting these datasets (e.g., European Centre for Medium-Range Weather Forecasts, Oak Ridge National Laboratory) are constantly working to address known deficiencies and improve resolution and physical representation of global, regional, and local climate (Hersbach et al., 2020; Thornton et al., 2021). Despite the demonstrated utility of interpolated/reanalysis/remote sensing data to propel climate and hydrological science across data sparse regions (Zhang et al., 2000; Derksen, et al., 2008; Murfitt & Brown 2017), it is important to emphasize that this research does not advocate for these types of data to completely replace *in situ* observed data from meteorological stations, nor should it be used to justify the current trend of governments to deactivate/reduce monitoring stations (Shiklomanov et al., 2002;

Mlynowski et al., 2011; Orihel et al., 2014; Lavoie, 2017). Hence, the academic community, citizen scientists and the general public are encouraged to continue to actively lobby policy makers to ensure that adequate resources are available to maintain and expand the continuous *in situ* monitoring of climate variables. These *in situ* data are vital as they are incorporated as inputs to many interpolation/reanalysis data assimilation products and are also used in routine validation of climate and hydrological model outputs and remote sensing products (Hersbach et al., 2020; Arias et al., 2021; Thornton et al., 2021).

5.2.2 Atmospheric-oceanic teleconnections and predictions

This dissertation provides an initial framework to understand the effects of strong AD modes on regional and local air temperature, snowmelt and precipitation in the NWT. However, it is assumed that there is a concurrent and mechanistic link between AD modes and surface climate variables. That is, it is hypothesised that both AD modes act independently to affect the surface climate in the NWT. To build upon this work, additional investigations will be needed to understand how the presence of multiple atmospheric-oceanic teleconnections will simultaneously (such as Arctic Oscillation, El Nino-Southern Oscillation, Pacific Decadal Oscillation, etc.) influence the hydroclimate in the NWT (Shabbar et al., 1997; McCabe & Dettinger, 1999). This study also recognises that teleconnections are not always independent and nonlinear (Jiang et al., 2014; Heo et al., 2021), and the amplified presence of these atmospheric-oceanic teleconnection patterns may be responsible for changes in other climate variables, such as SSR and lake surface temperature, observed in the NWT. Characterising the impact of each of these atmospheric-oceanic components on climate variables is a complex endeavour that will be critical to building a thorough understanding necessary to anticipate future changes in this region. Although this research

elucidates some aspects of the mechanisms between the AD and surface climate for the NWT, the development of additional insights regarding the relationship between these mechanisms and the observed changes across the NWT region would be necessary to further develop the predictive value. This is crucial and warrants more investigation as potential increase in strong AD is anticipated to lead to an increase in temperature and precipitation variability by 2100 (Cai et al., 2018) and thus may accelerate the hydrological and ecosystem changes observed in northern regions (Alexeev et al., 2015; Déry et al., 2009).

5.2.3 Radiation budget and LSWT

The analyses in this dissertation provide a first assessment of the spatiotemporal trends of annual and seasonal SSR receipt across continental NWT using Daymet data while simultaneously exploring its relationship with cloud cover and LSWT between 1980 and 2020. Although there is evidence of a negative correlation between total cloud cover and SSR, there is still a need to understand how cloud properties (*e.g.*, cloud's height, its size, and the particles that form the cloud) may influence the amount of SSR received by NWT. In addition, the intensity of other potential drivers, such as oceanic-atmospheric teleconnection (*e.g.*, such as the Arctic Dipole, Arctic Oscillation) and aerosols, may periodically influence the receipt of SSR. For example, studies, have reported reduction of sea ice and longer open water periods in the Arctic during negative AD (*e.g.*, Overland et al., 2012; Alexeev et al., 2015) and, under climate warming and sea reduction, wildland fires have increased (Alexeev et al., 2015) and are projected to continue to rise in northern Canada (Flannigan et al., 2009; Hanes et al., 2019). More frequent wildfires could lead to an augmented level of aerosols within the atmosphere that may influence cloud properties and subsequently the amount of SSR that reaches the NWT. The numerous ways in which aerosol-

radiation and aerosol-cloud interactions occur are complex and are significant sources of uncertainty in climate modelling and prediction (Arias et al., 2021). Therefore, enhanced knowledge of the causes of SSR trend patterns could be utilised to improve climate models and minimise uncertainty in future climate projections (Wild, 2009).

This dissertation focused only on one component of the energy budget, that is, SSR, its trends and its relation to LSWT. Hence, a natural extension of this research would be to quantify long-term changes in the various components of the energy budget (e.g., incoming and outgoing longwave radiation, etc.) to acquire a better understanding of the anthropogenic and natural disruptions in the Earth's radiation balance that underpin regional warming in lakes across the NWT. Furthermore, LSWT variability may depend on a combination of physical and chemical characteristics of the lake (e.g., mean depth, trophic status, dissolved organic carbon, vegetation) and other local climate conditions (e.g., air temperature, wind direction and speed) (Bigras, 1990; O'Reilly et al., 2015; Thompson et al., 2020). Hence, investigating LSWT sensitivity to these processes will necessitate additional investigation across the NWT.

5.3 References

- Arias, P.A., N. Bellouin, E. Coppola, R.G. Jones, G. Krinner, J. Marotzke, ..., & K. Zickfeld, (2021) Technical Summary. In *Climate Change 2021: The Physical Science Basis. Contribution of Working Group I to the Sixth Assessment Report of the Intergovernmental Panel on Climate Change* [Masson-Delmotte, V., P. Zhai, A. Pirani, S.L. Connors, C. Péan, S. Berger, N. Caud, Y. Chen, L. Goldfarb, M.I. Gomis, M. Huang, K. Leitzell, E. Lonnoy, J.B.R. Matthews, T.K. Maycock, T. Waterfield, O. Yelekçi, R. Yu, and B. Zhou (eds.)]. Cambridge University Press, Cambridge, United Kingdom and New York, NY, USA, pp. 33–144. doi:10.1017/9781009157896.002.
- Alexeev, V.A., Euskirchen, E.S., Cherry, J.E. & Busey, R.C. (2015). Tundra burning in 2007—Did sea ice retreat matter? *Polar Science*, 9(2), 185–195. doi: <https://doi.org/10.1016/j.polar.2015.02.002>.
- Bailey, W. G., Oke, T. R., & Rouse, W. R. (1997). *The surface climates of Canada*. Montreal: McGill-Queen's University Press.
- Bigras, S. C. (1990). Hydrological regime of lakes in the Mackenzie delta, Northwest Territories, Canada. *Arctic and Alpine Research*, 22(2), 163-174. doi:10.1080/00040851.1990.12002778.
- Bristow, K. L., & Campbell, G. S. (1984). On the relationship between incoming solar radiation and daily maximum and minimum temperature. *Agricultural and Forest Meteorology*, 31(2), 159-166. doi: [https://doi.org/10.1016/0168-1923\(84\)90017-0](https://doi.org/10.1016/0168-1923(84)90017-0).

- Bush, E. & Lemmen, D.S., editors (2019). Canada's Changing Climate Report Government of Canada, Ottawa, ON. 444 p. <https://changingclimate.ca/CCCR2019/>.
- Cai, L., Alexeev, V.A., Walsh, J.E. & Bhatt, U.S. (2018). Patterns, impacts, and future projections of summer variability in the Arctic from CMIP5 models. *Journal of Climate*, 31(24), 9815–9833. doi: <https://doi.org/10.1175/JCLI-D-18-0119.1>.
- Derksen, C., Brown, R., & MacKay, M. (2008). Mackenzie Basin Snow Cover: Variability and Trends from Conventional Data, Satellite Remote Sensing, and Canadian Regional Climate Model Simulations. In: Woo, Mk. (eds) Cold Region Atmospheric and Hydrologic Studies. The Mackenzie GEWEX Experience. Springer, Berlin, Heidelberg. doi: https://doi.org/10.1007/978-3-540-73936-4_13.
- Déry, S.J., Hernandez-Henríquez, M.A., Burford, J.E. & Wood, E.F. (2009). Observational evidence of an intensifying hydrological cycle in northern Canada. *Geophysical Research Letters*, 36(13), L13402. doi: <https://doi.org/10.1029/2009GL038852>.
- Flannigan, M., Stocks, B., Turetsky, M., & Wotton, M. (2009). Impacts of climate change on fire activity and fire management in the circumboreal forest. *Global Change Biology*, 15(3), 549-560. doi: <https://doi.org/10.1111/j.1365-2486.2008.01660.x>.
- Government of the Northwest Territories [GNWT]. (2018). 2030 NWT Climate Change Strategic Framework. https://www.enr.gov.nt.ca/sites/enr/files/resources/128-climate_change_strategic_framework_web.pdf.

- Hanes, C. C., Wang, X., Jain, P., Parisien, M. A., Little, J. M., & Flannigan, M. D. (2019). Fire-regime changes in Canada over the last half century. *Canadian Journal of Forest Research*, 49(3), 256-269. doi: <https://doi.org/10.1139/cjfr-2018-0293/>.
- Heo, E., Sung, M., An, S. & Yang, Y. (2021). Decadal phase shift of summertime Arctic Dipole pattern and its nonlinear effect on sea ice extent. *International Journal of Climatology*, 41(9), 4732–4742. doi: <https://doi.org/10.1002/joc.7097>.
- Hersbach, H., Bell, B., Berrisford, P., Hirahara, S., Horányi, A., Muñoz-Sabater, J., . . . Thépaut, J. (2020). The ERA5 global reanalysis. *Quarterly Journal of the Royal Meteorological Society*, 146(730), 1999-2049. doi: <https://doi.org/10.1002/qj.3803>.
- Jiang, R., Gan, T.Y., Xie, J. & Wang, N. (2014). Spatiotemporal variability of Alberta's seasonal precipitation, their teleconnection with large-scale climate anomalies and sea surface temperature. *International Journal of Climatology*, 34(9), 2899–2917. doi: <https://doi.org/10.1002/joc.3883>.
- Lavoie, J. (2017). Key Arctic Research Station Set to Close Because of Liberal Government's Funding Cuts. Access on August 15th, 2022 from <https://thenarwhal.ca/key-arctic-research-station-set-close-because-liberal-government-s-funding-cuts/>.
- McCabe, G.J. & Dettinger, M.D. (1999). Decadal variations in the strength of ENSO teleconnections with precipitation in the western United States. *International Journal of Climatology*, 19(13), 1399–1410. doi: [https://doi.org/10.1002/\(SICI\)1097-0088\(19991115\)19:133.0.CO;2-A](https://doi.org/10.1002/(SICI)1097-0088(19991115)19:133.0.CO;2-A).

- Mlynowski, T. J., Hernández-Henríquez, M. A., & Déry, S. J. (2011). An evaluation of hydrometric monitoring across the Canadian Pan-Arctic region, 1950–2008. *Hydrology Research*, 42(6), 479-490. doi:10.2166/nh.2011.105.
- Murfitt, J., & Brown, L. C. (2017). Lake ice and temperature trends for Ontario and Manitoba: 2001 to 2014. *Hydrological Processes*, 31(21), 3596-3609. Doi: <https://doi.org/10.1002/hyp.11295>.
- Orihel, D., Swanson, H., & Venkiteswaran, J. (2013). Scientists on saving science. *Limnology and Oceanography Bulletin*, 22(3), 76-78. doi: <https://doi.org/10.1002/lob.201322376>.
- O'Reilly, C. M., Sharma, S., Gray, D. K., Hampton, S. E., Read, J. S., Rowley, R. J., . . . Zhang, G. (2015). Rapid and highly variable warming of lake surface waters around the globe. *Geophysical Research Letters*, 42(24), 10,773-10,781. doi: <https://doi.org/10.1002/2015GL066235>.
- Overland, J.E., Francis, J.A., Hanna, E. & Wang, M. (2012). The recent shift in early summer Arctic atmospheric circulation. *Geophysical Research Letters*, 39(19), L19804. doi: <https://doi.org/10.1029/2012GL053268>.
- Shabbar, A., Bonsal, B. & Khandekar, M. (1997). Canadian precipitation patterns associated with the Southern Oscillation. *Journal of Climate*, 10(12), 3016–3027. doi: [https://doi.org/10.1175/1520-0442\(1997\)0102.0.CO;2](https://doi.org/10.1175/1520-0442(1997)0102.0.CO;2).

- Shiklomanov, A. I., Lammers, R. B., & Vörösmarty, C. J. (2002). Widespread decline in hydrological monitoring threatens pan-arctic research. *Eos, Transactions American Geophysical Union*, 83(2), 13-17. doi: <https://doi.org/10.1029/2002EO000007>.
- Thompson, H. D., Déry, S. J., Jackson, P. L., & Laval, B. E. (2020). A synoptic climatology of potential seiche-inducing winds in a large intermontane lake: Quesnel Lake, British Columbia, Canada. *International Journal of Climatology*, 40(14), 5973-5986. doi: <https://doi.org/10.1002/joc.6560>.
- Thornton, P. E., Shrestha, R., Thornton, M., Kao, S., Wei, Y., & Wilson, B. E. (2021). Gridded daily weather data for north America with comprehensive uncertainty quantification. *Scientific Data*, 8(1), 190. doi:10.1038/s41597-021-00973-0.
- Wild, M. (2009). Global dimming and brightening: A review. *Journal of Geophysical Research: Atmospheres*, 114 doi: <https://doi.org/10.1029/2008JD011470>.
- Zhang, X., Vincent, L. A., Hogg, W. D., & Niitsoo, A. (2000). Temperature and precipitation trends in Canada during the 20th century. *Atmosphere-Ocean*, 38(3), 395-429. doi:10.1080/07055900.2000.9649654.

Appendices

Supplemental information for Chapter 2

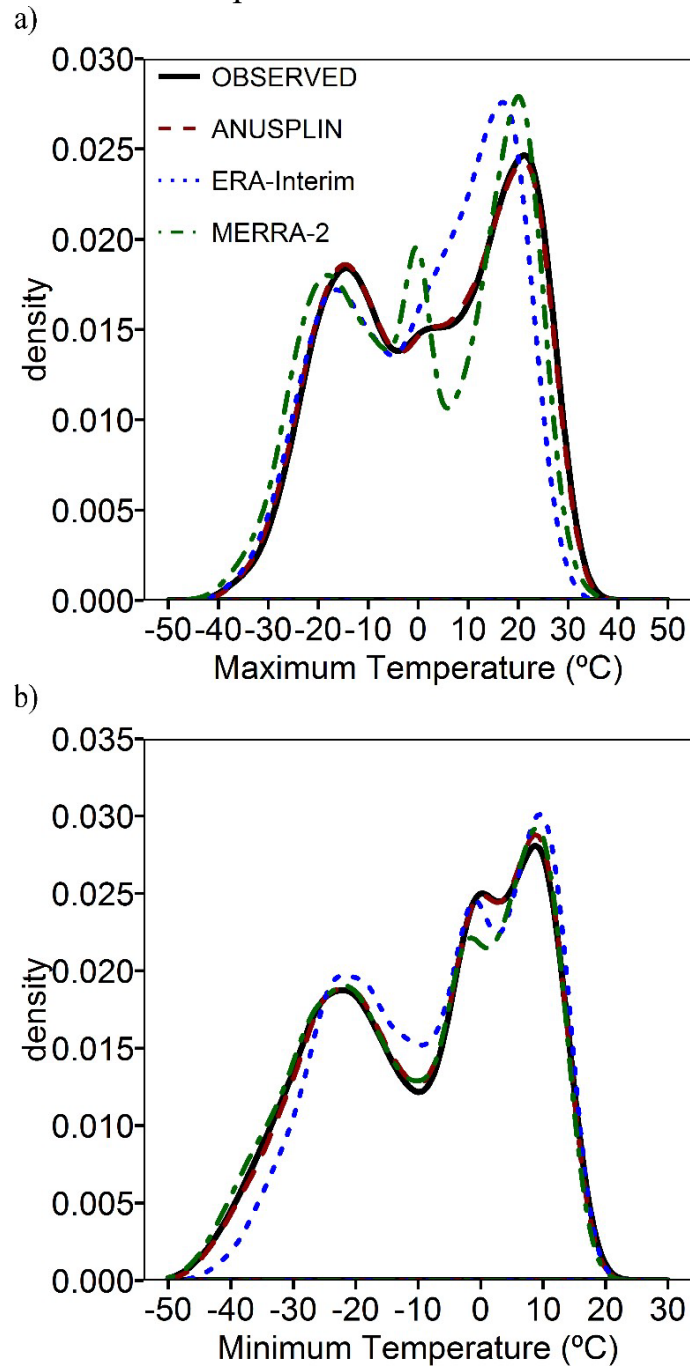


Figure S2.1 Probability distribution functions for (a) observed daily maximum temperature, and (b) daily minimum temperatures for ANUSPLIN, ERA-Interim, and MERRA-2 for Fort Simpson, NWT, from 1980 to 2013.

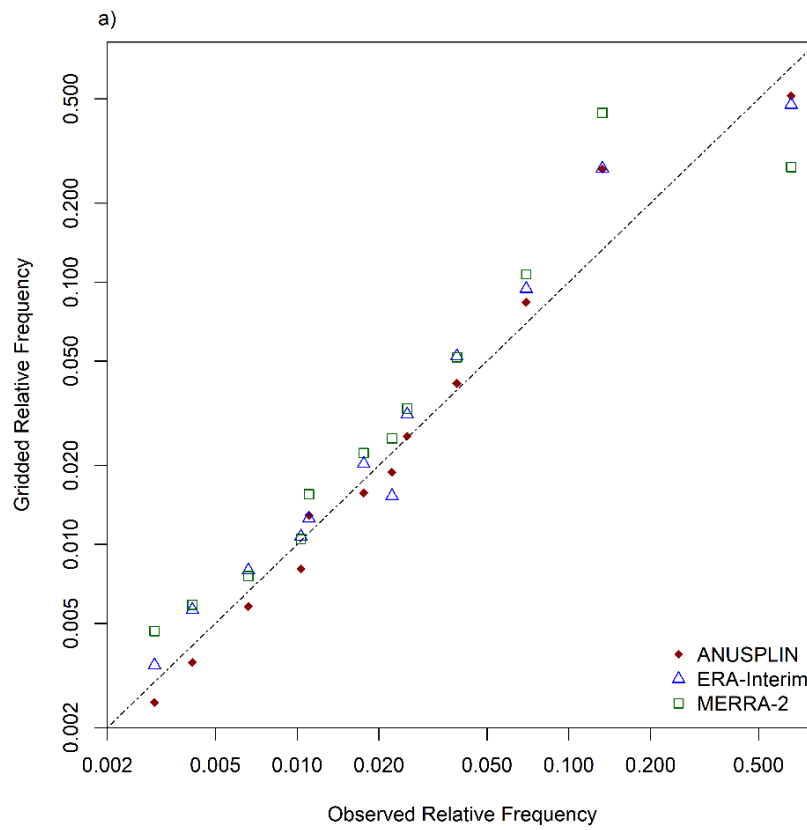


Figure S2.2 The relative frequency of daily precipitation as a function of precipitation amounts on log scale. The dash 1:1 line indicates a gridded relative frequency equal to observed data.

Table S2.1 Summary of statistical methods and R-packages used.

Statistic		Expected	Range	function	package	Reference
Mean Error	ME	0	$-\infty$ to ∞		hydroGOF	Zambrano-Bigiarini, 2014
Mean Absolute Error		0	$-\infty$ to ∞		hydroGOF	Zambrano-Bigiarini, 2014
Root mean square error	RMSE	0	0 to ∞		hydroGOF	Zambrano-Bigiarini, 2014
Kolmogorov-Smirnov	KS	0	-	ks.test		R Core team, 2016
Pearson's correlation coefficient	R		-1 to 1			R Core team, 2016
Breusch and Pagan	BP			bptest	lmtest	Hothorn <i>et al.</i> , 2015
Autocorrelation	acf	0	-1 to 1	acf		R Core team, 2016
Nash-Sutcliffe Efficiency	NSE	1	$-\infty$ to 1		hydroGOF	Zambrano-Bigiarini, 2014
Wang-Bovik	WB		-1 to 1	coded		Mo <i>et al.</i> , 2014

Hothorn, T., Zeileis, A., Farebrother, R., W., Cummins, C., Millo, G., Mitchell, D. (2015). *Lmtest: Testing Linear Regression Models*. version 0.9-34 R Foundation for Statistical Computing, Vienna, Austria. <https://cran.r-project.org/package=lmtest>.

Mo, R., Ye, C., & Whitfield, P. H. (2014). Application potential of four nontraditional similarity metrics in hydrometeorology. *Journal of Hydrometeorology*, 15(5), 1862-1880. doi <https://doi.org/10.1175/JHM-D-13-0140.1>.

R Development Core Team. 2016. R: A language and environment for statistical computing: R Foundation for Statistical Computing. <https://www.R-project.org/>.

Zambrano-Bigiarini, M. (2014) hydroGOF: Goodness-of-fit functions for comparison of simulated and observed hydrological time series. Version 0.3-8. R Foundation for Statistical Computing, Vienna, Austria. URL <https://cran.r-project.org/web/packages/hydroGOF>

Table S2.2 A summary of the statistical performance measures between observed and gridded daily maximum temperature, minimum temperature, and precipitation data for all climate stations. The following abbreviations are used: Mean error (ME), Mean absolute error (MAE), Root-Mean-Square error (RSME), Nash-Sutcliffe model efficiency (NSE), slope, Wang Bovik (WB) index and Pearson correlation coefficient (R).

Location		Maximum Temperature							Minimum Temperature							Precipitation						
		ME	MAE	RMSE	NSE	slope	WB	R	ME	MAE	RMSE	NSE	slope	WB	R	ME	MAE	RMSE	NSE	slope	WB	R
	'best'	0.00	0.00	0.00	1.00	1.00	1.00	1.00	0.00	0.00	0.00	1.00	1.00	1.00	1.00	0.00	0.00	0.00	1.00	1.00	1.00	1.00
Fort Reliance	ANUSPLIN	-0.23	1.00	1.91	0.99	0.99	1.01	0.99	0.39	1.06	1.85	0.99	0.99	1.02	0.99	0.06	0.39	1.08	0.78	0.79	0.86	0.88
	ERA-INTERIM	-1.45	2.20	2.70	0.97	1.00	1.01	0.99	0.08	2.17	2.79	0.97	0.94	1.00	0.99	0.23	0.82	2.04	0.21	0.59	0.61	0.60
	MERRA-2	-1.54	3.56	4.62	0.92	1.08	0.99	0.97	-1.16	3.96	5.16	0.90	1.08	0.99	0.97	0.54	1.03	2.36	-0.06	0.70	0.52	0.59
Yellowknife	ANUSPLIN	-0.19	0.84	1.69	0.99	0.99	0.99	0.99	-0.25	1.30	2.00	0.99	0.97	0.99	0.99	0.03	0.46	1.27	0.74	0.74	0.86	0.86
	ERA-INTERIM	-1.09	1.69	2.15	0.98	0.99	0.99	0.99	0.70	1.82	2.40	0.98	0.92	0.99	0.99	0.03	0.73	1.99	0.37	0.48	0.60	0.62
	MERRA-2	-2.01	3.34	4.52	0.92	1.12	0.97	0.98	-1.37	3.46	4.74	0.92	1.11	0.97	0.98	0.33	0.93	2.33	0.14	0.62	0.56	0.60
Fort Simpson	ANUSPLIN	-0.34	0.75	1.45	0.99	1.00	1.00	1.00	0.15	0.96	1.64	0.99	0.98	0.99	0.99	-0.02	0.55	1.67	0.76	0.75	0.86	0.87
	ERA-INTERIM	-1.54	2.56	3.18	0.97	0.92	0.99	0.99	1.56	2.38	3.17	0.96	0.92	0.98	0.99	0.05	0.99	2.65	0.40	0.52	0.63	0.65
	MERRA-2	-2.07	3.17	4.06	0.94	0.99	0.98	0.98	-0.67	2.51	3.29	0.96	0.99	0.98	0.98	0.35	1.18	3.08	0.19	0.59	0.57	0.59
Scotty Creek	ANUSPLIN	-0.58	1.44	2.12	0.98	0.99	0.96	0.99	1.33	2.27	3.15	0.96	0.94	0.94	0.98	0.23	1.49	3.85	-0.36	0.13	0.16	0.16
	ERA-INTERIM	-1.41	2.49	3.18	0.96	0.94	0.98	0.99	3.74	3.97	5.06	0.90	0.89	0.96	0.98	0.45	1.43	3.55	-0.18	0.32	0.35	0.36
	MERRA-2	-1.79	3.39	4.29	0.93	0.97	0.96	0.97	1.86	3.28	4.21	0.93	0.93	0.96	0.97	1.06	1.97	4.99	-1.33	0.46	0.25	0.31
Hay River	ANUSPLIN	0.02	1.00	1.72	0.99	1.00	0.99	0.99	0.05	1.18	1.85	0.98	1.00	0.99	0.99	0.01	0.55	1.54	0.73	0.72	0.84	0.85
	ERA-INTERIM	0.12	2.10	2.78	0.97	0.98	0.98	0.98	2.33	2.65	3.34	0.95	0.95	0.98	0.99	0.06	0.86	2.26	0.42	0.50	0.63	0.66
	MERRA-2	-1.79	3.83	4.84	0.90	1.10	0.96	0.97	0.80	4.51	5.45	0.87	1.19	0.95	0.97	0.43	1.09	2.82	0.10	0.66	0.56	0.60
Fort Smith	ANUSPLIN	-0.26	0.76	1.52	0.99	1.00	1.00	1.00	0.45	1.01	1.73	0.99	0.99	0.99	0.99	0.00	0.48	1.42	0.78	0.75	0.87	0.88
	ERA-INTERIM	-1.18	1.95	2.47	0.98	0.94	0.99	0.99	1.63	2.25	2.89	0.96	0.94	0.99	0.99	0.11	0.89	2.36	0.39	0.51	0.63	0.64
	MERRA-2	-1.63	2.90	3.83	0.94	1.07	0.98	0.98	-0.80	2.67	3.60	0.94	1.06	0.98	0.98	0.24	0.96	2.47	0.33	0.62	0.64	0.65
Fort Liard	ANUSPLIN	0.07	0.50	1.00	1.00	0.99	1.00	1.00	-0.05	0.51	0.89	1.00	0.99	0.99	1.00	-0.06	0.44	1.85	0.77	0.74	0.87	0.88
	ERA-INTERIM	-2.84	4.14	4.98	0.91	0.87	0.96	0.97	0.16	2.42	3.32	0.95	0.92	0.97	0.97	0.13	1.58	3.71	0.09	0.34	0.42	0.44
	MERRA-2	-1.46	3.89	4.93	0.91	0.90	0.95	0.96	-0.22	2.65	3.54	0.94	0.93	0.96	0.97	0.58	1.85	4.30	-0.22	0.46	0.41	0.43
Fort Nelson	ANUSPLIN	-0.04	0.69	1.40	0.99	0.99	0.99	1.00	0.43	0.83	1.39	0.99	0.98	0.99	1.00	-0.02	0.70	1.97	0.77	0.80	0.93	0.88
	ERA-INTERIM	-0.99	2.97	3.74	0.94	0.87	0.97	0.98	1.74	2.51	3.49	0.94	0.91	0.97	0.98	-0.08	1.19	2.99	0.47	0.55	0.71	0.69
	MERRA-2	0.16	3.07	4.01	0.93	0.91	0.96	0.97	1.11	2.69	3.71	0.93	0.90	0.96	0.97	0.38	1.30	3.26	0.37	0.73	0.76	0.70

Supplemental information for Chapter 4

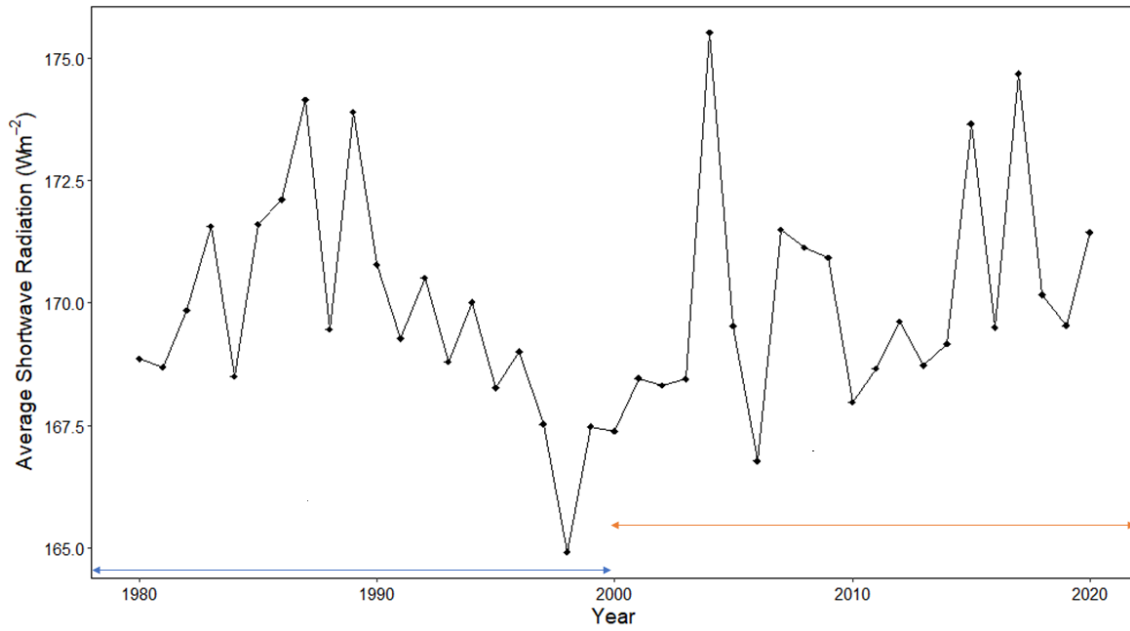


Figure S4.1 Example of year-to-year variability mean shortwave radiation during the 1980 to 2000 and 2001 to 2020 periods.